Development and Characterization of Fe-NiTi-Cr Reinforced Metal Matrix Composites Made by Powder Metallurgy

Melkayehu Legesse Tesfaye

A Thesis Submitted to Department of Mechanical Engineering

School of Mechanical, Chemical and Materials Engineering

Presented in Partial Fulfillment of the Requirement for the Degree of

Masters in Manufacturing Engineering

Office of Graduate Studies

Adama Science and Technology University

June, 2023

Adama, Ethiopia

Development, and Characterization of Fe-NiTi-Cr Reinforced Metal Matrix Composites Made by Powder Metallurgy

Melkayehu Legesse Tesfaye

Advisor: Dr. Devendra Kumar Sinha

A Thesis Submitted to Department of Mechanical Engineering

School of Mechanical, Chemical and Materials Engineering

Presented in Partial Fulfillment of the Requirement for the Degree of Master's in Manufacturing Engineering

Office of Graduate Studies

Adama Science and Technology University

June, 2023

Adama, Ethiopia

CANDIDATE'S DECLARATION

Declaration I hereby declare that this Master Thesis entitled "**Development, and Characterization of Fe-NiTi-Cr reinforced Metal Matrix Composites Made by Powder Metallurgy**" is my original work. That is, it has not been submitted for the award of any academic degree, diploma or certificate in any other university. All sources of materials that are used for this thesis have been duly acknowledged through citation.

Melkayehu Legesse Tesfaye	___________________	________________
Name	Signature	Date

RECOMMENDATION OF ADVISOR

I the advisor of this thesis, hereby certify that I have read the revised version of the thesis entitled "**Development, and characterization of Fe-NiTi-Cr reinforced metal matrix composites made by powder metallurgy**" prepared under my guidance by Melkayehu Legesse Tesfaye submitted in partial fulfillment of the requirements for the degree of Mater's of Science in Manufacturing Engineering. Therefore, I recommend the submission of revised version of the thesis to the department following the applicable procedures.

Dr. Devendra Kumar Sinha	____________	____________
Advisor	Signature	Date

APPROVAL OF ADVISOR

I the advisor of the thesis entitled "**Development, and characterization of Fe-NiTi-Cr reinforced metal matrix composites made by powder metallurgy**" and developed by Melkayehu Legesse Tesfaye hereby certify that the recommendation and suggestions made by the board of examiners are appropriately incorporated into the final version of the thesis.

Dr. Devendra Kumar Sinha	 ______________	______________
Advisor	Signature	Date

APPROVAL BY BOARD OF EXAMINERS

We, the undersigned, members of the Board of Examiners of the thesis Melkayehu Legesse Tesfaye have read and evaluated the thesis entitled "**Development, and characterization of Fe-NiTi-Cr reinforced metal matrix composite made by powder metallurgy**" and examined the candidate during open defense. This is, therefore, to certify that the thesis is accepted for partial fulfillment of the requirement of the degree of Master of Science Manufacturing Engineering.

______________________	______________	______________
Chairperson	Signature	Date
______________________	______________	______________
Internal Examiner	Signature	Date
Getasew A. TADDESE (PhD)	______________	04/10/2023
External Examiner	Signature	Date

Final approval and acceptance of the thesis is contingent upon submission of its final copy to the Office of Postgraduate Studies (OPGS) through the Department Graduate Council (DGC) and School Graduate Committee (SGC).

______________________	______________	______________
Department Head	Signature	Date
______________________	______________	______________
School Dean	Signature	Date
______________________	______________	______________
Office of Postgraduate Studies, Dean	Signature	Date

ACKNOWLEDGEMENT

Before anything else, I want to express my heartfelt thankfulness to the Almighty God for providing me enough energy and health to finish my study with His help as to make use of my best achievements.

I want to express my sincere gratitude to my advisor**, Dr. Devendra Kumar Sinha. Dr. Devendra Kumar Sinha** is an extraordinary advisor to work with, and I am grateful for the opportunity to be a member of his team of researchers. His respectful professional conduct, because along with his sincere dedication and patience to help the students to be better versions of themselves in their research and future careers, make him an exceptional advisor to work with. I would like to take this opportunity to thank my friends, my teachers and other kindness people for giving their time and helpful suggestions during my work.

I have a great acknowledged and respect to my teachers Dr. Devendra, Dr. Moera Gutu, Dr. Dr. P.J. Ramulu, Dr. Guteta.K, and Dr. Habtamu Beri from the Mechanical Design and Manufacturing Engineering program for their excellent instruction and for sharing their knowledge of academically and personal experiences.

TABLE OF CONTENTS

ACKNOWLEDGEMENT v

TABLE OF CONTENTS vi

LISTS OF TABLES x

LISTS OF FIGURES xi

LISTS OF ACRONYMS xiii

ABSTRACT xv

CHAPTE ONE 1

INTRODUCTION 1

1.1 Background of the Study 1

1.2 Problem Statement 4

1.3. Research Questions 5

1.4. Objectives of the Study 5

1.4.1. General Objective 5

1.4.2. Specific Objectives 5

1.5. Significance of the Study 5

1.6. Scope of the Study 6

1.7. Research Motivation 6

1.8. Limitation of Study 6

1.9. Thesis Organization 7

CHAPTER TWO 8

LITERATURE REVIEW 8

2.1 Introduction to Composite Materials 8

2.2 Classification of Composite Materials 9

2.1.1 Polymer Matrix Composite 10

2.1.2 Ceramic Matrix Composite 10
2.1.3 Metal Matrix Composite 11
2.2. Ferrous Metal Matrix Composites (FMMC's) 13
2.2.1. Steel Metal Matrix Composites 13
2.2.2. Iron Based Metal Matrix Composites 13
2.3. Literature Survey Related to IMMC 13
2.3.1. Microstructural and Mechanical Properties of IMMC's 13
2.3.2. Corrosion and Tribological Behavior of Reinforced IMMC's 18
2.3.3. Particle Reinforcement Composites 21
2.4. Nitinol Particle Reinforcement 21
2.5. Manufacturing Technology for Metal Matrix Composites 22
2.5.1. Liquid State Processing 22
2.5.2. Solid State Processing 23
2.6. Powder Metallurgy 23
2.6.1. Powder Preparation and Mixing: 24
2.6.2. Compaction 24
2.6.3. Sintering 25
2.7. Effects of Powder Metallurgy Process Parameters on Composites 26
2.7.1. Milling Time 26
2.7.2. Compaction Pressure 26
2.7.3. Sintering Temperature and Time 26
2.8. Application of Iron Metal Matrix Composites (IMMC's) 27
2.9. Gear Material 27
2.10. Fe-NiTi-Cr Metal Matrix Composites 28
2.11. Literature Summary 28

2.12. Research Gap 28
CHAPTER THREE 30
MATERIALS AND METHODS 30
3.1. Materials 30
3.1.1. Iron Based Metal Matrix..30
3.1.2. Nitinol Pre-alloyed Reinforcement Particles 30
3.1.3. Chromium..31
3.1.4. Molybdenum Disulfide (MoS2) 32
3.2. METHODS 33
3.2.1. Experimental Procedures..33
3.2.2. Design the Experiment for IMMC Fabrication 34
3.2.3. Specification of Weight Percentage Composition in Composite's 34
3.2.4. Mass and Volume Estimation of Matrix and Reinforcements in Composites 35
3.2.5. Powder Metallurgy Fabrication Techniques..38
3.2.6. Specimen Preparation for Microstructural Characterization..41
3.2.7. Microstructural Characterization Test of Sintered Specimen..42
3.2.8. Density of Composite Materials..45
3.2.9. Hardness Test..47
3.2.10. Compression Strength Test..48
3.2.11. Corrosion Test..49
3.3. Tools and Equipment Used in Research Study 51
CHAPTER FOUR 52
RESULTS AND DISCUSSIONS 52
4.1. Introduction..52
4.2. Analysis of Density and Porosity of Sintered Sample 52

4.2.1. Density of Composites 52
4.2.2. Porosity of Composite 53
4.3. Microstructural Characterization 55
4.3.1. XRD Analysis 55
4.3.2. Optical Microscopy 59
4.3.3. Scanning Electron Microscope (SEM) 61
4.3.4. FT-IR Analysis 62
4.4. Analysis Hardness Test 63
4.5. Analysis of Compression Test 65
4.6. Fracture Analysis Using SEM 67
4.7. Corrosion Study 68
4.7.1. Potentiodynamic Polarization Measurements 69
4.7.2. Electrochemical Impedance Spectroscopy (EIS) Analysis 72
4.7.3. Surface Investigation After Corrosion 73
CHAPTER 5 75
CONCLUSION AND RECOMMENDATION 75
5.1. Conclusions 75
5.2. Recommendation 76
5.3. Future Work 77
REFERENCES 78

LISTS OF TABLES

Table 3.1 Properties of Iron, Nitinol Powder and Chromium. 32
Table 3.2 Properties of MoS2 Powder..32
Table 3.3 Reinforced IMMC Made by Powder Metallurgy 34
Table 3.4 Mass and Volume Fraction of Matrix and Reinforcements in Composite.................37
Table 3.5 Tools and Equipment Used in the Research Work..51
Table 4.1 Composition and Samples Design 52
Table 4.2 Experimental Density, Relative Density and Porosity 54
Table 4.3 Crystalline Sizes of Samples Using XRD Data 57
Table 4.4 Crystalline Sizes, Dislocation Density and Lattice Strain Experimental Calculation 58
Table 4.5 Experimental Results of Hardness Values..64
Table 4.6 Tafel Polarization Experimental Parameters Values 70

LISTS OF FIGURES

Figure 1.1 Classification of Composites Based on Reinforcing Elements. 2
Figure 1.2 Effects of Corrosion on Gear. 3
Figure 2.1 Number Research's Paper Per Year (Sing et al., 2022). 9
Figure 2.2 Classification of Composite Materials (Rajak et al., 2019); (Ashebir, 2022). 10
Figure 2.3 Classification of MMC's (Kumar et al., 2020). 12
Figure 2.4 Particle Reinforced Composites 21
Figure 2.6 Compaction Process (Panda, 2016). 25
Figure 3.1 Material Used in The Research Work 31
Figure 3.2 General Flow Chart for Experimental Procedure 33
Figure 3.3 Dimension of Predesigned Die 35
Figure 3.4 Photos of High Energy Planetary Ball Milling 39
Figure 3.5 Photos of (A) Mounting Press set up and (B) Compacted Specimen (Green Part) .40
Figure 3.6 (A), The Furnace Set Up and (B) The Sintered Samples 41
Figure 3.7 Sample Preparation 42
Figure 3.8 (A) Sample Prepared for Test, and (B) OM Test 45
Figure 3.9 Photos of Weighting Balance for Measuring (A) Weight in Air And (B) Suspended Weight in Water 46
Figure 3.10 Vickers Hardness Test and Measurements 48
Figure 3.11 (A) UTM (Compression test) set up and (B) the compressed Sample 49
Figure 4.1 Physical Propeties of Sintered Samples 54
Figure 4.2 XRD Spectrum of IMMC at Different Reinforcement Content 56
Figure 4.3 Comparison Between Crystalline Size (CS), Dislocation Density (DD) And Lattice Strain (LS) Using Bar Chart 59
Figure 4.4 Optical Micrographs of S1, S2, S3, And S4 Before and After Etchant at Different Magnification 60
Figure 4.5 Porosity Analysis of Using Imagej Software from OM Image 61
Figure 4.6 SEM Micrographs of (S1, S2, S3 And S4) at 20μm 62
Figure 4.7 FT-IR Spectrum of IMMC's and for (S1) 63
Figure 4.8 Bar Chart Average Vickers Hardness (HV) of (S1, S2, S3, And S4) 65
Figure 4.9 Stress- Strain Diagram of (S1, S2, S3, And S4) 66

Figure 4.10 (A) Average Vickers Hardness and Compressive Strength, and (B) Improvement Recorded 67
Figure 4.11 Fractography Analysis Using SEM for (S2) and (S3) at 50μm and 100 μm 68
Figure 4.12 The Tafel Polarization Plot of Iron and IMMC's 70
Figure 4.13 Electrochemical Impedance Nyquist Plots of Pure Iron and IMMC In 3.5 Wt% NaCl Solution. 72
Figure 4. 14 OM Micrographs of Corroded for (S1, S2, S3, and S4) at 100μm 73
Figure 4.15 SEM Micrographs Before and After Corrosion........ 74

LISTS OF ACRONYMS

ASTM	American Society for Testing Materials
CMC	Ceramics Metal Composite
CR	Corrosion Rate
DD	Dislocation Density
Ecorr	Corrosion Potential
EDS	Energy Dispersive Spectroscopy
EIS	Electrochemical Impedance Spectroscopy
FMMC	Ferrous Metal Matric Composites
FTIR	Fourier Transform Infrared Spectroscopy
FWHM	Full Width Half Maximum
HV	Vickers Hardness
Icorr	Corrosion Current
IMMC	Iron Metal Matrix Composite
JCPDS	Joint Committee on Powder Diffraction Standards
LS	Lattice Strain
MMC	Metal Matrix Composites
MOS2	Molybdenum Sulphide
MPa	Mega Pascal
NFMMC	Non-Ferrous Metal Matrix Composite
NITINOL	Nickel Titanium -Naval Ordnance Laboratory
NI-TI	Nickel Titanium
NMC	Nickel Metal Matrix Composite
OCP	Open Circuit Potential
OM	Optical Microscopy

PM	Powder Metallurgy
PMC	Polymer Metal Composite
SCE	Standard Calomel Electrode
SiC	Silicon Carbide
SEM	Scanning Electron Microscopy
Rp	Polarization Resistance
TMC	Titanium Metal Composite
UCS	Ultimate Compressive Strength
UTM	Universal Testing Machine
VHN	Vickers Hardness Number
XRD	X-Ray Diffractometer
wt%	Weight Percentage
ρsint.	Sintered Density
μ(%)	Protection Efficiency

ABSTRACT

In the modern developed world, new materials are being discovered at a rapid rate. The main issues with employing iron are its short lifespan, low strength-to-weight ratio, poor corrosion resistance, and increased density. The goal of this thesis study was to create high-hardness, and corrosion-resistant Fe- metal matrix composite materials for use in industrial and automotive applications. The composite was created using powder metallurgy with additions of different weight percentages of base metal iron (81 wt%), Nitinol (5, 7.5, 10) wt%, Chromium (10, 7.5, 5) wt%, and 4 wt% MoS2 smart reinforcing particulates at the same milling time (2 hours), compaction pressure (60 MPa), and sintering temperature (1100°C). After proper fabrication of samples, phases analyzed by XRD, distribution and microstructure morphology by (OM, SEM), the physio mechanical properties (density, porosity, Vickers hardness and compression), and corrosion behavior sintered samples were characterized, and analyzed. The XRD results showed that the (Fe-Cr) and (Fe-Ni) (kamacite) phases were exhibited and due to small reinforcing particle addition, the smaller peaks not identified. From OM micrographs the grain distribution was analyzed and SEM showed particles distributed finely in base matrix. (Fe-5%NiTi-10%Cr-4%MoS2) shows minimum pores (4.37%), high relative densities (95.6%), uniform microstructure, higher Vickers hardness (465HV) with 86% improvement, compressive strength (636MPa), with (76%) corrosion protection efficiency with minimum corrosion rate was investigated. Increment of both reinforcement (NiTi and Cr) up to 10 wt.% shows there were an improvement in all sectors, yet the mechanical characteristics and corrosion behavior of iron metal matrix composites are significantly improved by the addition of chromium. The addition of promising particles increases the manufactured Iron Metal Matrix Composite (IMMC) hardness and corrosion resistance compared to base metal pure iron. The new reinforced IMMC material is thus expected to have potential uses in the automobile industry, as well as a variety of other structural applications.

Keywords: *Iron Metal Matrix Composite, Powder Metallurgy, Nitinol, Chromium, Vickers Hardness, Corrosion resistance*

CHAPTE ONE

INTRODUCTION

1.1 Background of the Study

The development and innovation of advanced materials that meet the requirements of developing new applications is an essential area of study in the manufacturing industry. Because of today's rapid modernization and advancements, the production of high-quality alloys is becoming an important issue to fulfill the interesting, and the implementation of smart materials for successfully completing various tasks in terms of weight, strength, strength-to-weight ratio, and cost reduction has been increasing (Aydogmus, 2015); (Singh et al., 2022). Modern industry is largely dependent on the development of novel technologies that improve product quality while maintaining low manufacturing costs. Because of their low density and superior mechanical properties, composite materials are the smartest material that will have a role in the future.

A composite material is made up of elements that are created by mechanically combining pre-existing ingredient materials to produce a new material with special properties when compared to monolithic material properties (T.Somasekhar and P Niteesh kumar, 2018). Metal matrix composites (MMC) are a type of composite material made by mixing two or more components that have superior qualities to the individual components (the matrix phase). Reinforcing elements in metal matrix composites (MMC) typically include ceramic whiskers, continuous or discontinuous fibers, and particles (Öksüz et al., (2014); (Chauhan et al., 2017). Depending on the size and shape of the reinforcement material, metal matrix composites can be, classified as whiskers, monofilament and particles. The shape and size of the reinforcement affect the properties of the produce material and different fabrication method is, needed. Powder form of reinforcements can be termed as particulates.

Metal Matrix Composites (MMCs) have gained popularity due to their ability to provide a wide variety of mechanical and physical qualities. They have distinct compositions, microstructures, and properties, including low density, excellent strength, high hardness, fracture toughness, corrosion resistance, and wear resistance, high stiffness and high temperature stability, ductility, and have extensive applications in the bio-medical, aerospace, and automotive industries (Campbell, J. 2015); (Rajasekar et al., 2018); (Raturi, 2019). The size and volume proportion of the reinforcing components have the greatest impact on composite characteristics (Khuntia and Samal, 2019).

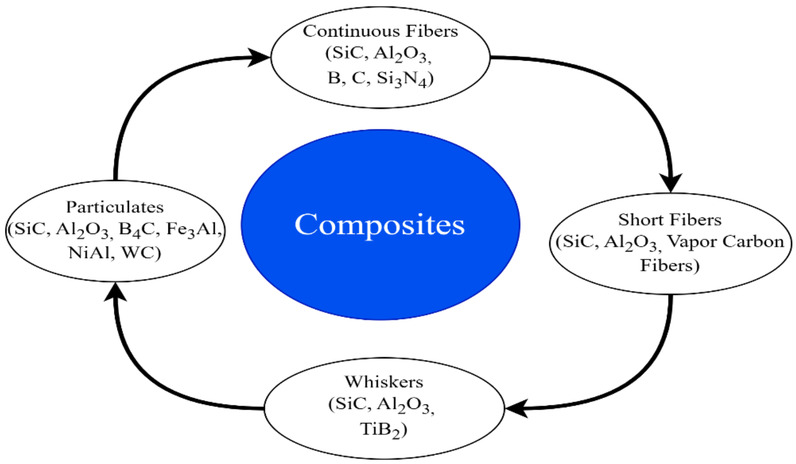

Figure 1.1 Classification of Composites Based on Reinforcing Elements (Panda, 2016).

For improved wear resistance, thermal stability, and predictable isotropic mechanical and frictional qualities in the MMC, hard particles, often ceramic, such as SiC, silica, are used. Additives such as graphite, MoS2, and boron nitride exhibit stability and damping qualities under constant friction, (Li et al., 2019). With the advancement of industry, the need for service performance and life of mechanical components has steadily increased. Mechanical elements, such as gear, are quickly destroyed due to surface wear under constant operating conditions.

Aluminum (Al), magnesium (Mg), copper (Cu), iron (Fe), titanium (Ti), steel, cast iron, and various other matrices are employed in MMCs (Singh et al., 2022). Aluminum (Al) and magnesium (Mg) alloys have received a great deal of attention in recent decades as a potential material of choice for significant weight reductions, (Miller et al., 2016). So far, the majority of nonferrous MMC's created have been based on the popular aluminum matrix with various reinforcements such as oxides, carbides, borides, nitrides, and fly ash.

Since ferrous metal matrix composites (FMMC's) are less investigated and created than NFMMC's, they are used for fewer real-world applications. However, ferrous Fe-based alloys have recently gained popularity in structural, automotive, actuators, filters, sensors, aerospace engineering, microcontrollers, and robotics due to their good mechanical properties, low cost, excellent workability, high ductility, high shear stress, and high machinability (Lee et al., 2015).

Steel, cast iron, and pure iron are the three types of ferrous MMC’s (Khuntia and Samal, 2019). To avoid oxidation and interaction with the reinforcements, FMMC’s must be synthesized with the greatest care. FMMC fabrication techniques are classed as solid-state (powder metallurgy, hot isostatic pressing, cold compaction and sintering) or liquid-state (stir casting, squeeze casting) (Chandel et al., 2021).

Powder metallurgy (PM) is a process for creating more dense, precise, and robust MMC components (Dad Chandio et al., 2019). Powder metallurgy is an established technique because clarify geometries with exact sizes and shapes may be manufactured at a high production rate while remaining cost-effective (Meignanamoorthy and Ravichandran, 2018). It is made by combining small powders of metals or ceramic materials, pressing them into a suitable form, and then heating the compressed material in a controlled environment to join the material sintering. Researchers are looking for ways to improve elastic behavior, high temperature stability, and other performance, but strength-to-weight ratio, corrosion resistance and creep capacity remain problems.

Figure 1.2 Effects of Corrosion on Gear (El-Saeed et al., 2009); (Chami et al., 2021).

Adding the good corrosion resistance smart metal particles to iron metal matrix is one of the significant studies of many researchers to improve the corrosion properties of the ferrous material (Varadaraj et al., 2023). In many applications, the expense of reducing the useful life of iron-based materials owing to corrosive attack is substantial. Increasing the silicon carbide content of the iron matrix to at least 12% is one technique to lower the rate of material corrosion (Olani et al., 2023). Generally better values of structural and mechanical properties are, carried out by many researchers for iron-based metal matrix. However, based on the existing literature, Fe-NiTi-Cr metal matrix composites has not been previously, developed.

The goal of this work is to develop an iron-based metal matrix composite reinforced with nitinol and chromium for automotive and industrial applications. The fabrication had been done with powder metallurgy, and the synthesis of iron-based reinforced metal matrix composite have fabricated at different weight percentage of reinforcing particulates. XRD have used to examine phase processes, SEM used to characterize morphology of composites, and OM for evaluating grain size and homogeneity. The hardness tested by Vickers hardness test machine, porosity and density analyzed by Archimedes principles, compression done by universal testing machine, and corrosion of the composited material have analyzed by potentiodynamic polarization and electrochemical impedance spectroscopy.

1.2 Problem Statement

In today's developed environment, the discovery of new materials is evolving at a rapid rate. Short life, low strength-to-weight ratio, low corrosion resistance, and increased density are all issues in this regard. Iron-based composite used in a variety of automotive and industrial products. Metal matrix composites have been identified as having significant employment potential in a wide range of applications, including actuators, filters, pipe joints, fasteners, springs, gears, brakes, crane rails, and special connectivity (bolts, nuts, screws, rivets). A greater quality-to-weight ratio is an industrial need that is difficult to meet using a single material or even in combination. In terms of strength to weight ratio, iron metal still lacks the attribute, causing the material's the effectiveness to be lower.

High fuel prices, as well as environmental concerns about energy usage and air pollution, have raised the need for efficient transmission systems. Transmission gears experience cyclic loads as they enter and exit their gear mesh. The successive loading causes cyclic bending stress in the gear root and contact stress on the flank surface that surrounds the gear tooth. As a result, the friction between the matrix and the reinforcement must be reduced in order to have the mechanical and tribological behavior of the composite (Dyachkova et al., 2020). By considering the above challenges, the development of iron-based MMC hardness and corrosion resistant materials reinforced with nitinol, chromium, and molybdenum for appropriate matrix-reinforcement mixing was chosen.

1.3. Research Questions

Having all the above-mentioned facts about the fabrication process and characterization of iron matric composites in the introductory part and statement of the problem, the following research questions are raised.

A. what are the most significant process parameters during fabrication in powder metallurgy?

B. At what conditions the best corrosive iron matrices composites are achieved?

C. At what process parameters the best mechanical and metallurgical characteristics of iron composites material is achieved?

D. What is the effect of reinforcements on mechanical and metallurgical properties of the composite?

E. How does the corrosion is improved with respect to hardness after reinforcement addition?

1.4. Objectives of the Study

The general and the specific objectives of the study described as follows:

1.4.1. General Objective

The general objective of the study is to develop, and characterize of Fe-NiTi-Cr reinforced metal matrix composite made by powder metallurgy.

1.4.2. Specific Objectives

- ✓ To fabricate Fe-NiTi-Cr reinforced metal matrix composite through powder metallurgy.
- ✓ To characterize phase, microstructural evolution, and uniformity of grain distribution in the composite material through XRD, SEM, and OM respectively.
- ✓ To investigate porosity, density and hardness of synthesized composite material.
- ✓ To investigate the compression strength and fractography of the developed composite material.
- ✓ To study the corrosion behavior and surface after corrosion of the developed composite material.

1.5. Significance of the Study

Now a day ‘s, manufacturing industries such as automotive industries, and aerospace industries are highly in need of lightweight, harder, stronger components using costeffective composite materials. The significance of the study is to manufacture, characterize, and investigate the mechanical properties of Fe-NiTi-Cr reinforced metal matrix composites in order to increase their corrosion and wear resistance. The study concentrates on the service life and corrosion resistance of composites by lowering the weight of automotive and industrial components in order to save fuel. Learning and understanding how to prevent porosity in samples helps improve the mechanical and physical qualities of produced materials, allowing them to last longer. As a result, this research is critical in translating my theoretical knowledge into practical practice and acts as motivation for future research initiatives.

1.6. Scope of the Study

The development of nitinol and chromium-reinforced iron-metal matrix composites to improve corrosion resistance and wear was the primary focus of research. Powder metallurgy techniques were used in the fabrication process, which was characterized by XRD for phase transformation, SEM for microstructure, and OM for grain size refinement. The hardness tested by Vickers hardness test machine, porosity and density analyzed by Archimedes principles, compression done by universal testing machine, and corrosion of the composited material have analyzed by potentiodynamic polarization and electrochemical impedance spectroscopy. The appealing features of Fe-NiTi-Cr composites make them appealing for a wide range of industrial and automotive applications.

1.7. Research Motivation

Due to their high damage and low corrosion attributes, reinforced iron-based metal matrix composites are no more available for researchers to design and analyze. Composites with slightly enhanced mechanical and metallurgical characteristics are created. As a result, the emphasis of this study is on regulating and improving the mechanical and metallurgical performance of the produced composites. The addition of smart reinforcing particles Nitinol and Chromium improves mechanical and metallurgical properties over the basic matrix.

1.8. Limitation of Study

Difficulties in fabrication of iron-based metal matrix composites are:

- ✓ Uniform distribution of reinforcement: It can be challenging to achieve a uniform distribution of the reinforcing phase in the metal matrix, particularly if the reinforcing phase's particle size is small. This may result in particle clustering or a non-uniform distribution, which might change the general characteristics of the composite.

- ✓ High melting point: Because iron has a high melting point, melting and casting the metal into various shapes can be difficult.

1.9. Thesis Organization

The overall structure of this document can be summarized as follows:

Chapter one, Background of study, problems statement, objectives of study, research scope, research motivations, research limitations. Overview of the literature on this area of study has been provided shortly. **Chapter two**, Fabrication method of MMC'S, application, the geometry of the matrix and reinforcement, the matrix and reinforcement utilized in metal matrix composites, the influence of reinforcement on microstructure, mechanical characteristics, corrosion, and compression were all reviewed. **Chapter three,** Material selection and experimental procedure and testing, analysis method. **Chapter four**, several test findings and discussions on produced samples have been discussed and evaluated, and **Chapter five**, Summarize, conclusions and recommendation the future study. Finally, Reference and various appendix listed.

CHAPTER TWO

LITERATURE REVIEW

This chapter introduces the classification of composite materials, their production techniques, their enhanced effect on mechanical characteristics, wear behavior, and microstructural characterization of metal matrix composites to put the research issue into context. The review of the published literature on iron-based metal matrix composites and its applications. gaps in the literature have been identified and presented in this summary of the literature survey.

2.1 Introduction to Composite Materials

A composite material is a material system composed of an appropriate mixture or combination of two or more macro, and micro components separated by interfaces yet with differing forms and chemical compositions. A composite material is one that combines a considerable proportion of the properties of both the reinforcing phase (which contains the discrete components) and the matrix component (which contains the continuous phase), resulting in a better combination of properties (Bodunrin et al., 2015); (Mavhungu et al., 2017). This composite material has a high strength-to-weight and modulus-to-weight ratio, as well as outstanding fatigue and wear and corrosion resistance. These applications require materials with increased specific strength, hardness, wear resistance, and dimensional stability at high temperatures.

The properties of composite materials are heavily influenced by the qualities of their constituents, their distribution, and their interactions. The morphology of the reinforcement (shape, size, and particle distribution) has a considerable impact on the composite qualities in addition to the type of starting material. The contribution of individual components to the overall qualities of the composite is determined by the concentration distribution and orientation of the reinforcement. Non-ferrous matrix composites (NFMMC's) are a key application field among the various MMC's (A. Singh et al., 2022).

However, the consistency of FMMC research has been carried out in a variety of applications, including heavy-duty road vehicles and railways (Paswan et al., 2021). FMMC synthesis necessitates extreme caution to avoid oxidation and reactivity with strengthening agents. Lower temperature requirements in the P/M range not only safeguard ferrous materials from reactions with the environment and reinforcements, but also contribute to environmental protection by saving material, energy, and post-processing. MMCs have arisen as a new class of materials over the last two decades to meet demanding applications in aerospace, automotive, marine, sports, and bio-implants (Singh et al., 2022).

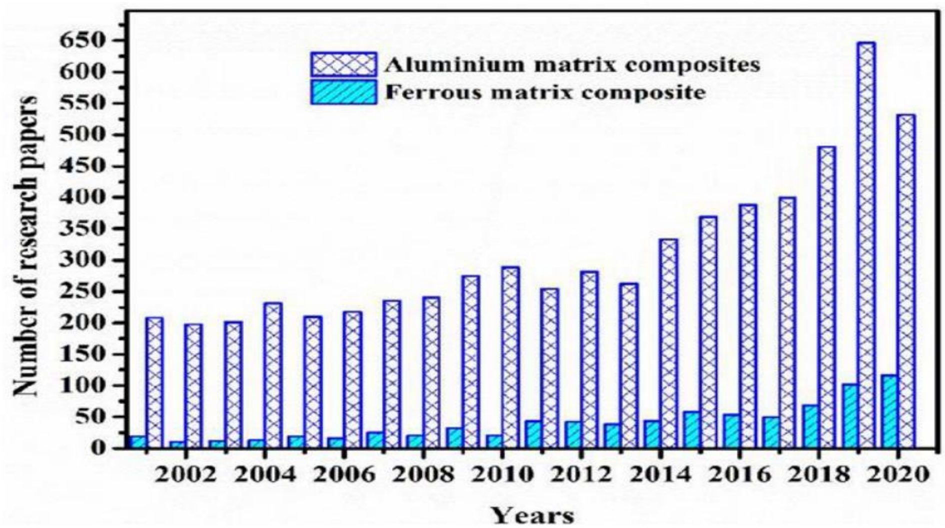

Figure 2.1 Number Research's Paper Per Year (Sing et al., 2022).

Until 2019, there were 6–8 times as many research articles on aluminum matrix-based composites as there were on ferrous matrix-based composites. However, a slight decline has been seen for composites made with aluminum in 2020. This information is a strong indicator that more research papers are being published annually, which is good news for ferrous matrix-based composites.

2.2 Classification of Composite Materials

Chandra Kandpal et al. (2018) Composites can be divided into many categories according to their types of matrices, reinforcement, size, content, etc. The following are the primary composite material classifications: Based on the matrix phase's science, and the dispersion phase (reinforcement shape) material.

Composites are divided into metal matrix (MMC), polymer matrix (PMC), and ceramic matrix composites (CMC) based on the chemical properties of the matrix phase measurements. Composites are further subdivided into particle-reinforced composites and fiber-reinforced composites, and structural composites distinguished by the geometry of the reinforcement (Kesarwani et al., 2015); (Cheng et al., 2016); (Rajak et al., 2019).

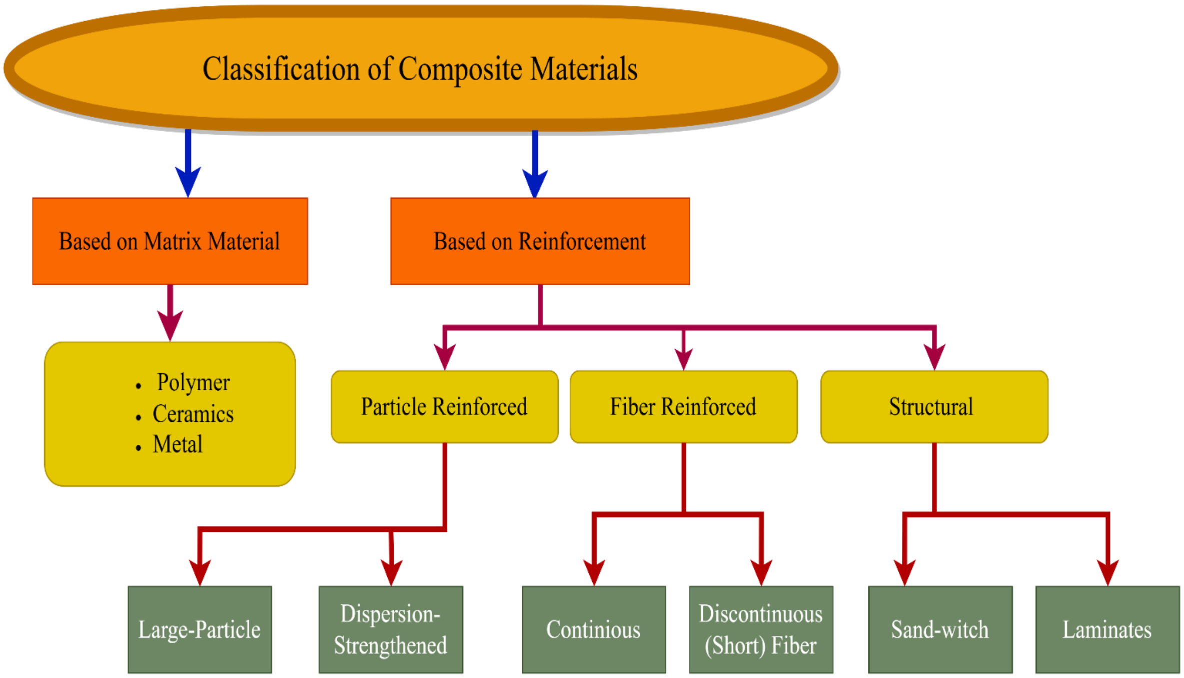

Figure 2.2 Classification of Composite Materials (Rajak et al., 2019); (Ashebir, 2022).

2.1.1 Polymer Matrix Composite

The matrix phase in polymer matrix composites is a polymer, whereas the reinforcing phase is an organic, inorganic, or hybrid material. Polymer matrix composites outperform metal and ceramic matrix composites in various ways, including low density, high ductility, high impact absorption capacity, low production cost, and so on (Tai et al., 2012); (Sharma et al., 2020). Polymer matrix composites have always fascinated the scientific community because they have superior mechanical qualities such as stiffness, fatigue resistance, and corrosion resistance compared to many other materials, making them excellent for a wide range of engineering applications. (Sajan and Philip Selvaraj, 2021); (Kangishwar et al., 2023).

2.1.2 Ceramic Matrix Composite

Ceramic matrix composites (CMC) are made up of ceramics as the primary constituent and metals or other inorganic materials as the reinforcing phase. Ceramics have a high melting point, a high compressive strength, a high strength at high temperatures, and are resistant to oxidation. SiC-based ceramic materials' unique mix of qualities enables its usage in a wide range of engineering applications, including nuclear, defense, metallurgical, food, chemical, oil production and refining sectors, aerospace vehicles, airplane brake systems, and breakdown cranes (Kaledin et al., 2023) and traditionally, advanced structural ceramics have been best suited for mechanical, structural, tribological, and thermal shock resistant applications (Shvydyuk et al., 2023).

2.1.3 Metal Matrix Composite

Anand and Tiwari, (2022) because of their intelligent mechanical and thermomechanical qualities, metal matrix composites are gaining favor in a variety of industrial, automotive, and aerospace applications. MMCs are created by fusing two or more materials with distinct chemical, physical, and mechanical properties. Aluminum, magnesium, copper, iron, titanium, steel, cast iron, and other metal matrices are commonly employed in MMC research (Singh et al., 2022).

The majority of MMCs created to date are based on a common aluminum matrix with diverse reinforcements such as oxides, carbides and borides, nitrides, and fly ash. Aluminum-based MMCs dominate practically every NFMMC application, from road transportation vehicles to satellite launchers. Ferrous metal matrix composites, in addition to non-ferrous metal matrix composites, are potential possibilities for aircraft and road transportation. The graphical representation of data acquired from the web of science validated the idea that aluminum matrix composites predominated (Hathaway et al., 1997).

According to (Kumar et al., 2020) many studies have been conducted to help guide future study in the field of iron matrix-based composites. However, aluminum-based composites will experience a modest dip in 2020. However, as compared to aluminum-based composites, they provide substantial obstacles for researchers interested in working with iron-based composites (Wang et al., 2020). As a result, substantial scientific and efficient efforts should be performed to identify alternative perspectives in the development of iron-metal matrix composites for new application domains. At high temperatures, all metals become more reactive. Ferrous metals like iron and its alloys like steel oxidize at temperatures considerably below their melting points (Degnan and Shipway, 2002).

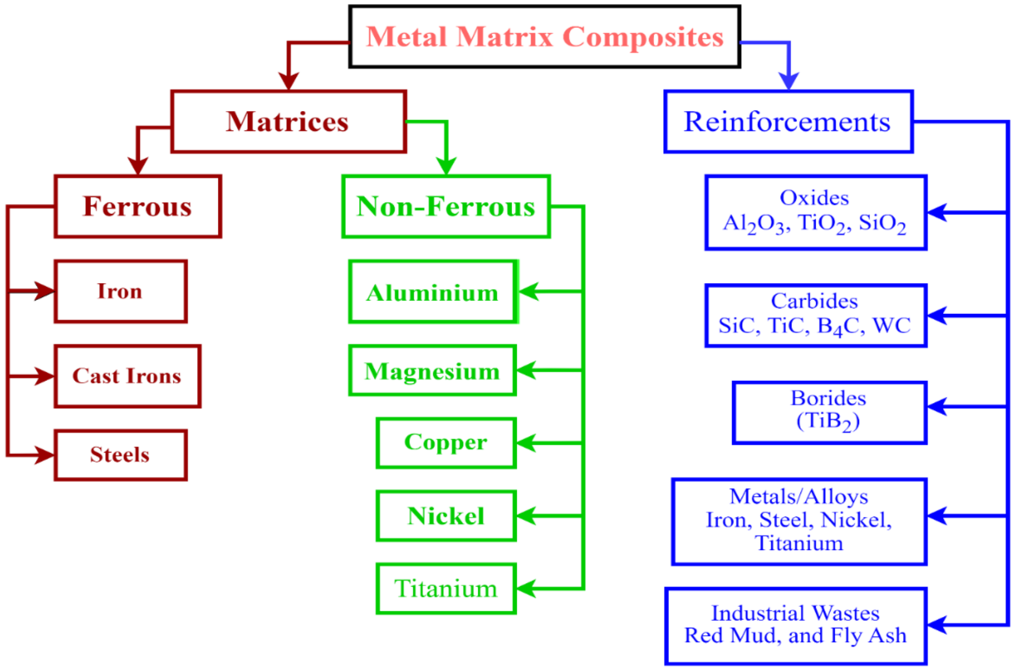

Figure 2.3 Classification of MMC's (Kumar et al., 2020).

2.1.3.1. Aluminum Metal Matrix Composites

Aluminum metal matrix composites are one type of material that has been shown to meet the highest requirements in applications demanding light weight, high stiffness, and moderate strength. Reinforcing particles added to pure aluminum metal are reported to improve composite mechanical qualities such as tensile strength, hardness, and wear resistance Bahari et al. (2012). Aluminum-magnesium alloy (AlMg) is an important engineering material for mechanical applications due to its low density, high thermal conductivity, and increased machinability in the automotive, aerospace, marine and mineral processing industries (Chandel et al., 2021).

2.1.3.2. Titanium and Nickel Metal Matrix Composites

Titanium matrix composites (TMC's) are made up of a titanium matrix with continuous reinforcing fibers. The main advantage, depending on the type of reinforcement, is great strength and stiffness. Titanium and its alloys are gaining popularity in research for a variety of uses, including the automotive and aerospace industries. Composite coating based on nickel-based metal matrix (NMC's) for better magnetic characteristics, increased wear and corrosion resistance, and repair parts. Because of their outstanding wear and corrosion resistance, strong resistance to adhesion and abrasion, and high bonding strength, they are widely utilized in industry (Parande et al., 2018); (Hayat et al., 2019); (Karmakar et al., 2021).

2.2. Ferrous Metal Matrix Composites (FMMC's)

In terms of literature and practical applications, ferrous metal matrix composites (FMMC) are older but less utilized than non-ferrous metal matrix composites (NFMMC). Cast iron, steel, and iron are the three main types. FMMC is usually manufactured using steel, cast iron, and pure iron molds. Iron-based metal-matrix composites have numerous engineering uses (Singh et al., (2022); (Jha et al., 2022).

2.2.1. Steel Metal Matrix Composites

Because of their simplicity of synthesis and mechanical tribological characteristics, ceramic-reinforced steel matrices are important materials (Fallahdoost et al., 2014). Steel's major application in aviation and ground transportation can result in a variety of stress and wear issues. According to (Parashivamurthy et al., 2001) wear resistance is one of the appealing features that contribute to MMC's better frictional properties.

2.2.2. Iron Based Metal Matrix Composites

Iron is an essential substance in physical metallurgy because it can be alloyed with other elements to produce well-known products like steels and super alloys. Iron-based metal matrix composites with superior physical, mechanical, and tribological properties have recently been created and successfully used in a variety of areas including automotive, aerospace, sports, and rail transportation. During this age of tremendous growth, research seeks to investigate alternatives to traditional materials. Metal matrix composites have enormous potential because they can impart characteristics that traditional alloys cannot.

2.3. Literature Survey Related to IMMC

Several iron-based composites have been studied to improve their mechanical and tribological properties at varying weights. Different reinforcements are used in wt.%. The most related works are described here:

2.3.1. Microstructural and Mechanical Properties of IMMC's

Hui et al. (2000) titanium powder (99.8 wt% purity, average particle size 45 μm) and graphite powder (99.5 wt% purity, average particle size 45 mm) were prepared by ball milling for 4 hours. The chemical compositions of the base metal alloys used in this work are as follows (% by weight):C 0.12, Cr 25.8, Ni 14.5, Si 1.7, balance Fe. The Fe-Cr-Ni alloy was melted in a medium induction furnace under a protective atmosphere of flowing argon. Once the melt reached a certain temperature, titanium and graphite powder precursors with desired compositions were added to the melt. Subsequently, TiC particles were synthesized in the molten state.

Tensile creep tests were performed in air over a temperature range of 973-1123 K and a stress range of 40-160 MPa. Creep was measured using a linear variable differential transformer. The creep test temperature was kept within 1K. Measurements were made with a thermocouple placed as close as possible to the center of the gauge length of the sample. The steady-state creep rate for each subsequent stress level was determined by linear regression at 0.5% strain. The creep life of composites containing 5 and 10 vol% TiC particles is longer than that of the matrix alloy. The creep strain rate of the composite increases with increasing volume fraction of TiC particles at all applied stresses and temperatures.

Bahari et al. (2012) studied Al-Fe-Cr-Ti nanocomposite structures using XRD and AFM techniques. It obviously depends on the manufacturing method and the combination of Ti and Al content. Acetic acid was added to the solvent over 30 minutes at room temperature. This solution was then mixed with titanium chlorides TiCl4, Al2O3, Fe2O3, and FeCr2O4 at 0 °C in specific molar ratios to obtain different contents. The sol was stirred at 60° C. until it gelled and ethanol was removed (approximately 24 hours). The temperature gradient during the test run was 5 degrees/minute and the samples were placed in the oven for 2 hours at various firing temperatures.

The composition, structure and surface morphology of Al2O3-TiO2-SiO2 powders were studied using XRD and AFM techniques. AFM and XRD results show that due to the increased dislocation density in the highly deformed regions, the crystal splits into sub grains separated by small-angle grain boundaries, and the sub grains rotate to form nanograins with random orientations relative to each other. is shown to form Grain refinement is caused by a significant increase in dislocation density, followed by the formation of sub grains with dense dislocation walls, a gradual increase in sub grain boundary misorientation, and finally a dislocation density Ultra-fine particle with reduced are fully developed.

Chauhan et al. (2017) has conducted research on induction hardening of powder metallurgically treated Fe-Cr/Mo alloys. Pre-alloyed powders Fe-3Cr-0.5Mo, Fe-1.5Cr-0.2Mo and Fe-0.85Mo were mixed at 0.4 wt%, 0.6 wt% and 0.8 wt% and tested by compression at 500, 600 and 700 MPa. bottom. Alternatively, the compacts were sintered at 1473 K for 1 hour and then cooled at 6 K/min.

Hardness varied from HV 600 to HV 375 from the surface of the sample to the interior of the case-hardened region. The best combination of properties and hardening depth was achieved for Fe-1.5Cr-0.2Mo alloy with 0.6 wt% C. A 0.6 wt% sintered Fe-1.5Cr-0.2Mo alloy has a high tensile strength of 457.7 MPa, an elongation of 6.4% and a hardness of HV 233. The maximum hardness of the alloy after induction hardening is HV 600. The case depth is 2.5 mm. Therefore, among the studied alloys, the Fe-1.5Cr-0.2Mo alloy containing 0.6 wt% C is the most suitable for automotive gears and engine parts.

Duriagina et al. (2020) used a powder metallurgy approach to synthesize and investigate the structural formation features, phase compositions and properties of the model alloys Fe75Cr25, Fe70Cr25Zr5 and Fe69Cr25Zr5B1. The sintering process was carried out in an electric furnace with a tungsten cathode under a pure argon atmosphere on a water-cooled copper anode under a pressure of 6×10 4 Pa. The sintered alloy was annealed in an electro corundum tube at a temperature of 800° C. for 3 hours. XRD analysis was performed using diffractometers DRON-3.0M and DRON-4.0M. Microstructural investigation and phase identification were performed using a REMMA-102-02 scanning electron microscope.

Microhardness was measured with a PMT-3M microhardness tester. Using microstructural formation features of model alloys and phase transformations determined in the Fe-Cr, Fe-Cr-Zr, and Fe-Cr-B-Zr systems, the chemical composition of alloyed gypsum during ferrite formation was investigated. It can be improved. and ferritic-martensitic stainless-steel coatings, using these alloys, especially Fe75Cr25, Fe70Cr25Zr5 and Fe69Cr25Zr5B1, as new materials with specific functional properties.

By alloying up to 5% zirconium in Fe-Cr based model alloys, it is possible to obtain a composite microstructure consisting of a solid-solution-based mechanical mixture of basic Feα(Cr) solid solution on Laves-Fe2Zr and FeCrZr. The microstructure stabilizes at high temperature as a result of the of intermetallic precipitates at grain boundaries or the process of Zr segregation at grain formation boundaries.

Chu et al. (2021) characterized the microstructure and investigated the mechanical behavior of the high-entropy alloys Fe-Ni-Co-Cr and FeNiCoCrMn produced by powder metallurgy. Elemental powders of Fe, Ni, Co, Cr and Mn with high purity (>99.7 wt%) and small particle size (<45 µm) were first mixed for 5 hours. Subsequently, the mixed powder was dry-milled for 45 hours and then wet-milled in ethanol (process control agent) for 5 hours to obtain Fe-Ni-Co-Cr and Fe-Ni-Co-Cr-Mn mechanical alloying powders. Milling was performed in a high-energy planetary ball mill at 300 rpm using high-performance stainless-steel vials and tungsten carbide balls (10:1 ball-to-powder ratio).

After 0, 5, 15, 30, 45 and 50 hours of grinding, powder samples were taken to study the phase evolution during the MA process. After wet milling, the ground powder was placed in a vacuum chamber to evaporate the ethanol at 60°C. Finally, the dry powder was compacted using the spark plasma technique on a spark plasma sintering device at 1000 °C. with a residence time of 8 minutes. The microstructure of the samples was observed by transmission electron microscopy with energy dispersive spectroscopy (EDS) analysis.

Compression tests were performed at room temperature using an Instron 5500 test system at a strain rate of 1×10^{-3}. Three Φ 3 mm × 4.5 mm cylindrical compression specimens were tested for each sample. The Vickers hardness of the samples was measured using a digital microhardness tester (HVS-1000) with a load of 300 g and a dwell time of 15 seconds before discharge. Data reported were the arithmetic mean from 10 different positions for each sample. In addition, the densities of Fe-Ni-Co-Cr and FeNiCoCrMn bulk alloys were determined according to Archimedes' principle using high-purity ethanol.

From these investigations, the mean grain size of the FCC primary phase in the bulk Fe-Ni-Co-Cr alloy is about 416 nm, whereas the mean grain size of the FCC primary phase in the bulk FeNiCoCrMn alloy is about 547 nm. Clearly, the small grain size of the FCC primary phase in the Fe-Ni-Co-Cr alloy seems to be the main contributor to the improved mechanical performance.

Khazaal et al. (2022) have successfully developed hybrid iron-based metal matrix composites (MMC) reinforced with volume fractions of 0, 1, 2, 3, and 4% in defined mixtures (80% Al2O3 and 20% ZrO2) by powder metallurgy, investigated its mechanical properties of hybrid composites. Depending on the reinforcement content, 80% alumina and 20% zirconium powder reinforced iron matrix composites were produced by powder metallurgy techniques. Fractured and compressed four different specimens after compression and sintering using five different volume fractions of 80% Al_2O_3 and 20% ZrO_2 (0%, 1%, 2%, 3%, 4%) hardness test. The powder was compacted at 640 MPa and sintered at 1120°C in the presence of argon gas. Purity, density, average particle size and shape were measured using a dosimeter, particle size analyzer and SEM.

Iron-based metal matrix composites were prepared and subjected to various mechanical tests such as impact, compression, tensile and hardness tests, as well as X-ray diffraction (XRD) and SEM microstructure to measure the mechanical and physical properties of the metal matrix Composite. The best mechanical properties were obtained at (97% + 3% (80% Al_2O_3 + 20% ZrO_2)) of all reinforcement volume fractions, and the composites had matrix properties with respect to compressive strength of 61%, 37%, and 7% better. Hardness or radial compressive strength SEM proved the presence of three phases, $FeAl_2O_4$ and $FeZrO_2$ as pure materials, in addition to Fe and Al_2O_3.

Ivannikov et al. (2022) have prepared and studied the microstructure and mechanical properties of high-entropy Fe-Cr-Ni-Mo-W alloys from elemental powders. They produced high entropy alloys of 35Fe30Cr20Ni10Mo5W (wt%) and 30Fe30Cr20Ni10Mo10W (wt%) manufactured using powder metallurgy. Powder blends for hot pressing processes are prepared by mixing and mechanically alloying elemental powders. Hardened chromium steel balls with a diameter of 5.5 mm were used for grinding with a ball-to-powder weight ratio of 5:1. Hot pressing was performed at a pressure of 30 MPa and a temperature of 1200 °C for 30 minutes. The maximum density of the confined material of 8.14 ± 0.02 and 8.40 ± 0.01 g/cm^3 and the compressive strength of 2430 ± 30 MPa and 2460 ± 35 MPa were obtained in the powder mixture after mechanical grinding for 10 h at 5 wt.% or 10% W. Powder morphology, microstructural evolution, and chemical composition analysis were characterized using a Hitachi 4700 scanning electron microscope with energy dispersive X-ray spectroscopy (EDS). Compressive strength measurements at room temperature were performed on an Instron 3382 at a loading rate of 1 mm/min. Hardness was evaluated according to the Rockwell method using a hardness tester TR 5006. At least 10 measurements were taken to calculate the average value.

These studies show that mechanical alloying contributes to bulk and tapped densities, as well as increased densities of green bodies made from powder mixtures. Increasing the mechanical alloying time decreased the molybdenum and tungsten peaks, which also contributed to the formation of BCC and FCC phases in the powder. An intermetallic compound Ni_3Fe was also present in the powder. The low physical density values of the agglomerates prepared by pressure sintering from powders after 2.5 h and 5 h grinding is consistent with low compressive strength and hardness. The highest density agglomerates from the powder exhibited the highest compressive strength and hardness values at room temperature after milling for 10 hr.

Jha et al. (2022) developed a mathematical model to predict the density and hardness of Fe-ZrO_2 metal matrix composites produced by powder metallurgy. The three process parameters considered are: Sintering temperature (900-1100 °C), weight percentage of ZrO_2 (10-30), and sintering time (1-3 hours). Iron-based metal matrix composites are widely applied in the automotive, aerospace and railway sectors. Sintering time and ZrO_2 weight percent, and their interaction, have a large effect on density, while ZrO_2 weight percent independently affects hardness.(Olani et al., 2023) With the addition of hard ceramic reinforcement, the hardness of Fe-SiC-ZrO_2 increases from 327.4 HV to 477 HV for iron and composites, respectively, compared to the base metal, and the corrosion behavior of the reinforced Fe matrix shows favorable corrosion.

2.3.2. Corrosion and Tribological Behavior of Reinforced IMMC's

Li et al. (2019), developed the interfacial bonding and wear behavior of iron matrix composites reinforced with ceramic particles. Using zirconia-strengthened alumina particles and Ni-Ti composite powder as raw materials, particle-strengthened high-Cr cast iron was manufactured by infiltration casting. 1mm diameter particles containing 80 vol.% ZrO_2 were selected as reinforcement for high Cr cast iron matrix composites. Ni and Ti elemental powders (40–50 µm) were thoroughly mixed in ethanol using alumina grinding balls for 24 hours. Coated particles are formed by sintering in a graphite mold protected from an argon atmosphere. The sintering temperature was 1500°C, which is slightly higher than the melting point of Ni (1428°C), and the sintering holding time was 1 hour.

The compressive strength of the preforms was measured using a universal mechanical testing machine. Its chemical composition is: Cr 15 wt%, C 3.1-3.2 wt%, Si 0.5-1.0 wt%, Mn 0.6-0.7 wt%, Mo 1.0-1.5 wt%, balance Fe. The casting temperature for the Cr15 matrix was 1550°C, slightly higher than the industry standard (1420°C) to improve the fluidity of the molten iron. This study shows that the wear resistance of the composite improved significantly with increasing stress, reaching 12.6 times that of the reference Cr15 sample. This is mainly because the interface is tightly bound by the Ni-Ti transition layer and forward particles also withstand major wear forces and protect the surrounding iron matrix from further damage. The smaller grain size of alumina relative to the Fe-Cr matrix improved the wear and strength properties of the composite (Shamsuddin et al., 2013).

Zhou et al. (2021) Coated strengthened aluminum particles are formed by sintering in a graphite mold protected from an argon atmosphere. The sintering temperature was 1500°C, which is slightly higher than the melting point of Ni (1428°C), and the sintering holding time was 1 hour. The compressive strength of the preforms was measured using a universal mechanical testing machine. Its chemical composition is: Cr 15 wt%, C 3.1-3.2 wt%, Si 0.5-1.0 wt%, Mn 0.6-0.7 wt%, Mo 1.0-1.5 wt%, balance Fe. The casting temperature for the Cr15 matrix was 1550°C, slightly higher than the industry standard (1420°C) to improve the fluidity of the molten iron.

This study shows that the wear resistance of the composite improved significantly with increasing stress, reaching 12.6 times that of the reference Cr15 sample. The smaller grain size of alumina compared to the Fe-Cr matrix improved the wear and strength properties of the composite. A good metallurgical bond is formed between the substrate and the coating and no cracks occur. The microhardness and wear resistance of the coating first increase and then decrease. Also, the wear resistance of the coating was significantly improved compared to that of the substrate, and both the hardness and wear resistance of the coating decreased with increasing Cr content (Han et al., 2019). Small additions of 0.1 and 0.3 wt% Cr to NiTi slightly improved the pitting resistance of the resulting alloys, as the pitting potentials of all Ni-Cr samples in 0.9% NaCl shifted to more noble values. increase. The addition of chromium also decreased the corrosion rate of the alloy in 0.9% NaCl Obadele et al. (2015).

Composite samples were manufactured using a powder metallurgy process. Powders of iron, graphite and silicon carbide were mixed for 1 hour and pressed under a pressure of 750 MPa. After pressing, the composite was sintered at 1100°C for 1 hour. Both wear and corrosion resistance are improved by increasing the proportion of ZrO2 reinforcing particles up to 10% by weight compared to composites based on Fe-Ni matrix (Singh et al., 2018). As the silicon carbide content increased, the hardness of the composite increased and the corrosion resistance decreased (Karabulut et al., 2022).

Kheradmand et al. (2022) Tribological characterization of reinforced Fe matrix composites with hybrid reinforcement from C, Cu and SiC particles was studied. They designed and characterized Fe, SiC, Cu, and C metal matrix composites (MMCs) with optimal SiC content to achieve sufficiently good anti-wear performance. Fe, Cu, graphite, BaSO4 (Fe-11Cu-6.5G-6BaSO4) and 2, 4, 6, 8, 10 wt% SiC powders (ranging from 45 to 150 µm) were milled to fabricate composites. Subsequently, it was sintered by hot pressing under conditions of 1000° C. and 400 MPa in an atmosphere furnace. The wear and coefficient of friction (COF) of the samples were then measured over 1000 m at 20 N and 700 rpm. SEM recordings and EDS analysis were also used for wear mechanisms.

Examination of the wear surface revealed that the wear mechanism was dominant at the beginning of the sliding distance, with plastic deformation, adhesive wear and oxidation being activated as the sliding distance increased. Weight loss by increasing SiC to the optimum value is reduced by10%. Increasing the SiC content reduced the sample weight and improved the wear resistance. Therefore, with low wear rate and suitable coefficient of friction, Fe-11Cu-10SiC-6.5G-6BaSO4 composites can be used for aircraft brake pad applications. High and stable coefficient of friction (0.3 to 0.5) for the requirements imposed on brake lining materials for automotive applications.

J. Li et al. (2020) The study of Fe-Ni matrix composites containing various amounts of graphite (Gr) and the microstructure and properties of the composites fabricated by the spark plasma sintering system "SPS" have been investigated in detail. The results show that the Fe–Ni matrix composites are mainly composed of Fe, NiWCr, FeNi, FeCr, Fe3C, Fe3W3C, (Cr, Fe)7C3, core eutectic structure (pearlite/Fe3C) and Gr. The variation of average microhardness of Fe-Ni matrix composites depends on Gr content. It increased initially, but then tended to decrease as the Gr content increased. At 3 wt% Gr addition, the average microhardness reaches a maximum of about 355.3HV, which is about twice that of 16Mn steel. In addition, increasing the Gr content to 3 wt% under the same conditions resulted in the formation of a composite layer with high hardness and continuous low shear strength on the wear surface, resulting in the lowest wear rate of Fe–Ni matrix composites.

Bratu et al. (2013) By PM approach, Fe scrap was used to prepare low-cost Fe-Cu alloy matrix nanocomposites supplemented with hybrid NbC and granite scrap. It works by collecting surplus iron stock from previous industrial processes and grinding it into powder using a high-energy ball mill. Fe-10 vol% Cu matrix nanocomposites were subsequently fabricated and reinforced with different volume percentages of hybrid NbC and granite nanoparticles. The prepared composite material was subjected to a sintering process at 1150° C. for 1 hour in an argon atmosphere. Finally, the physical and tribo-mechanical properties of the sintered nanocomposites were measured. Since these nanocomposites are exposed to high temperatures during fractionation, aim to reduce the coefficient of thermal expansion so that they can be widely used in industrial applications automotive brakes, and transmissions (Issa et al., 2023).

2.3.3. Particle Reinforcement Composites

Metal matrix composites can be divided into three categories: whiskers, monofilaments, and particles, depending on the size and shape of the reinforcement. Particulate fillers are working to increase wear resistance, decrease shrinkage, decrease friction, and improve high temperature performance. In smaller quantities than a fiber, the particle will also transfer the load to the matrix. As a result, a particle reinforcement will become more rigid but rarely stronger Chauhan et al. (2020).

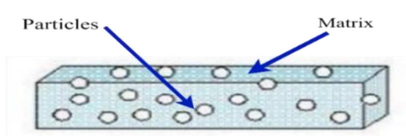

Figure 2.4 Particle Reinforced Composites

The qualities of the material generated are influenced by the size and shape of the stiffeners, necessitating various manufacturing techniques. For instance, stir casting can be used to create whisker MMC, whereas powder metallurgy is frequently used to create particles. Mechanical compatibility (low but matrix-matched coefficient of thermal expansion), chemical compatibility, thermal stability, high modulus, high compression, superior processability, and economics are the main characteristics of particulate materials (Ajith James Cyriac, 2005); (Karl Ulrich, 2006).

2.4. Nitinol Particle Reinforcement

Nickel Titanium, also called Nitinol, is a metal alloy made of nickel and titanium, with almost equal amounts of each element's atomic weight. In recent years, many NiTi-based actuation devices are under development for aerospace and automotive applications (Jiang, 2012). Metal matrix composites with smart material strengthening have greater yield strength and composite strength because of the application of compressive stress at the crack tip and the production of compressive residual stress (Furuya, 1996).

Strength and elongation of the yield are enhanced by the increased NiTi concentration. As NiTi content rises, these advantages become less significant. At high temperatures, NiTi fiber reinforced aluminum metal matrix composites have increased yield strength (Song & Sun, 2000); (Xie et al., 2007). NiTi is used in aero-space industries due to its distinctive properties of pseudo-elasticity, bio-compatibility, corrosion resistance and shape memory effect (Sharma et al. 2015). (López et al., 2009); (Barrado et al., 2009) a highly damped high-strength NiTi-Mg composite was also developed and characterized (Lee et al., 2010).

On a larger scale, bonded NiTi tubes to a soft Fe core to create a composite coaxial wire exhibiting high strain recovery and damping potential (Hao et al., 2012). High strength, low modulus, and large elastic strain in addition to having a very high strength (1.65 GPa), Nb nanowire-reinforced NiTi composites also have a high elastic strain (>6%) and a low Young's modulus (26 GPa). nanocomposites of deformed metal Hao et al. (2013). Composites made with TiNi contents of 20% and 30% meet high strength and modulus requirements at service conditions of 150-200 °C and stress levels of 50-70 MPa (Aydogmus, 2015).

2.5. Manufacturing Technology for Metal Matrix Composites

Different methods are used to create MMCs. The final qualities of MMC are significantly influenced by the production process. MMC employs tried-and-true metal manufacturing techniques with the necessary changes. The desired MMC qualities, cost, alloy matrix, distribution of reinforcing components (particles or fibers), and product application all play a role in selecting the best procedure. The methods typically employed to synthesize MMC can be broadly divided into solid-state and liquid-process methods (Singh et al. 2022). Following is a classification of the numerous fabrication procedures used to create MMC:

2.5.1. Liquid State Processing

A manufacturing procedure where molten metal is combined with a dispersed phase and solidifies. Stirring casting, squeezing casting, composite casting, and injection molding are the categories.

2.5.1.1. Stir Casting

Stir casting is a procedure for creating liquid-state composites that combines molten metal with reinforcement through mechanical stirring. Due of its low melting point, the aluminum-based MMC finds extensive use in stir casting procedures. However, the stir casting method is unable to regulate the homogeneous distribution of the ceramic reinforcing particles in the metal matrix due to their low density and wettability. Capable of press pressure of 650MPa, preheat temperature of 225°C and melting temperature of 700°C for better mechanical response and metallographic structure (Karthik et al., 2019). Stir casting is not recommended for materials with particularly substantial density variances between the base metal and the reinforcement due to these issues. In order to dissolve, oxidize, and poison the environment, ferrous metals require more energy. Stir casting is often not a good fit for the creation of FMMC (Bharat & Bose, 2021); (Singh et al., 2022).

2.5.2. Solid State Processing

Solid-state fabrication of MMCs is a process that results from the binding of MMCs by interdiffusion between the matrix metal and the dispersed phase in the solid state under high temperature and pressure. Improved wear resistance and adoption of surface treatment technology Ren et al. (2019), improvement metallurgical bond and improvement bond quality (Chauty et al., 2020), In ultrasonically assisted casting, particle reinforcement can be applied to this technique, ensuring a nearly uniform and fine particle distribution. It can be classified as powder metallurgy based on the recrystallized grain structure (Vijayavel et al., 2020), The material's mechanical characteristics, fatigue life and strength, reduction of grain size, and improvement of hardness and wear were all enhanced by friction stir treatment.

2.6. Powder Metallurgy

PM is a net-shape/near-net-shape molding process that can produce large volumes of complex geometries with a wide range of properties that are used to synthesize denser, more precise, and more robust MMC components (Meignanamoorthy and Ravichandran, 2018). Powder metallurgy is a technology that mixes fine powders such as metals and ceramics, forms them into the desired shape, and heats and bonds (sinters) the compressed materials in a controlled atmosphere. This is one of the best ways to compact powder composites in a mold to achieve desirable properties such as reduced porosity and a more uniform distribution of reinforcement, as well as adequate compaction of the ground powder (Kumar, Bharti, and Dixit, 2021).

Powder metallurgy uses powders of metals or alloys as raw materials to produce highly accurate finished parts at competitive costs, saving energy and time. Sintering in air maintains a temperature below the melting point throughout the process (Khazaal et al., 2022).

It consists of the following steps:

2.6.1. Powder Preparation and Mixing:

Proper mixing of powder is very important for product consistency. Binders and/or lubricants are added to the mixture before mixing the powders. The function of lubricants is to minimize wear and reduce friction. Wet or ball mill thoroughly mixes various powders in appropriate proportions. Mixing technology and prepared powder quality are well controlled (Sankhla et al., (2022); (Panda, (2016).

2.6.2. Compaction

It can be defined as "the process of filling a mold with powder, compressing the powder with a hard punch to shape it, and removing it from the mold". The mixed powder composite is then compacted in a rigid mold under pressure (150-900 MPa) (Sinka, 2007).   Figure 2.6 general die compaction process diagram. The higher the pressing pressure, the higher the compact density, are among the processes in the compacting process.

A lubricant, such as graphite, molybdenum sulphide ought to be used between the die wall and the powder to allow for die compression. This is because the friction between the powder and die wall during die compression results in an uneven density distribution, which leaves the green body with residual stresses. When the PM pieces are subsequently subjected to high temperature consolidation, this could result in undesirable flaws like pores and cracks, (Honnaiah et al., 2023).

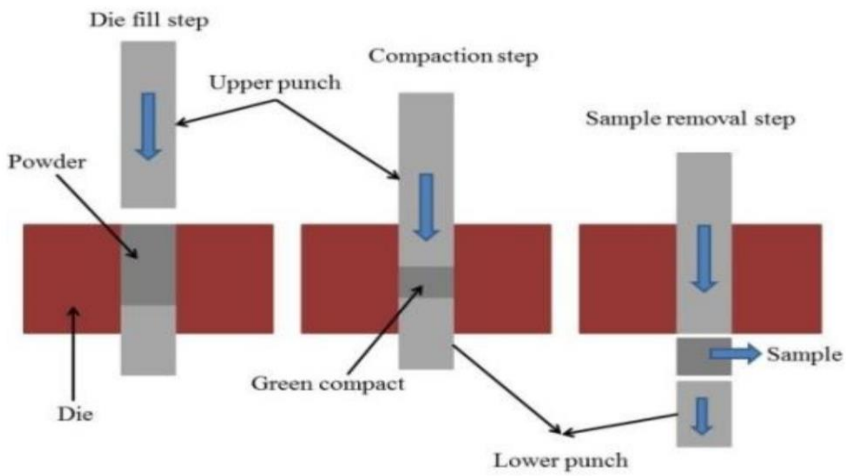

Figure 2.5 Compaction Process (Panda, 2016).

For the requisite compaction qualities, additional lubricant elements such as MoS2, Mg, and paraffin waxes are required. These lubricants are utilized to make the powder compact during the fabrication process by reducing friction between die and powder.

2.6.3. Sintering

Heat treating a powder composite or compact below its melting point to increase strength by bonding particles. During sintering, the green compact is usually heated in a protection atmosphere such as argon, hydrogen or nitrogen. The individual powder's particles (which were either loose or physically bonded together) are bonded to produce a solid structural part with the desired properties (Fisika et al., 2008). The sintering temperature done below the melting point of the matrix material and usually it carried out at 60 to 75% of the melting point of the components (Wang et al., 2021). By regulating the different conditions, sintering can occur without any shrinkage; no net dimensional change is quite probable (Manohar et al., 2020), resulting in strongly bound structures.

Physical and mechanical qualities of the materials can be improved by using the sintering process after compacting the powder under regulated conditions (Adnan Khan et al., 2020). As the sintering temperature rises, so do the rate and size of every change that takes place during the process (Panda, 2016). Sintered self-lubricating bearings, sintered magnets, and other PM materials, as well as sintered automotive structural components and gears (Meignanamoorthy and Ravichandran, 2018); (Yong et al., 2021); (Khazaal et al., 2022).

2.7. Effects of Powder Metallurgy Process Parameters on Composites

2.7.1. Milling Time

Milling time refers to the duration of time a milling process takes to complete. The milling time can vary depending on several factors such as the complexity of the design, the type and hardness of the material being machined, and the specific milling process being used (Singh et al., 2019). The amount of powder decreases with crystalline size as lattice strain rises over the course of milling (Parveen et al., 2021).

Increases in milling time led to an increase in the compressible strength and ductility of porous steel sintered at 1200 °C (Xie et al., 2023). To accomplish the homogenous dispersion of the reinforcement into the metal matrix, the ball milling procedure is important. Depending on the ingredients to be mixed and the intended outcomes, blending time might range from a few minutes to several days (Skotnicova et al., 2015).

2.7.2. Compaction Pressure

Compaction pressure refers to the force applied on the composite powder to form it into a desired shape before sintering. The most crucial step in powder metallurgy is powder compaction. This means that practically all desirable material qualities, including shape, size, density, porosity, hardness, and other mechanical properties, may be adjusted during this process Manohar et al. (2020). It relates to the composite's mechanical characteristics, density, compressive strength, microstructure, and strong bonds between the reinforcement and matrix (Manohar et al., 2020); (Kumar et al., 2021). The primary purposes of this cold compaction are as follows: (Ankur & Singh., 2021).

- ✓ To produce the appropriate shape,
- ✓ To manage the dimensions,
- ✓ To manage porosity and
- ✓ To add enough strength to allow for handling.

2.7.3. Sintering Temperature and Time

The compacted powder is heated during the powder metallurgy (PM) sintering process to fuse the individual particles together, creating a harder, stronger product with increased strength. The sintering temperature is lower than the melting point of the powder metallurgy material's primary constituent. In one hour, the sintering temperature rises from 1000 to more over 1300 °C. When several iron-based PM composites were sintered at high temperatures, their mechanical and physical properties were enhanced, and the apparent porosity of the sintered samples was reduced Fisika et al. (2008); (Delavari et al., 2011); (Jabur, 2013). The wet-milled composite powder sintered at 1300 °C for two hours results in a maximum hardness of 450 VHN and a compressive strength of 525 MPa (Meher et al., 2021).

2.8. Application of Iron Metal Matrix Composites (IMMC's)

Many different automotive, manufacturing, construction, and aerospace industries can make use of metal matrix composites (Jha et al., 2022). Cylinder head, main crankshaft bearing, engine block, and cylinder block are examples of outside parts. Aluminum matrix, which has a low melting point and poor strength, is not as well suited for high-temperature wear-resistant materials as ferromagnetic matrix composites (Bahari et al., 2012). Iron-based metal matrices are employed in a variety of applications in the automotive, military equipment, industrial, and building materials sectors based on these characteristics (Zakaria, 2014). Building materials such as nuts, bolts, rivets, fasteners, gears and wind turbines (Issa et al., 2023). It's crucial to increase wear and corrosion resistance. When selecting different gear materials, consideration should be given to strength, brittleness, and corrosion resistance.

2.9. Gear Material

Gears are crucial mechanical components that transmit power between the prime mover and the driving portions. In order to overcome gear difficulties, the choice and development of materials for gears is crucial, and this has led to a research interest in this area (Sankar and Nataraj, 2011); (Milani et al. (2005). The severe stresses that transmission gears frequently endure might concentrate stress on the active flanks and root fillets of the gears. To have enough strength and hardness to endure fatigue, the material must then be properly developed in terms of its chemical composition, mechanical qualities, and heat treatment techniques. Therefore, an emphasis on materials design and development should be appropriate for the intended function (Höhn et al., 2012).

Hardness sufficient to withstand root cracks and surface damage is one of the criteria when selecting materials for gears. It must also have the strength to sustain the impact emphasizes applied to the gear pair. In other words, gear materials need a robust core to prevent brittle fracture under high impact loads and a hard outer layer to offer appropriate fatigue and wear resistance. As a result, consideration needs to be given to design of materials and material development to reduce potential stress concentrations with the goal to meet gear choice of materials criteria (Wu and Hwang, 2010).

2.10. Fe-NiTi-Cr Metal Matrix Composites

Numerous research from the past few years have shown the usage of brand-new smart metal particles as the reinforcing phase in metal matrix composites made of titanium, aluminum, copper, iron, and nickel. The world of design has given the hybrid metal matrix, one of the reinforcing elements for MMCs, exceptional consideration in the coming year. Nitinol and Cr are two of these typical smart metal reinforcements that are used to strengthen press matrix because of their excellent wear resistance, excellent corrosion resistance, and hardness (Chauhan et al., 2017); (Duriagina et al., 2020). A primary candidate for strengthening IMMC's composites with applications that call for hardness, a high melting point, high damping capacity, wear resistance, corrosion resistance, and weakness resistance is nitinol and Cr.

2.11. Literature Summary

The following observations can be organized using the literature review as a guide. Researchers in the past have developed and studied a variety of composite materials. The main advantage of MMC materials is their improved mechanical properties, especially in the areas of strength, hardness, stiffness, and wear resistance. Metal matrix composites based on iron have lately been developed and effectively used in a wide range of industries, including the automotive, aviation, sporting goods, and rail transportation. Additionally, it will increase the number of mechanical engineering disciplines where these composites can be used, particularly in the structural and automotive industries where it is crucial to obtain better wear performance and higher mechanical characteristics inside intelligent reinforcements. The literature review made it abundantly evident that choosing the right reinforcement, as well as its number, size, and appropriate process parameters, was essential for attaining the intended results. varied types of reinforcement, varied reinforcement particle sizes, different production procedures, and diverse testing settings have all been used in various research projects.

2.12. Research Gap

Regarding several studies on iron metal matrix composites, some promising particles have also been included to increase the mechanical, and metallurgical behaviors of iron. There has been a lot of research on iron-based metal matrix composites, but relatively little has been done on NiTi alloy, a smart material. Therefore, the goal of the thesis paper is to offer the scientific contribution of NiTi, which can be used in a variety of applications, within addition of chromium to the iron matrix, due to its promising properties. The features of a metal matrix composite based on ferrous iron that is reinforced with smart materials (nitinol and chromium) and the presence of MoS2 for improved friction between the matrix and reinforcement for mechanical and metallurgical behaviors have not yet been studied in detail. The effects of various weight percentages of reinforcing elements, including chromium and nitinol, on the microstructure, physical and mechanical, corrosion, and compressive behavior of the Fe matrix were examined in this study.

.

CHAPTER THREE

MATERIALS AND METHODS

This chapter covered the materials used to create iron-based metal matrix composites, sample preparation techniques, experimental procedures, and testing setups, as well as the tools and instruments used and data analysis techniques. Pure Iron powder as matrix and reinforcement Nitinol, Chromium (Cr) and small amount of molybdenum (MoS2) was used for dry lubricants. They were selected based on cost, properties, and availability.

3.1. Materials

3.1.1. Iron Based Metal Matrix

Recently, iron-based metal matrix composites have been created and successfully used in a variety of industries, including: Electronics, manufacturing, tools and machinery, automobiles, structural elements of buildings, bridges, industrial applications, and other aircraft (Huang et al., 2014); (Klarzak et al., 2018); (Singh et al., 2022). It has a low tensile strength and a high weight-to-strength ratio, is easily damaged, and is susceptible to corrosion and rust (Dhanesh, Kumar, Fayiz, et al., 2021). Therefore, unless corrosion-resistant, wear-resistant, and fatigue-resistant materials like ceramics, chromium, and aluminum are added, its application is constrained. Chemical composition of Iron (Fe) metal powder, element Pb (0.02), As (0.0005), Cu (0.05), Mn (0.05), S (0.05), Ni (0.02), Zn (0.01) and Fe balance in weight percentages.

Iron powder was chosen since it is more workable, stronger, and suitable for a number of uses in the construction and automotive industries in order to function better in metal matrices by creating heat. The pure iron powder was purchased from Parshwamani metal manufacturer, India with an average particle size of (50-150μm), density 7.874 g/cm3 at 25 ºC, and 99.99% purity) used as matrix.

3.1.2. Nitinol Pre-alloyed Reinforcement Particles

NiTi is a smart metal alloy powder composed of approximately equal atomic percentages of nickel and titanium. Nitinol metal alloy is one of the most useful alloys used for various purposes. Properties such as high tensile strength, high fatigue strength, fracture toughness, corrosion resistance, and improved damping properties of metals are achieved in metal alloys through nitinol reinforcement and increased tensile strength.

Aluminum, magnesium, steel, and even ceramic composites are frequently manufactured using nitinol as a reinforcing material (Chauhan et al., 2020); (Balokhonov et al., 2022) Surface roughness and hardness of NiTi composites increase from 0% to 12% as NiTi reinforcement content increases. Incremental addition of dense (1% or less) and exceptionally porous NiTi (Parande et al., 2018); (Mishra, 2023). Nitinol powder was selected as the first reinforcement due to the above excellent properties.

3.1.3. Chromium

Chromium is a white, hard, excellent, and brittle metal that has a high level of corrosion resistance. Chromium is utilized as a wear-resistant coating on some automotive parts to increase their lifespan. In many industrial applications, its hardness, corrosion resistance, high temperature, and tensile strength make it one of the most crucial components. This increases the hardness of the newly formed composite (Bairwa et al., 2021). Chromium is added to the iron matrix in varying amounts (5%, 7.5%, and 10% Cr), with the remaining material being Fe powder. Testing for corrosion on these samples revealed that adding Cr to the Fe matrix did, in fact, greatly reduce corrosion (Konishi et al., 2005).

Microstructural analyses reveal that the chromium reinforcement is spread equally throughout the iron matrix and that there are no internal defects (Varadaraj et al., 2023). When the metal matrix in a martensitic matrix has enough chromium, corrosion and wear resistance is achieved (Hill et al., 2011). Chromium powder was chosen as the secondary reinforcement due to excellent hardness, wear resistance and corrosion resistance properties.

Figure 3.1 Material Used in The Research Work

Table 3.1 Properties of Iron, Nitinol Powder and Chromium (Purity>99.98%) (Deepan Bharathi Kannan et al., 2016); (N. Sharma et al., 2015); (Chauhan et al., 2020).

Properties	Pure Iron	Nitinol powder	Chromium powder
Particle size	50-150 µm	50 µm	50 µm
Density	7.874 g/ cm^3	6.45 g/ cm^3	7.1 g/cm^3
Melting point	1538 °C	1310 °C.	2150°C
Hardness	50-150 HV	400-600 HV	600-800 HV
Poisons ratio	0.291	0.3	0.2
Ultimate tensile strength	350 MPa	754 - 960 MPa	760 MPa
Compressive strength	300 MPa	900- 1400 MPa	430 MPa
Fracture toughness	10-50 MPa	30-80 MPa	150 MPa
Appearance	Black	Grey	Bright grey
Elongation	1-5%	15.5%	2-10 %
Elastic Modulus	200 GPa	70-90 GPa	248 GPa
Thermal conductivity	80 W/ (m. K)	20-25 W/ (m. K)	90 W/ (m. K)

3.1.4. Molybdenum Disulfide (MoS2)

It is a silver-black solid that occurs as the mineral molybdenite, the primary ore of molybdenum. Due to its low coefficient of friction, it is often used as a dry or solid lubricant. Iron-based composites' capacity to sinter and process of densification are improved by molybdenum disulfide during the sintering process (Olani et al., 2023). MoS2 was chosen as the reinforcement due to its friction control during mixing and compression, free movement at high temperatures.

Table 3.2 Properties of MosS2 Powder (Gonfa et al., 2022)

Properties	Value
Density	5.06 g/cm^3
Particle size	1.5µm
Melting point	1185 *°C*
Purity	99.99%

3.2. METHODS

3.2.1. Experimental Procedures

In this work, iron matrix composite samples reinforced with nitinol and chromium were created using a powder metallurgical procedure. The following figure depicts the mixing, compacting, sintering, manufacturing, and testing steps. Figure 3.2 depicts a general flow map of current research activities.

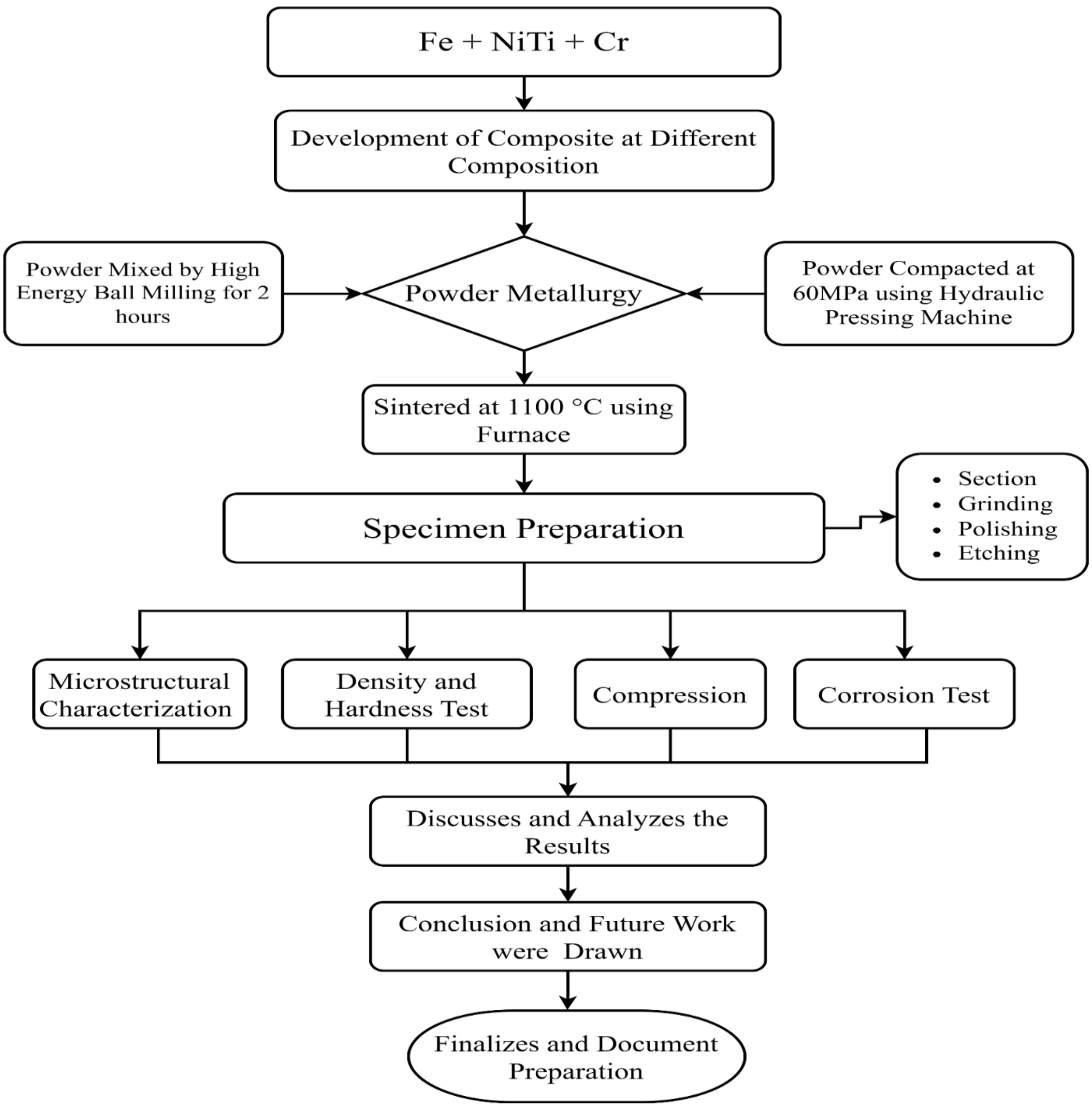

Figure 3.2 General Flow Chart for Experimental Procedure

3.2.2. Design the Experiment for IMMC Fabrication

Depend on the literature reviews, the new samples of Fe-based MMC were fabricated by selecting four samples, then from those samples, then the synthesized samples were selected for characterization and testing. The composites were manufactured in advance based on the basic input process parameters (milling time, compaction pressure, sintering temperature, sintering time, weight fraction of reinforcement) at the same mixing time (2 hours) and 60MPa, fabricated by powder metallurgy. Each sample, sintered for 2 hours and temperature of 1100°C.

Table 3.3 Reinforced IMMC Made by Powder Metallurgy

Sample's	Materials (in Weight %)			
	Fe	NITINOL	Cr	MoS2
S1	81%	5%	10%	4%
S2		7.5%	7.5%	
S3		10%	5%	
S4	100%	-	-	-

3.2.3. Specification of Weight Percentage Composition in Composite's

The mechanical, corrosion and wear properties of the developed composites strongly depend on the weight percentage (wt%) of the reinforcement. Therefore, the weight percent composition of nitinol and chromium used in this research work was assumed based on a literature review, and the researchers' successive work was used to determine the weight percent composition of the reinforcement for each sample to be considered.

Kalepu and Nallu, (2021) experimental investigation and optimization of mechanical properties of nitinol reinforced composites. Powdered nickel-titanium (Ni-Ti) was added as a reinforcing material in different proportions of up to 10% by weight. MMC with 4 and 6 wt% reinforcement gave better results than those with 2 and 8 wt% reinforcement, respectively. The impact strength of composites with 8 wt% additive showed better durability compared to 2, 4, and 6 wt% reinforced MMC. Addition of 8 wt% Ni-Ti powder to the metal matrix was found to resist fracture due to the applied load. As the additive weight percentage increases, the porosity increases and the strength, performance, and quality of the composite decrease (Baradaraj et al., 2023); (Günen et al., 2023) Chromium additions (3 wt%, 4 wt%, 5%, 6 wt%, 8%, 10 wt%, and 12 wt%) in the metallic matrix showed good microhardness in alloys, fracture toughness, and good wear resistance. So even if the wt% composition of reinforcement addition is possible till 30%, as studied by (Ramanathan et al., 2019). Therefore, by comparing the several paper, we decided the maximum reinforcements in this research study were 19 wt% (10% NiTi, 5% Cr, and 4% MoS_2).

3.2.4. Mass and Volume Estimation of Matrix and Reinforcements in Composites

The total mass of matrix and reinforcement required to fabricate Fe-NiTi-Cr composite specimens was determined based on the dimensions of the prefabricated dies and punches for testing hardness, microstructure, compression, corrosion and wear. It is determined from the total amount of specimens required. The dimensions of ready-made dies and punches are as follows: The inner diameter and height of the mold are 10mm and 15mm, respectively, and the punch diameter is 10mm, with a small clearance for inserting into the mold during powder compaction by the hydraulic press. Based on the dimensions above, the iron matrix and Fe-NiTi-Cr composites were fabricated with the height/length (L) and diameter (D) shown in below. The dimensions of the samples made are limited to the production of short length cylindrical samples due to the capabilities of the hydraulic press. Parameters of die and punch Dimension (mm) of pre-designed die:

- ✓ Outer diameter of die 50mm
- ✓ Inner diameter of die 20mm
- ✓ Length of the die 50mm
- ✓ Diameter of the punch 20-clearance
- ✓ Length of the punch 50mm

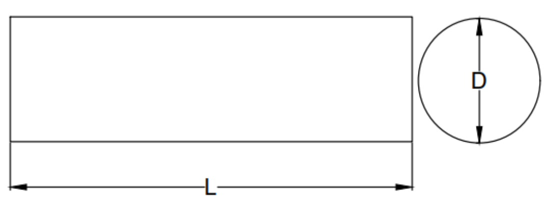

Figure 3.3 Dimension of Predesigned Die

Pre-made dies and punches were used to create the required number of samples. Based on the following types of tests performed as per standard;

- The hardness and microstructure specimens are 15mm long with a diameter of 12 mm.

- The compression test specimen has a length of 15 mm and a diameter of 12 mm.
- The corrosion specimen has length 12mm and 7mm diameter.
- The wear specimen has a length of 12 mm and a diameter of 6mm.
- Removal of material by hand saw, file, Grinding allowance 10mm consideration.
- Then, the total length and diameter of the composite are the summation of all tests.

L= hardness and microstructure (15mm) + compression (15mm) + corrosion (12mm) + Wear (12mm) + allowance (10mm) = 64mm.

D = 12mm

The required volume of material for a cylindrical sample is calculated using Eq (3.1);

$$V = \frac{\pi}{4} D^2 \times L \tag{3.1}$$

Where V= volume of sample in mm^3, L=length of sample in mm, and D=diameter sample in mm VT= the total volume of material required for each sample in mm^3

$$V = \frac{\pi}{4} (12mm)^2 \times 64mm = 7238.229\ mm^3 = 7.24\ cm^3$$

For four samples , $V_T = 7.24\ cm^3 * 4 = 28.96\ cm^3$The total volume of material required for sample fabrication includes both matrix and reinforcement materials and for four (4) sample fabrications V_T = $28.96\ cm^3$.

Table 3.4 Mass and Volume Fraction of Matrix and Reinforcements in Composite

Sample	Fe		Nitinol		Cr		MoS2	
	V (cm^3)	Mass	V (cm^3)	Mass	V (cm^3)	Mass	V (cm^3)	Mass
Sample 1	5.864	46.01g	0.362	4.67g	0.724	2.57g	0.29	1.5g
Sample 2	5.864	46.01g	0.543	3.5g	0.543	3.86g	0.29	1.5g
Sample 3	5.864	46.01g	0.724	2.33g	0.362	5.14g	0.29	1.5g
Sample 4	7.24	56.8g	-	-	-	-	-	-
Total volume required	24.832 cm^3		1.629 cm^3		1.629 cm^3		0.87 cm^3	

Density of Iron (Fe) = 7.847 g/ cm^3, Density of Nitinol (NiTi) = 6.45 g/ cm^3 Density of chromium (Cr) = 7.1 g/ cm^3, Density of Molybdenum disulfide (MoS2) = 5.06 g/ cm^3

The weights of matrix material (Fe) and reinforcement materials (NiTi, Cr, MoS2) for each sample of given composition are estimated as follows: The mass of a material is the product of the volume of the material and the density of the material (m=V*ρ). Therefore,

Total weight of (Fe) = Total volume of (Fe) * density of (Fe) = 24.832 cm^3 *7.847 g/ cm^3 =195g

Total mass of Nitinol = Total volume of (nitinol) * density of (nitinol)

= 1.629 cm^3 $*$6.45 g/ cm^3= 11g

Total mass of (MoS2) = Total volume of (MoS2) * density of (MoS2)

= 0.87 cm^3*5.06 g/ cm^3= 4.5g

Total weight (mass) required for the work is 211g.

3.2.5. Powder Metallurgy Fabrication Techniques

Powder metallurgy is one the most economical process for fabricating the near net particulate reinforced MMCs and thereby allowing greater flexibility, a significant reduction in manufacturing costs due to minimizing machining process and minimized scrap losses. Powder metallurgy is the most economical technique for producing MMC and can prevent agglomeration and segregation of reinforcing particles (Che et al., 2019). In powder metallurgy, the homogeneity of the mixture is better controlled, the components are produced with good dimensional stability and good ductility, and the homogeneity of the mixture is improved, (Krone et al., 2004); (Raturi et al., 2019); (Bharat and Bose, 2021); (A. Singh et al., 2021).

In this research work, the main objective of the selection of powder metallurgy was to produce hybrid metal matrix composites with the best mechanical properties to manufacture tool material with high wear resistance and corrosion resistance. The experimental procedure is adopted to fabricate the entire specimens of matrix and reinforcements using Powder metallurgy (PM) process. The steps of powder metallurgy technique are shown as follows (Khazaal et al., 2022). The manufacturing with powder metallurgy process can be divided into three basic sequence steps:

3.2.5.1. Powder Mixing

Mixing refers to blending different types of powders uniformly, and it is very important to distribute them evenly within the matrix in order to achieve the desired performance of the selected powders in composite manufacturing. High energy ball milling machines have been used for this purpose. Metal alloy powders are ball milled in a high velocity chamber using zirconia balls. High-energy ball mills are also used to produce fine particles from alloy powders, ensuring the physical and structural integrity of the final part.

Measured weight percents of nitinol and chromium were added to the iron matrix powder and mixed. Four weight percent (4%) MoS2 was added to the composite powder mixture to prevent buckling, prevent matrix powder from flowing out of the mold, and minimize friction between mold and powder, Sharma et al. (2019). After mixing was completed, the mixture was stored in an evacuated tube to prevent oxidation from risk to air.

Figure 3.4 Photos of High Energy Planetary Ball Milling

In this study, 5% and 10% pre-alloyed nitinol powder and chromium 10% and 5% were mixed in sample one and three vice versa, and both reinforcements were mixed at equal weight percentages (7.5%) in sample two within an equal proportion of iron matrix (81%) and mixed using a high-energy ball mill. A high energy planetary ball mill was used to mix the powder by using zirconia balls, (Jha et al., 2022). The milling conditions adopted in the present research work are: Milling Parameters:

- ✓ Milling speed: 200 rpm
- ✓ Milling time: 2hours
- ✓ Ball diameter: 10 mm
- ✓ Ball-to-powder weight ratio: 10:1
- ✓ Temperature of milling (at room temperature).

3.2.5.2. Powder Compaction

Powder compaction is the process of compressing the Fe-NiTi-Cr-MoS2 mixed powder in a mold using a hydraulic mounting press. The mixed powder was accurately weighed using a weighting balance. The powder mixture was pressed into a cylindrical shape (d=12mm, h=15mm) using a carbon steel die using a hydraulic press with a load of 120 kN. Cold pressing was performed at a pressure of 60 MPa (Olani et al., 2023) and a holding time of 10 minutes produce raw compacted samples of heights 15mm and diameter of 12 mm. Typically, the tool is held vertically and the punch tool forms the bottom of the cavity. The compressed samples are then ejected from the mold cavity. The density of compacted powders is directly proportional to the pressure applied.

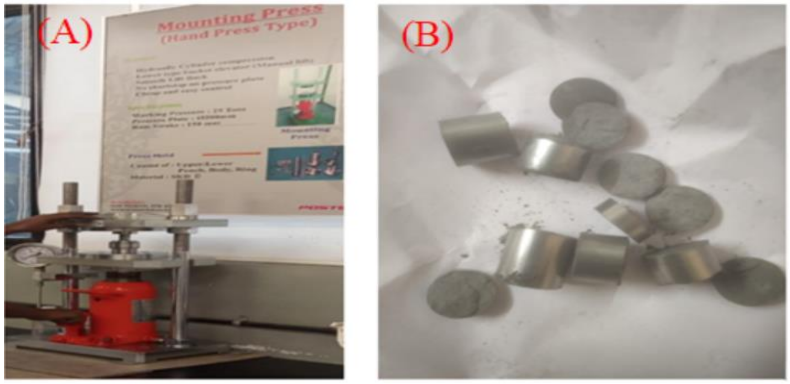

Figure 3.5 Photos of (A) Mounting Press set up and (B) Compacted Specimen (Green Part)

3.2.5.3. Sintering

The green compressed does not have sufficient strength and the particles are loosely bound together and may crash even at low loads. It may also contain interparticle voids. Sintering is performed after compaction to eliminate porosity and create metallic bonds between powder particles. Solid phase sintering is the process of heating the green compact to a temperature 70-90% below the melting point of the base matrix for a specific sintering time to achieve chemical bonding between the porous combined particles (Das et al., 2022). After deformation, particle formation and growth, and cooling, the powders combine to form solid pieces. During sintering, bonding occurs between agglomerated powder particles (Sharma et al., 2019); (Issa et al., 2023).

Sintering should be performed in a controlled atmosphere to prevent oxidation of the compact surface (Karabulut et al., 2022). In this study, Samples were dried at (150) °C for (30) min in the oven and green compacted samples of Fe-NiTi-Cr-MoS2 (S1, S2, S3 and S4) were subjected to a sintering process. The densified samples were heated in a High Temperature Box Furnace by using MoS2 heater (at ASTU, material lab.) a heating rate of 10 °C/min to a sintered temperature of 1100 °C for 120 min (with argon gas introduced for atmospheric control at flow rate of 10 liters/min with a hold time of 20 min (Shamsuddin et al., 2008); (Shamsuddin et al., 2014); (Duriagina et al., 2020).

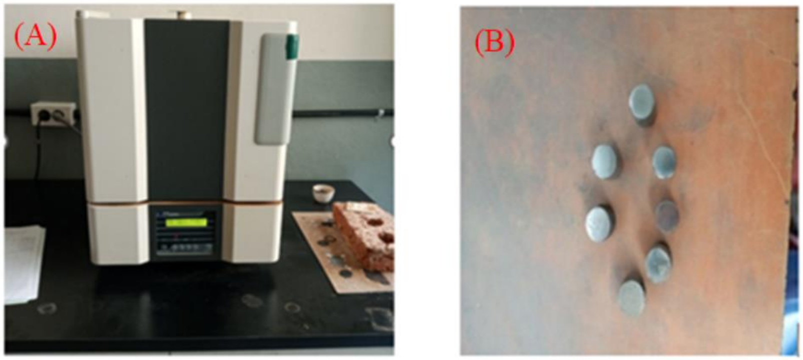

Figure 3.6 (A), The Furnace Set Up and (B) The Sintered Samples

3.2.6. Specimen Preparation for Microstructural Characterization

After the manufacturing of composite materials by powder metallurgy, composite green sintered samples were prepared for microstructural characterization, mechanical, physical, and corrosion testing. Samples were prepared by grinding, polishing, etching, hand sawing, and file to remove excess material and minimize dimensions to obtain the required sample geometry and dimensions for various tests according to ASTM standards.

The main steps for sample preparation (optical microscopy, scanning electron microscopy, X-ray diffraction) are: Cutting (sectioning), grinding (rough and fine grinding), polishing, etching, and then microscopic inspection.

3.2.6.1. Sectioning

A cross-section of the sample to be tested was created by cutting the prepared sample. Use a hand saw and file to reduce the size of the sample to be placed on the stage of the light microscope, as shown in the figure 3.7 (A).

3.2.6.2. Grinding and Polishing

The sintered Fe-NiTi-Cr-MoS2 composite samples were progressively finely ground using emery paper and ground with a grinder for hardness testing and microstructural analysis. The purpose of grinding and polishing is to obtain a flat, mirror-like surface without excessive distortion. This he achieves in three steps. Rough sharpening, fine sharpening, and polishing. Polishing is the process of rendering the Fe-NiTi-Cr-MoS2 composite samples scratch-free using sandpapers of progressively increasing grit from 240, 800, 1200, and 2000 as shown in figure 3.7 (C), It was then exposed to grinding using sand papers from coarse to fine grades with orientation of 90 degree from the previous direction of grinding, as shown in Figure 3.7, (B,). Polishing is the process of rubbing the sample with a diamond suspension to create a smooth, shiny surface while gradually reducing the pressure and rotation speed of the sanding disc in the RB 204 Metpol II model polishing process, as shown in the figure below 3.7, (D).

3.2.6.3. Etching

Polished samples of both matrix and composite were etched with the recommended nital solution of 4% nitric acid and alcohol mixed etchant, which was performed by simply immersing the sample in the prepared etchant for 30 seconds, as shown in figure 3.7, (E). The samples are then washed with distilled water before the microstructural characterization.

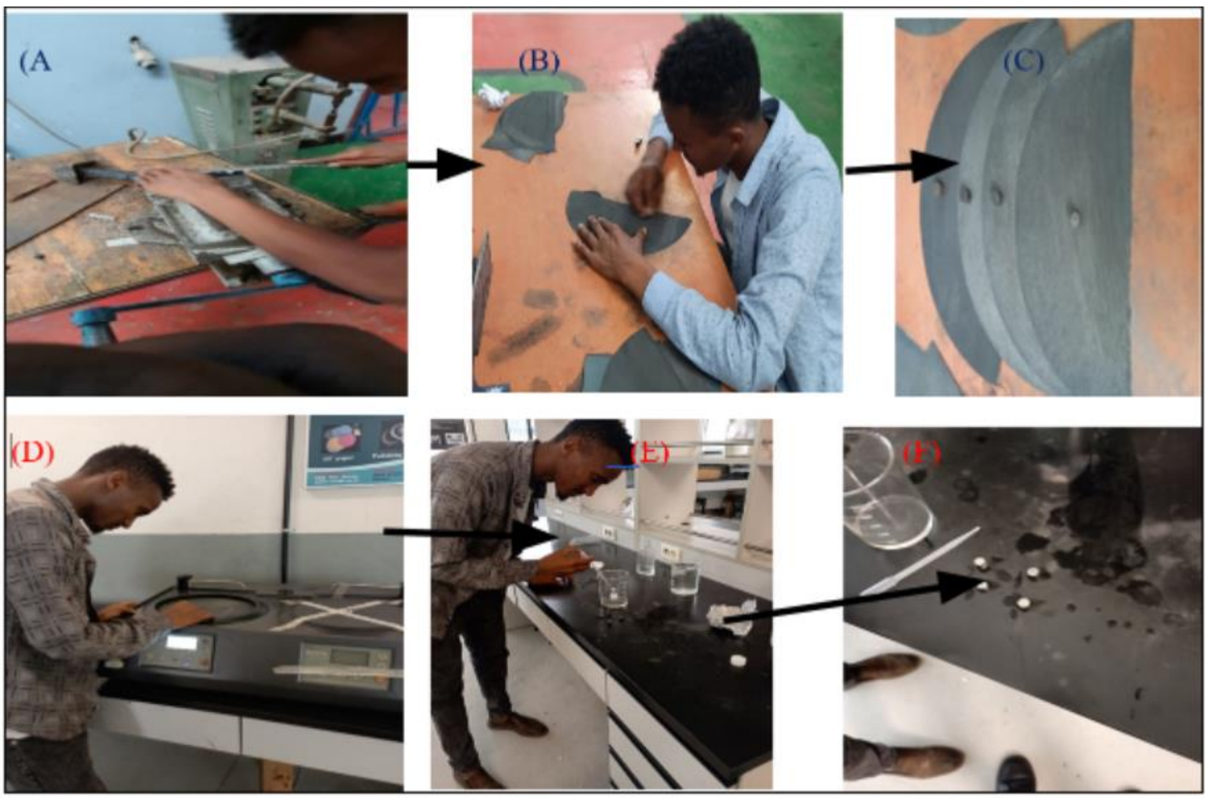

Figure 3.7 Sample Preparation

3.2.7. Microstructural Characterization Test of Sintered Specimen

In order to know the mechanical properties (hardness and compressive strength), and microstructural properties of Fe-NiTi-Cr-MoS2 composites, experimental test procedures measuring density and porosity values were performed. The purpose of microstructural testing is to know the microstructural properties of metals, such as: Grain size, segregation, distribution of different phases, types of constituent phase occurrences, and non-metallic inclusions such as slag and sulfides. As part of this study, X-RD, OM and SEM were performed for the above properties.

3.2.7.1. X-Ray Diffraction (XRD)

(A) Phases analysis in sintered composite

Using an X-ray diffractometer (XRD) with an XRD-7000 X-ray diffractometer Maxima model from Shimadzu Corporation (Japan), crystalline phases and elements of IMMC samples using respective sample preparation methods and sample holder devices. Phase analysis of the sintered samples was performed by X-ray diffraction (XRD, at ASTU) observation with Cu-Kα radiation at 40 kV and 30 (mA) at 2θ value in between (10^o-80^o) in 3°/min scan rate. Phase identification and quantitative phase analysis were performed by using origin pro-2022. The crystalline phase of the matrix and reinforcement's present in the sintered composite was analyzed.

(B) Determination of crystalline size and lattice strain by XRD peak Analysis

X-RD peak profile analysis by Gauss method is employed to calculate the microstructural parameters namely crystalline sizes, mean squared lattice strain, root mean squared strain, and dislocation density (Venkateswarlu et al., 2014) of Fe-NiTi-Cr by using XRD data. A study of X-ray peak broadening revealed that the intensity of X-ray diffraction lines depends on the elemental composition of the sample and its preparation conditions. The observed X-ray diffraction peaks can be correlated to atomic planes and useful for analyzing the atomic fine structure of prepared samples. The relationship between the crystal grain size and the full width at half maximum (FWHM) of diffraction peak was deduced by Scherrer for the first time, known as the Scherrer equation as shown in equation (3.2). By using the Scherrer equation, we can quantitatively calculate the relationship between the FWHM of diffraction peak and the crystal grain size (Venkateswarlu et al., 2014). The Scherrer equation for crystalline size;

$$D = \frac{K\lambda}{\beta\cos\theta} \tag{3.2}$$

Where, D crystallite size

λ XRD radiation of wavelength (μm)

K is Shape factor can be 0.62 - 2.08.

θ is Braggs angle in degree

β is line of broadening at FWHM in radians or measurement of the full width at half maximum of the radian peak located at any 2θ.

Dislocation density is a measure of the number of dislocations within a unit volume of the crystal. It was determined using XRD data with relate to crystalline size (Borbély and Groma, 2001); (Rai et al., 2023).

$$\delta = \frac{1}{D^2} \tag{3.3}$$

Lattice strain is the local deviation of atoms in the crystal structure from their equilibrium positions. This can be caused by various factors such as doping, defects, and external magnetic fields (Augustin and Balu, 2017). Lattice strain can be measured by diffraction techniques that detect changes in the interplanar spacing of crystal lattices. In principle, if the lattice strain is uniform in a particular crystallographic direction, the corresponding d-spacing will change. The presence of non-uniform stress is usually caused by non-uniform stress causing peak broadening. Mathematically calculated using equation (3.4) from XRD data.

$$\varepsilon = \frac{\beta}{4\tan\theta} \tag{3.4}$$

3.2.7.2. Optical Microscope (OM) and Scanning Electron Microscope (SEM)

The structure of a prepared material surface as seen with an optical (optical) microscope Huvitz HR-300 (at ASTU, material lab.). A metallurgical optical microscope was used to examine the sintered Fe-NiTi-Cr samples, as shown in the figure below. The sample matrix and composites mentioned in sample preparation and polishing were etched with the recommended 4% nital etchant, the sample was immersed in the prepared etchant for 10 seconds and rinsed with distilled water and then dried before being run the test as shown figure 3.7. Four photomicrographs of the sample were taken for microstructural characterization. In this study, OM is used to uniformly distribution of composites and determine grain size.

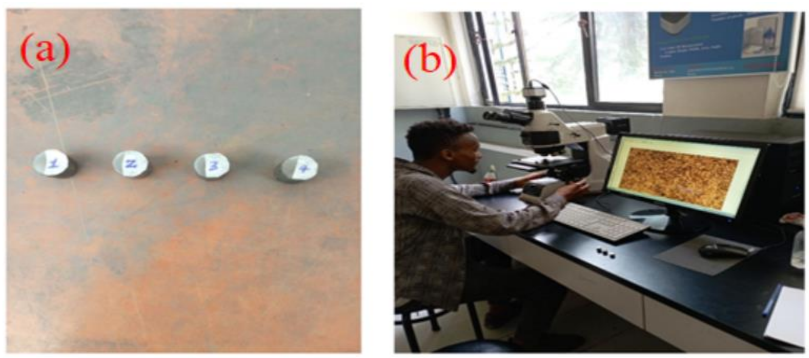

Figure 3.8 (A) Sample Prepared for Test, and (B) OM Test

Morphological analyzes were performed using SEM (at ASTU, Biology lab.). After cutting the sample to shape, the sample was assembled using hacksaw, file and polishing. The sectioned specimens were polished with 800, 1200 and 2000 emery papers of various grit and finally with a rotating wheel using a polishing cloth. SEM was used to analyze morphology and fractography. The chemical bonding between materials and functional group in a synthesis material was studied by FT-IR spectrometer in the range of 4000-400 cm-1 Ft/IR-6600 type A (at AASTU, Industrial chemistry laboratory).

3.2.8. Density of Composite Materials

Density is the mass per unit volume of matter. The density of the sample was, examined after sintering. Procedure for calculating the mass density of composite materials, (Kevin Beck, 2020). Procedure to determine density of samples were: (1) Determine the matrix and reinforcement densities of the composite, (2) Divide by 100 to convert the contribution of matrix and reinforcement to the composite into a decimal number a number between 0 and 1, (3) Multiply each decimal by the corresponding matrix and reinforcements, and (4) generally adding together the products from step 3.

(A) Theoretical densities

Theoretical density is an important parameter for estimating the porosity of a material after sintering. The theoretical densities of the composite samples were determined by determining the space occupied by the composite matrix and reinforcement at their respective densities, based on the mixing rule of (Ahmad et al., 2017); (Praveena et al., 2022).

$$\rho th = (\rho m * Vm) + (\rho r * (1 - Vm))^{n} \tag{3.5}$$

Where ρth, ρm and ρr represents theoretical density of composite, densities of matrix and reinforcements, respectively. Vm represent a fraction of the volume of matrix, 'n' is number reinforcements in composites. Consider that the produced iron metal matrix composite is the mixture of iron, nitinol, chromium, and Molybdenum disulfide (MoS2).

$\rho th = (\rho m * Vm) + \rho r1(1-Vm) + \rho r2(1-Vm) + \rho r3(1-Vm)$

where: ρr1, ρr2, and ρr3, densities reinforcement 1(nitinol), 2 (chromium), and 3 (Molybdenum disulfide) respectively.

$\rho th = (\rho Fe * VFe) + \rho NiTi*(1-VFe) + \rho rCr*(1-VFe) + \rho rMoS2*(1-VFe)$

(B) Experimental (Sintered) Density

The sintered density of composites can be calculated using Archimedes' principle. According to Archimedes' principle, when an object is immersed in water (or any other liquid), the force accomplished by the object is equal to the mass of the displaced water multiplied by gravity (i.e., the weight of the water).

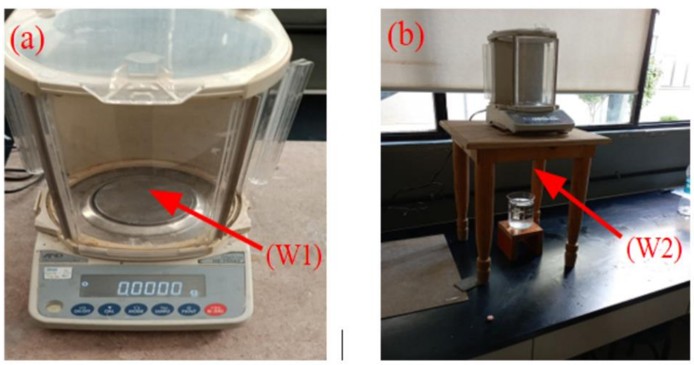

Figure 3.9 Photos of Weighing Balance for Measuring (A) Weight in Air And (B) Suspended Weight in Water

First of all, the sintered specimens were weighed in the air (W1), and then weighted in the distilled water (W2) by suspend in the water.

$$\rho Sint. = \frac{W1}{W1-W2} \times \rho w \quad (3.6)$$

Where ρSint. is sintered density of samples, W1 is weight of samples in the air, W2 is weight of samples in the distilled water and ρw is the distilled water density (1g/cm3) at 25°C Sambit Kumar Mohapatra, (2016).

(C) Relative-Density

The relative densities of the samples were calculated using the formula:

$$\rho r = \frac{\rho \text{Sint.}}{\rho \text{th}} \times 100\% \tag{3.7}$$

where ρr is the relative density (%) and ρth is the theoretically calculated density (g/cm³).

(D) Porosity of composite Materials

Porosity is the total empty spaces present in a material, or the open space between particles or the space enclosed by microstructures particles and is the presence of small openings or interstices within a material. Porous materials can absorb liquids and moisture and cause corrosion. The presence, size and distribution of porosity in composites play an important role in controlling mechanical properties and should be minimized to achieve desirable high performance in use. Porosity in composites occurs primarily through the addition of air bubbles to the slurry during disturbance or as an air unconditional around the reinforcing particles. The porosity is calculated by comparing the theoretical density and actual densities (Kulkarni et al., 2016).

$$\% \text{ Porosity} = 1 - \frac{\rho \text{Sint.}}{\rho \text{th}} \tag{3.8}$$

Where: ρSint. is the sintered density (g/cm³) and ρth is the theoretically calculated density (g/cm³).

Density of Iron (Fe) = 7.847 g/cm^3, Density of Nitinol (NiTi) = 6.45 g/cm^3 Density of chromium (Cr) = 7.1 g/cm^3, Density of Molybdenum disulfide (MoS2) = 5.06 g/cm^3.

3.2.9. Hardness Test

The main purpose of hardness testing is to evaluate the suitability of composites for specific engineering applications (hardness of composites is especially important for wear-resistant applications). A Vickers hardness tester consisting of a square right pyramidal diamond indenter with a base angle of 136° between the opposing faces was used to measure the hardness of the composite. Hardness testing of IMMC samples was performed according to ASTM E384-17 and cylindrical sample preparation was performed according to ASTM E3-95 using Vickers Hardness

Tester HVS-50 at (ASTU, Material lab.). All specimens for hardness and microstructural testing were prepared as 15mm diameter, 12 mm high cylinders and polished with 800, 1200, and 2000 grit sandpaper.

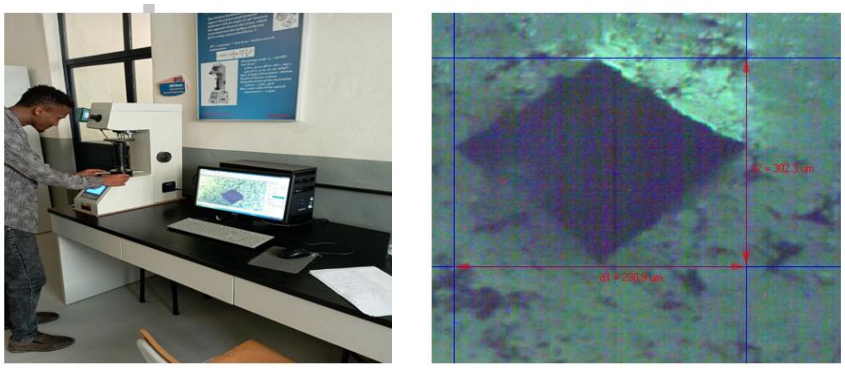

Figure 3.10 Vickers Hardness Test and Measurements

As shown in Figure (3.10), apply a uniform load without impact and push the indenter into the specimen. In this study, a test force of 20 kgf was applied for 7seconds at different positions three trials to obtain an average outcome value (Chauhan et al., 2017). The resulting indentation marks were optically analyzed at 10x magnification and the diagonal length determined to determine the hardness value. The VHT machine then automatically analyzed the HV number were using equation (3.9).

$$HV = \frac{\text{constant} \times \text{test force}}{surface\ area\ of\ identation} = \frac{0.102 \times 2F(\sin\frac{136°}{2})}{(d)^2} \qquad (3.9)$$

Where, HV is Vickers hardness value (kgf/mm2), F is the applied force for indentation (kgf) and d is the average length of the diagonals (d1 & d2) marked by the indenter in millimeters.

3.2.10. Compression Strength Test

Compression testing is used to obtain the compressive strength of a material and determine the elastic and compressive fracture material behavior (fractography) under an applied crushing load. In this study, the specimens were tested under uniaxial compressive loading on a universal testing machine (UTM) with a 50 kN capacity at room temperature (at ASTU, Mechanical lab). The compressive strength of the samples after sintering was measured by a compression testing machine universal testing machine with a strain rate of 10 s^{-1} at room temperature.

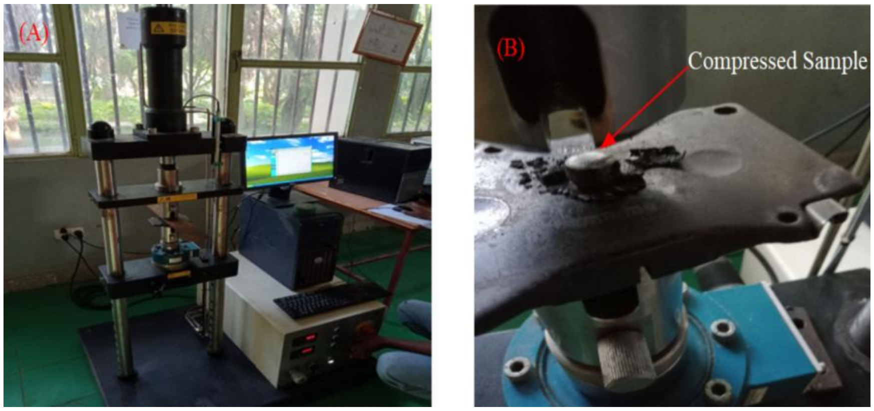

Figure 3.11 (A) UTM (Compression test) set up and (B) the Compressed Sample

The samples of IMMC were made according to ASTM E9-09 standard with a diameter of 10 mm. It has a height of 10mm and a length-to-diameter ratio of about one. Compressive strength was determined by gradually applying a load to an iron metal matrix composite sample calculated using the applied compressive load, force per cross-sectional area of the sample.

$$\mathrm{UCS} = \frac{\mathrm{F}}{\mathrm{A}} \qquad (3.10)$$

Where, UCS stand for Ultimate compressive strength, F is Ultimate compressive load and A is Cross-sectional area of samples.

The effect of the reinforcement composition, compaction pressure and sintering time on the compression test is, done. ASTM E9 testing covers the apparatus, specimens, and procedure for axial-load compression testing of metallic materials at room temperature.

3.2.11. Corrosion Test

Corrosion tests were performed by immersing the specimens in a 3% NaCl bath for one hours. The specimens for the testing were 12mm in diameter and 8mm in length. To eliminate any accidental marks from the surface of the specimen and make it mirror polished, composite specimens were polished with emery polishing paper 800, 1200, and finally with 12 m diamond paste on a double disc polishing machine. An electrochemical analyzer (SP300 EC-LAB, Biologic Science Instruments, ASTU, Material science laboratory) was used to perform the electrochemical measurements in a three-electrode cell.

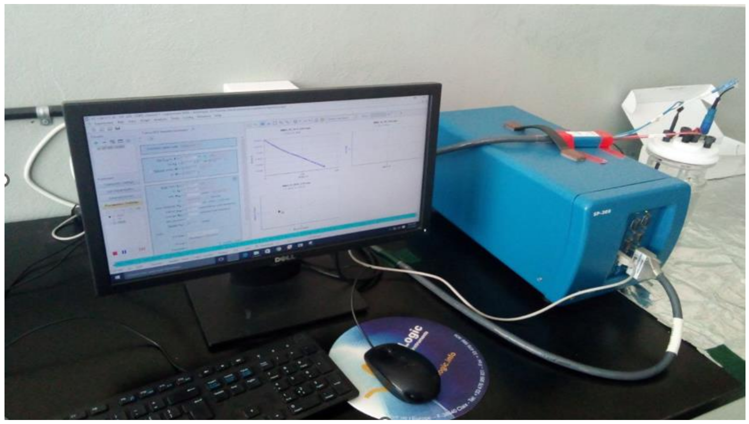

Figure 3.12 Electrochemical Analyzer

Working electrodes were iron-based composite specimens with an exposed area of 1cm2, an auxiliary (counter) electrode was graphite, and a reference electrode was standard calomel electrode (SCE) or mercury. Tafel curves were generated by automatically adjusting the electrode potential from -250 to +250 mV versus corrosion potential (Ecorr) at a scan rate of $1mVs^{-1}$. Experiments were carried out in order to investigate the effect of reinforcement content on the corrosion behavior of manufactured composites using powder metallurgy.

Tafel polarization curves include electrochemical parameters such as corrosion potential (Ecorr), corrosion current density (Icorr), corrosion rate (CR), and corrosion protection efficiency (μp%). The anodic and cathodic areas of Tafel plots were used to calculate corrosion potential (Ecorr) and corrosion current density (Icorr). Corrosion rate measurement was calculated by using formula:

$$\text{Corrosion rate (CR)in } (mmpy) = 0.13 Icorr.(Ew/d) \tag{3.11}$$

Where Icorr is corrosion current, Ew is equivalent weight of samples in (g), and d is density of samples in (g/cm^3). The following relationship was used to compute protective efficiency from the measured Icorr values:

$$\mu_p(\%) = \left(\frac{I^{\circ}corr - \mathrm{I}^{\mathrm{i}}corr}{Icorr}\right) \times 100\% \tag{3.12}$$

Where $\boldsymbol{I^{\circ}corr}$ ***and*** $\mathbf{I^{i}}\boldsymbol{corr}$ are values of corrosion current density for pure iron and for specimens with NiTi-Cr as reinforcement respectively.

3.3. Tools and Equipment Used in Research Study

Table 3.5 Tools and Equipment Used in the Research Work

S.No	Tools/Equipment	Function
1	Powder Metallurgy	To fabricate the composites materials
2	Ball Milling Machine	Grinding the Fe matrix and the nitinol, chromium particle reinforcements into extremely fine powders
3	Weighing Machine	For calculating the specimens' weight and weight loss during various tests
4	Hydraulic Pressing Machine	Compressing the combined powder
5	Electrical muffle furnace	Green-compacted hybrid composite specimens are strengthened further by sintering them at a specific temperature.
6	Polisher and grinder	used to provide a surface quality that is superior and has a flat, mirror-like surface free from excessive distortion
7	Chemical etchant	(HNO3) Keeping waste, dust, and other particles away from the sintered hybrid composite specimens for microstructural analysis
8	XRD	Statistical phase analysis of a sample's phase composition Using the relative peak intensities, dislocation and lattice strain of crystallites
9	Optical Microscope	Fe matrix and nitinol/chromium hybrid composite specimens were studied structurally using these specimens.
10	SEM	for morphological characterization of the hybrid composite surfaces and analysis the impact of corrosion and fracture on surfaces.
11	FTIR	The functional groups and bond in Fe composite
12	Image J Software	To analysis the image for measuring grain size and porosity
13	Origin Pro-2022	To better analysis of the graph of data
14	Vickers Hardness	To test the hardness of the matrix and composite
15	UTM	To evaluate the hybrid composite specimens' compressive strength under loads that tend to compress size
16	Electrochemical Analyzer	. To test corrosion of sintered composite

CHAPTER FOUR

RESULTS AND DISCUSSIONS

4.1. Introduction

The experimental results of all the tests had discussed in this chapter. This study includes a variety of analyses of several tests. The composites of iron matrix with Nitinol and reinforced metal matrix Cr were analyzed for density, hardness, XRD, optical microscopy, SEM, compression, and corrosion test. This chapter also mentions the findings of all experiments, with an analysis and discussion of all synthesized effects, and a summary of the results is offered at the end.

4.2. Analysis of Density and Porosity of Sintered Sample

Analyzing the density and porosity in composite material is necessary due to the effects on the mechanical properties of the composite materials like hardness and compression. As a result, the smaller the better criterion for material density and porosity, and the larger the better criterion for material hardness and compressive strength (Bayu et al., 2021).

4.2.1. Density of Composites

Table 4.1 below shows the compositions and sample designations for four samples developed at fixed compaction pressure (60MPa), sintering time (2hours) and temperature (1100) from literature review.

Table 4.1 Composition and Samples Design

Sample Code	Sample Composition in wt.%
S1	Fe-5%NiTi-10%Cr-4%MoS2
S2	Fe-7.5%NiTi-7.5%Cr-4%MoS2
S3	Fe-10%NiTi-5%Cr-4%MoS2
S4	Pure iron

The theoretical density (ρth) is derived by adding the components inside the sample volume using the mixing rule for matrix and composite powders using equation (3.5), and the sintered density was measured experimentally using the Archimedes principles equation (3.6) in chapter, relative density to theoretical density were calculated using equation (3.7) from chapter 3. The densities of iron matrix, nitinol, Cr and MoS2 reinforcements are (7.87, 6.4, 7.1 and 5.06) g/cm^3 respectively. The density of Nitinol and Cr is lower than that of Fe, so the addition of nitinol and Cr reduces the density of the material. The theoretical density decreases slightly with increasing reinforcement weight.

Sample three (Fe-10%NiTi-5%Cr-4%MoS2) contains more nitinol, which is less dense than chromium, so the theoretical density decreases more than the other samples. Sample one (S1) exhibits high theoretical density values (7.591 g/cm^3) next pure iron (7.847 g/cm^3). As shown in Figure 4.1, there was a difference between the theoretical and sintered densities of the composites due to the downward segregation of voids and heavy particles (Olani et al., 2023). Although Fe has a higher density than nitinol, the addition of nitinol to the composite caused a drop in its total density, and increasing porosity percentage.

When mixing was completed, the blended particles began to clump together, and agglomeration could happen during the mixing stage, which the main reason for increasing the number of pores and decreasing the density (Shamsuddin, 2014). The sintered densities of samples (S1, S2, S3 and S4) were 7.257 g/cm^3,7.045 g/cm^3, 6.969 g/cm^3 and 7.06g/cm^3 respectively. So due to the addition chromium and nitinol less density than iron base metal, the theoretical density, experimental density and relative density of composite was decreased, the same result registered by (Jha et al. 2022).

4.2.2. Porosity of Composite

Porosity was calculated from the actual and theoretical densities by measuring the total void space within the composite. Equation (3.8) can be used to compute the porosity of the generated composites. Particles addition in the base matrix, trapping air between them, and interconnected in nature the main reason for generation of voids, therefore the percentage of porosity increases with the number of particles added (Li et al., 2020) and the porosity increases as the reinforcement content increases according to (Arif et al., 2017); (Lin et al., 2018). The porosity of all samples was determined using theoretical and experimental densities as shown in the table below.

Table 4.2 Experimental Density, Relative Density and Porosity

Sample	Theoretical Density	Sintered Density	Relative Density (%)	Porosity (%)
Sample 1	7.591 g/cm^3	7.259 g/cm^3	95.6	4.37
Sample 2	7.575 g/cm^3	7.045 g/cm^3	93.01	6.99
Sample 3	7.558 g/cm^3	6.969 g/cm^3	92.2	7.79
Sample 4	7.847 g/cm^3	7.06 g/cm^3	89.97	10.02

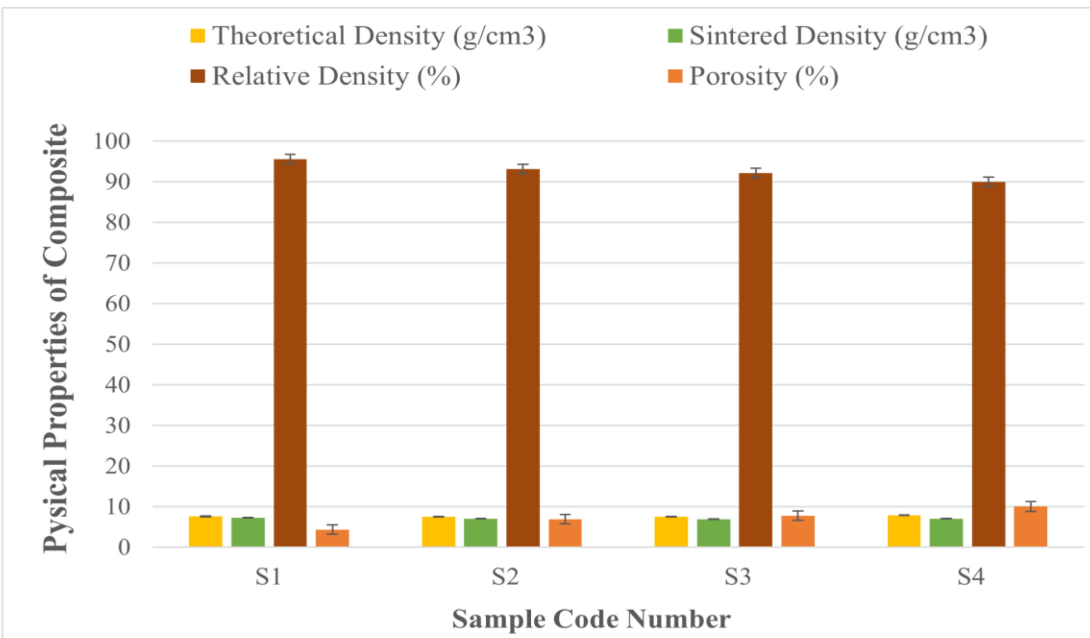

Figure 4.1 Physical Propeties of Sintered Samples

In (S4) pure iron and no reinforcing materials, it has greater porosity values due to the powder agglomeration. In contrast to the situation where pores are somewhat independent less than 5%, the porosity tends to be interconnected with an increase in porosity fraction greater than 5% (Chawla and Deng, 2005); (Bautista et al., 2008). It was discovered that increased pore size was closely correlated with increased pore shape irregularity (Ali Dad Chandio et al., 2019).

When the variance between the experimental density and theoretical density is increase (percentages of relative density is decreased) there is high probability the composite to be pores. so minimum porosity (4.37%) was obtained in sample one (S1), due to high relative density and more content of chromium which have small variance within base metal iron density, confirmed by reviewers (Chawla and Deng, 2005); (Meignanamoorthy and Ravichandran, 2018); (Ashebir, 2022).

4.3. Microstructural Characterization

4.3.1. XRD Analysis

4.3.1.1. Phase Analysis of sintered samples

The X-ray diffraction (XRD) pattern of Fe-5Nitinol-10Cr (S1), Fe-7.5Nitinol-7.5Cr (S2) and Fe-10Nitinol-5Cr (S3), were detected in angle between (10°-2θ-80°) at scan speed 3°/min. The samples' diffraction peaks were compared to XRD-JCPDS files of various materials, as shown figure (4.2). Smart materials Ni, and Cr, reinforcement in the Fe matrix can be seen as separate small peaks in XRD plotted graphs due to the addition of small percentages. The XRD analysis show the existence of Fe (high intensity peak) and enhancements (Ni and Cr), which are symbolized by various signs and XRD-JCPDS, in the composite matrix (Wang et al., 2021).

When the percentage of reinforcements is increased, the intensity of the reinforcements peaks were increased (Bahari et al., 2012); (N. Singh et al., 2018). It has been observed on the tallest peak at (2θ = 44.79°) and (110), (JCPDS card number: 037-0474), was present due to the high iron concentration. Fe-Ni (Kamacite), with a JCPDS card number of 035-1375, was produced at (2= 33.8°) and (111), the same phase reported by (Singh et al., 2018). The (054-0331, 034-0396, 041-1224) represent the JCPDS card numbers for the Fe-Cr (200) at an angle of (2= 64.4829°), agreed with (Bautista et al., 2008); (Li et al., 2020). Small peaks at (2θ=24.64°, (101) and JCPDS code, (004-0850) Ni and (2θ=55.42°, (220) and JCPDS code (006-0694) Cr has been detected.

Due to the low weight percentage, the reinforcements' peak intensity is smaller than that of the matrix and may even be below the limit for detection of the XRD technique (Olani et al., 2023). Due to the low concentration of molybdenum sulfide, titanium has not been found by XRD, but it may be present and react with nickel and the matrix phase. Small reinforcements have been added, hence an XRD test has not been able to validate the phase of every reinforced particle. The matrix phase of the reinforcing particle is unclear and is only visible at extremely modest peaks.

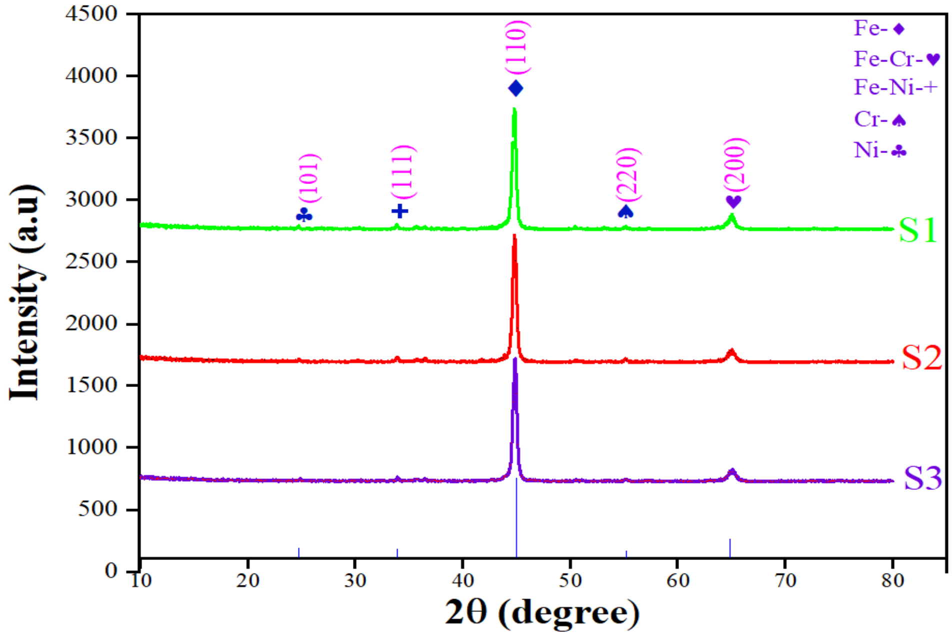

Figure 4.2 XRD Spectrum of IMMC at Different Reinforcement Content

4.3.1.2. Crystalline Sizes of Sintered Samples'

Equation (3.3) was used to determine crystalline size using the XRD data. Take K as 0.94 (recommended between (0.68-2.08) to calculate the Scherrer condition's most extreme acceptable run for Fe-NiTi-Cr (Lee et al., 2022), and since the average value is utilized, the diffraction peak point was calculated from the XRD data as 1.54056 (°), the X-ray diffraction wavelength, and as varied as possible.. There is consistency between the average grain size and the average crystalline size value of 27.87 μm found in the XRD data. Examining XRD data from crystals and OM measurements of grain size seem to have a good correlation

Table 4.3 Crystalline Sizes of Samples Using XRD Data

Parameters		Data from XRD peak analysis			
K	λ (Å)	Peak Position 2θ (°)	FWHM β (°)	D(μm) $D = \frac{K\lambda}{\beta\cos\theta}$	Average (D) (μm)
0.94	1.54056	43.8314	0.3	25.66	27.87 μm
		44.7982	0.4102	18.7	
		45.4705	0.24	31.89	
		64.4829	0.28	25.06	
		64.9977	0.65	10.77	

4.3.1.3. Dislocation Density and Lattice Strain of Composited Material

Since mixing, blending, compaction, and sintering had processed during the fabrication of iron based composite materials, the particles can interact and get circulated in the matrix (Saberi et al., 2009). Metal matrix composites' lattice strain increases and particle size decreases when milling time is increased (Bahari et al., 2012). Although these particles should flow uniformly, there was a possibility that defects like dislocations and lattice strain may emerge due to mixing imperfections, compaction, and temperature instability in the furnace.

In light of these problems, the parameters of micro structure have estimated using the XRD peak analysis Gauss method of the Scherrer formula. Peak variance analysis for the XRD Gauss method allows for a more precise determination of the microstructural characteristics of materials, such as lattice strain and dislocation density (Venkateswarl et al., 2014); (Altuntaş et al., 2022); (Zhu et al., 2023). The numerical dislocation density of sintered composite samples was estimated using equation (3.3) from chapter 3. Eq. (3.4) was used to calculate the lattice strain of the composite in terms of broadening lines and Bragg angles (Venkateswarlu et al., 2014).

Both dislocation density and lattice strain had calculated in the table (4.4). According to the table (4.4), When the proportion of chromium reinforcement increased from (5-10) wt% and the percentage of nitinol declined from (10-5), there was a decrease in crystalline size, an increase in lattice strain, and a rise in dislocation.

Table 4.4 Crystalline Sizes, Dislocation Density and Lattice Strain Experimental Calculation

Sample Code	Parameters Obtained from XRD Data		Experimental Calculation using Scherrer equation, (Venkateswarlu et al., (2014)		
	2θ (°)	FWHM β (°)	D(μm) $D = \frac{K\lambda}{\beta\cos\theta}$	$\delta *10^{-3}\ \mu m^{-2}$ $\delta = 1/D^2$	$\varepsilon *10^{-3}$ $\varepsilon = \frac{\beta}{4\tan\theta}$
Sample 1	43.8314	0.3	29.81	1.13	3.25
	44.7982	0.4102	21.88	2.09	4.34
	45.4705	0.24	37.48	0.71	2.49
	64.4829	0.28	35.034	0.81	1.94
	64.9977	0.65	15.13	4.37	4.45
Average	-	-	**27.87**	**1.73**	**3.3**
Sample 2	43.9313	0.32	27.96	1.28	3.46
	44.864	0.4008	22.39	1.99	4.24
	45.4905	0.28	32.13	0.97	2.91
	64.5229	0.2534	38.72	0.67	1.75
	65.026	0.78	12.61	6.28	5.34
Average	-	-	**26.76**	**2.24**	**3.54**
Sample 3	33.9389	0.2534	34.23	0.85	3.62
	43.9913	0.44	20.34	2.42	4.75
	44.8379	0.4088	21.96	2.07	4.32
	64.9877	0.79	12.45	6.45	5.41
Average	-	-	**22.4**	**2.95**	**4.53**

From sample one to sample three, the crystalline size reduces (from 27.87 m to 22.4 m). However, the dislocation density increases from 1.73μm^{-2} to 2.95 μm^{-2} and the lattice strain increases from 3.3 to 4.53. In this study, chromium up to 10% addition to iron metal matrix composites demonstrated a reduction in lattice strain and dislocation density.

The results in the table above lead me to the conclusion that the dislocation densities and lattice strain of composite materials rise when the crystalline size falls and vice versa, result have agreement with Khitouni et al. (2010); Bahari et al., (2012); Madhavi, (2019); Rai et al. (2023).

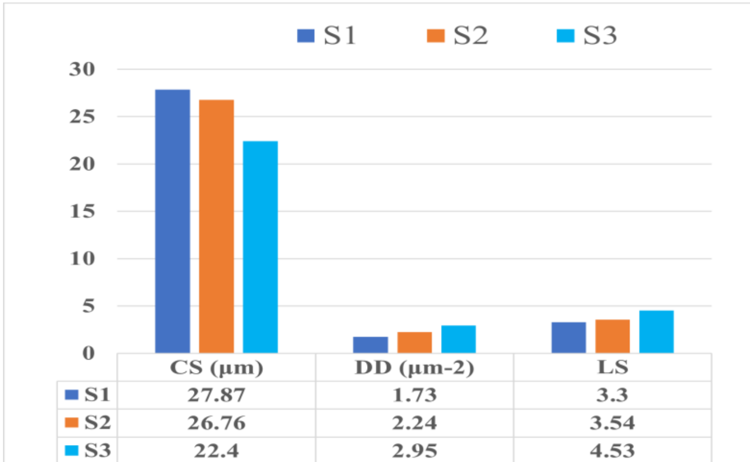

Figure 4.3 Comparison Between Crystalline Size (CS), Dislocation Density (DD) And Lattice Strain (LS) Using Bar Chart

4.3.2. Optical Microscopy

4.3.2.1. Distribution of Reinforcing Particles

The distribution of the reinforcing particles in the iron matrix was observed using optical microscopy (OM), as shown in Figure (4.4). before and after etching were depicted in the below image. The grain boundary is illustrated in the third column after being etched in 4% nital (nitric acid and distilled water) for 10 seconds. Etchant has a significant impact on the grain boundary as a result, allowing for improved clearing.

(S1)	(S1)	(S1)
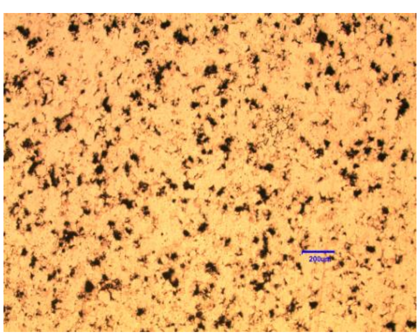	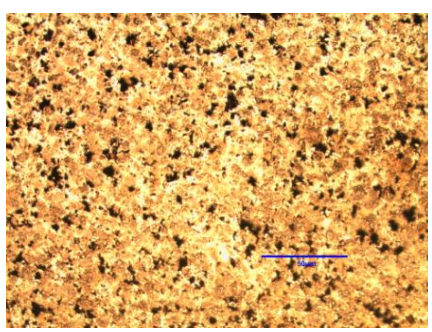	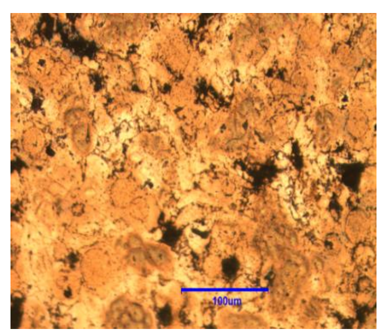
200μm (before etched)	50μm (after Etched)	100μm

(S2) 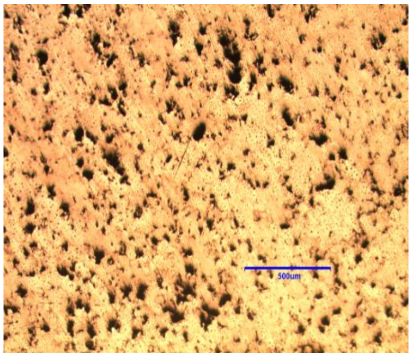 500μm (before etched)	(S2) 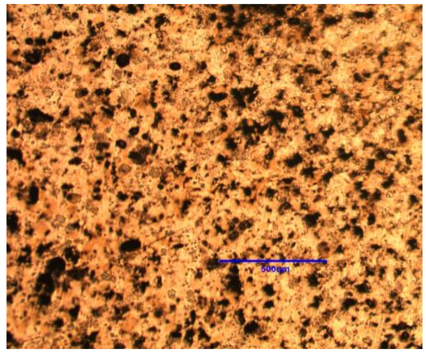 50μm (after Etched)	(S2) 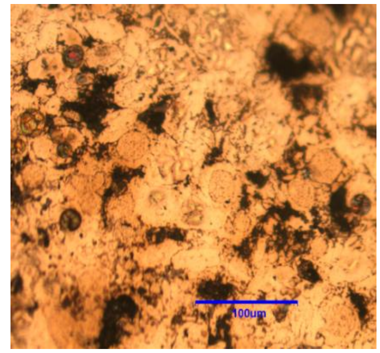 100μm
(S3) 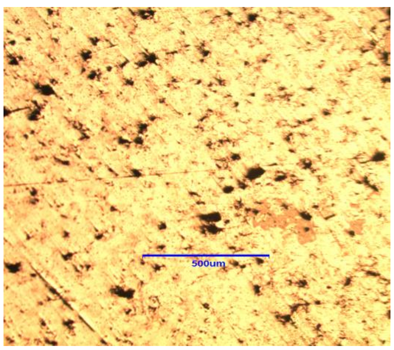 500μm (before etched)	(S3) 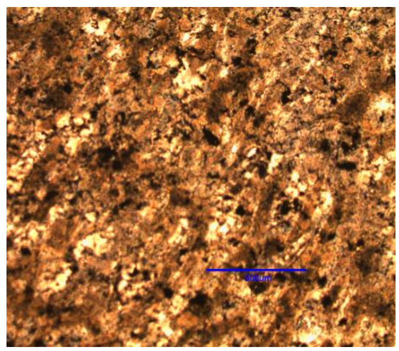 500μm (after Etched)	(S3) 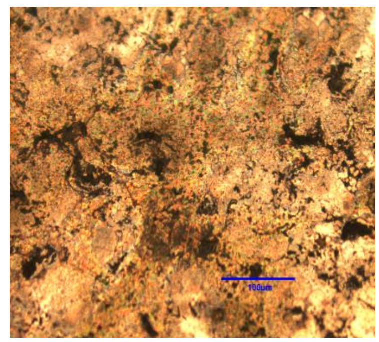 100μm
(S4) 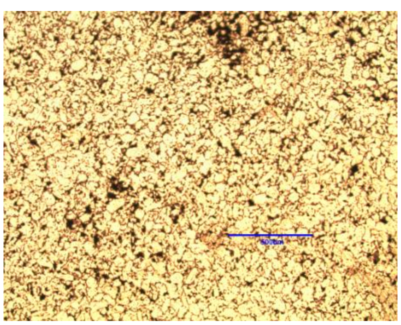 500μm (before etched)	(S4) 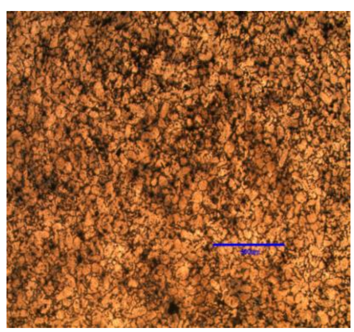 500μm (after Etched)	(S4) 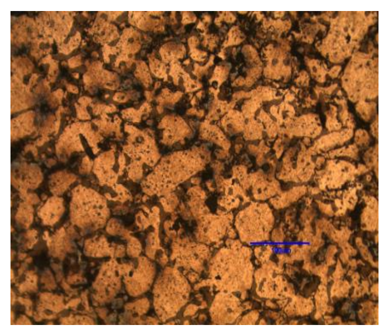 100μm

Figure 4.4 Optical Micrographs of S1, S2, S3, And S4 Before and After Etchant at Different Magnification

4.3.2.2. Grain Size of Sintered Samples

Using Image j software, the pore size distribution in relation to sintered density was calculated. The grain size was determined using Image J software based on a microscope's image. The line intersect approach was used to estimate the grain size, which ranged from 20.138 μm to 156.47μ

m, based on the OM image. The average grain size has been estimated to be 63.35 μm using trial data from several locations on the specimen image. Through analyzing the image through image j software 4.6%, 6.65%, 7.45%, and 10.05% were recorded for (S1, S2, S3, and S4) respectively.

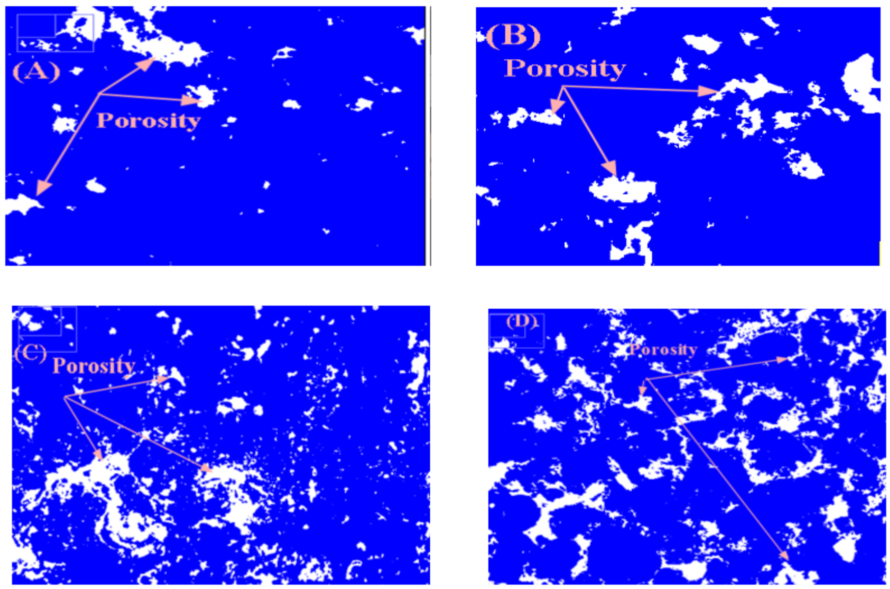

Figure 4.5 Porosity Analysis of Using Imagej Software from OM Image

4.3.3. Scanning Electron Microscope (SEM)

It is vital to do research on the distribution of reinforcements in composites since it has a significant impact on the final properties of powder metallurgy composites. SEM analysis revealed that the particles were uniformly distributed and that porosity was significantly decreased after sintering (Ali Dad Chandio et al., 2019).

Figure (4.6) shows the structure of the hybrid iron composite with some pore spaces produced by the evenly distributed nitinol and Cr reinforcement on the iron matrix. It is observed that the reinforcements (nitinol and Cr) have little to no agglomeration and are equally distributed throughout the Fe matrix. But in sintered pure iron, there is significant porosity and agglomeration of iron particles, which may be the result of inefficient mixing or blending of particles during mixing in a high energy ball milling machine and particle interconnected in nature.

The other samples (S1, S2, and S3) were sawn without significant agglomeration or disorder of the reinforcing particles due to the use of a molybdenum sulphide mixing agent. Hard particles can lead to improper mixing when added to an iron matrix, which can result in some broken lines, stressed lines, particle displacement that causes the composite to agglomerate, and some porosity holes formed by hard particles.

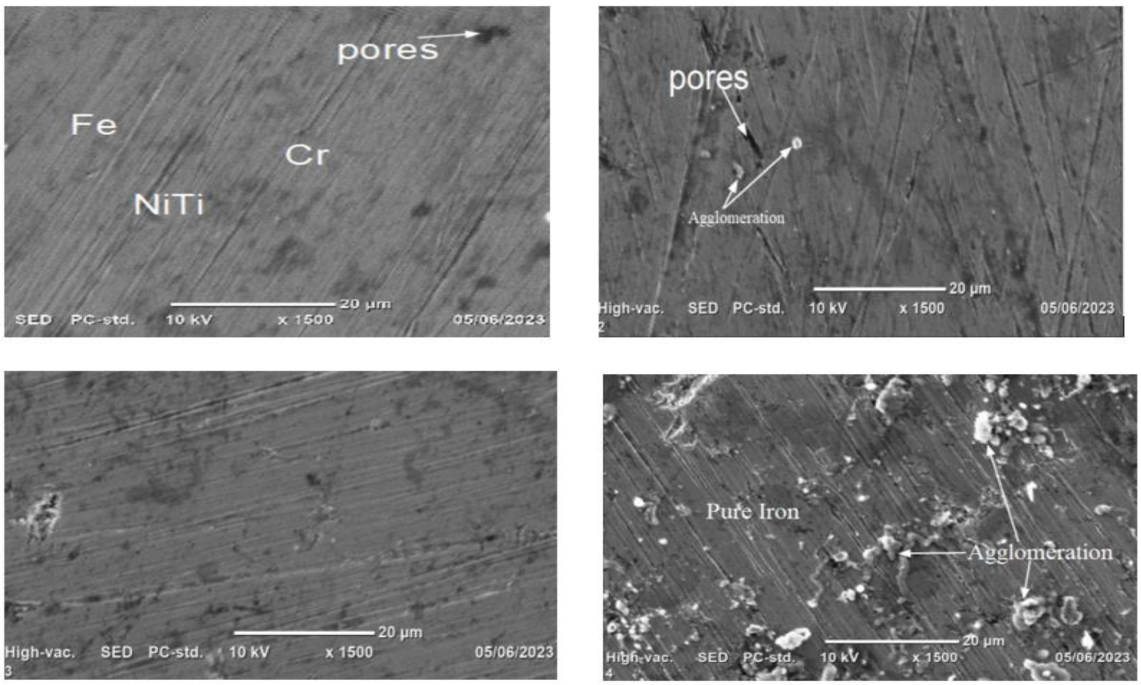

Figure 4.6 SEM Micrographs of (S1, S2, S3 And S4) at 20μm

4.3.4. FT-IR Analysis

The FT-IR absorption spectrum of crystalline solids is frequently used to explain the oscillation of ions in crystal structures. Between 1000 and 400 cm1, the major functional groups of Fe-O were observed to vibrate, as shown in figure... There is a peak between (400-800 cm-1) that is indicative of Fe-O vibrations. The IMMC's could display peaks at (409.18, 453.25, 555.15 and 750.18 cm-1) that are connected to the Fe-O bonds. The spectra of all manufactured samples contains two small wavelengths of absorption below 650 cm-1, verifying the composite samples' crystallization into a recognized crystal structure (Paswan et al., 2021). The spectrum exhibits a range of absorption between 592 and 670 cm-1, region 480 and 530 cm-1, and a tiny spectrum between 450 and 435 cm-1, and, all of which are in agreement with (Jacob and Khadar, 2010); (Paswan et al., 2021).

Small primary absorption zones between 480 and 530 cm-1 and below 450 cm-1 are attributed to changes in the length of the metal-oxygen (Fe3+O2), (Patange et al., 2013). Stretching vibration of (Fe-O) causes the higher frequency ranges to occur, whereas bending vibration causes the lower frequency regions to appear, (Bhowmik and Naresh, 2011); (Kumar et al., 2013). Between 650 and 750 cm-1, there is an increase in IR transmittance because of the absorption carried on by Fe-O stretching. Despite the fact that there is no absorption band from 750 to 3500 cm-1 or that there are no Fe-OH groups in the IMMCs. As a result, the produced samples have the capacity to resist corrosion since the surface of the IMMC's did not readily absorb the OH groups.

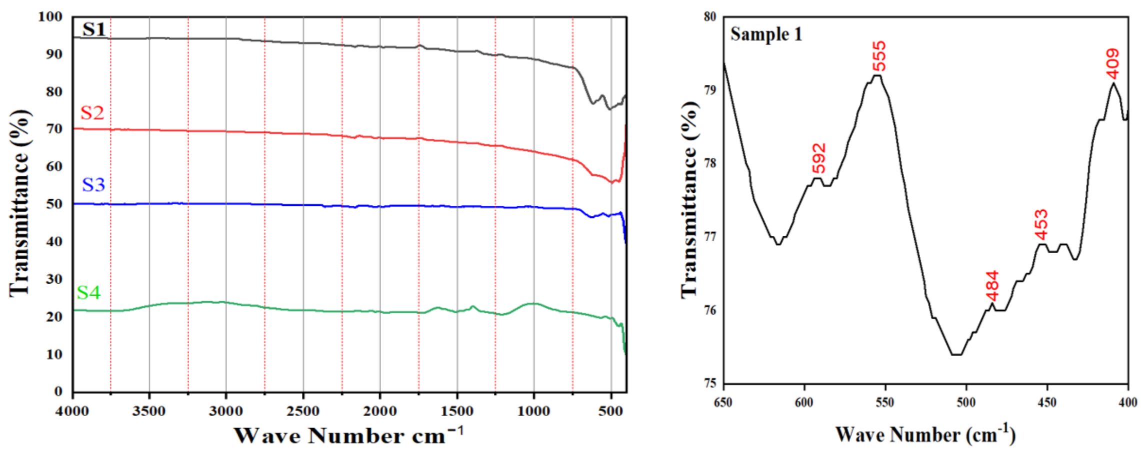

Figure 4.7 FT-IR Spectrum of IMMC's and for (S1)

4.4. Analysis Hardness Test

The hardness of Fe-NiTi-Cr composites was determined using the Vickers hardness test. Push the indenter into the specimen with a light, non-shocking load, as shown in figure 3.10 of Chapter Three. Equation (3.9) was used to calculate the Vickers hardness value. The Vickers hardness value of sintered specimens Fe-NiTi-Cr hybrid composites with varying reinforcement contents is shown in (appendix 2). The average hardness values for S1, S2, S3, and S4 are (465, 406, 371, and 249) respectively. Sample 1 (S1) has the highest hardness value, possibly 465 HV greater than pure iron's hardness of 249 HV, which agreed with (Chauhan et al., 2017); (Olani et al., 2023). The hardness values of the samples alter when the volume percent of the reinforcement changes due to the presence of smart particles, specifically nitinol and chromium.

The hardness of the sample increases by 1.86 times with an improvement of 86.5% when 10 weight percent of hard chromium particles and 5 weight percent of nitinol are added to matrix metal (Fe), as shown in table 4.6, (Kesarwani et al., 2015). The hardness increases from S1 to S4 as a result of the hard smart particles. The S1 IMMC sample's highest hardness measurement is 465, which is 1.86 times harder than the typical hardness of the matrix metal Fe, which confirmed with minimum dislocation density and lattice strain analyzed in section (4.3.1.3), (Venkateswarlu et al., 2014).

Sample two equal amount of (7.5 wt% NiTi and Cr) 1.6 times with improvement of 63.05%, and in sample three (10 wt% and 5 wt% Cr) 1.45 times within 48.99% were recorded. The addition of chromium and nitinol have increased the hardness, however with increment of nitinol more porosity is existed which affect the hardness of composite. As chromium percentage increases up to 10 wt% the hardness increase parallelly, and it has major significant effect on hardness than nitinol in this work. Experiments have revealed that as the weight fractions (nitinol and chromium) increase, so does the hardness (Chauhan et al., 2017); (Li et al., 2020); (Han et al., 2019). The reinforcing % has the biggest influence on hardness (Veličković et al., 2018); (Fanani et al., 2021);. (Chu et al., 2021).

Table 4.5 Experimental Results of Hardness Values

Sample's	Experimental Results of Hardness Value (HV)				
	Trial 1	Trial 2	Trial 3	Average (HV)	(%) Improvement
S1	445	452.5	497.4	465	86.5
S2	421.5	410.3	384.9	406	63.05
S3	380.6	373.7	359.2	371	48.9
S4	247.1	247.8	252.3	249	0

The percentage of improvement in material properties was calculated using the following equation:

$$\text{Improvement (\%)} = \frac{NEW\ (Xi) - Original\ (Xo)}{\text{Orignal (Xo)}} * 100 \quad (4.1)$$

New (Xi) is the average value of the IMMC samples and Orignal (Xo)is the average value of base metal (Fe).

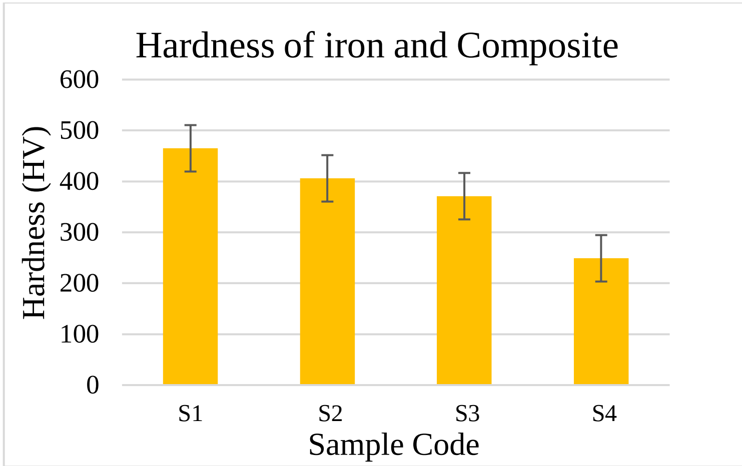

Figure 4.8 Average Vickers Hardness (HV) of (S1, S2, S3, And S4)

4.5. Analysis of Compression Test

The universal testing device was used to compress four samples. Figure (4.9) illustrates the stress-strain curve using data gathered during testing. The usual ultimate stresses for Fe-5%NiTi-10%Cr, Fe-7.5%NiTi-7.5%Cr, Fe-105NiTi-5%Cr, and sintered pure iron recorded are 636, 624, 575, and 547MPa, respectively. The results show that iron matrix samples with up to 19% reinforcements have somewhat higher yield strengths than samples made of the same components. In this study, the nitinol and Cr particles were added to the Fe matrix to improve the mechanical strength of the composite (Deepan Bharathi Kannan et al., 2016); (Chu et al., 2021); (Olani et al., 2023). The use of hard and smart particle powder resulted in a high compressive strength (Ivannikov et al., 2022). The increase in chromium up to 10% and the 5% increase in nitinol in each composite's stress-strain curves demonstrate ultimate stress, and sample two's compressive strength significantly improved as shown in figure (4.9).

Because of agglomeration, porosity in composites may affect the homogenous compressive strength. Along with the fracture formation and reduced ductility, the inclusion of tougher chromium and nitinol particles caused the matrix's plastic instability under compressive loading. The IMMC’s inconsistent elastic modulus and the reinforcement's nitinol damping properties (Chauhan et al., 2020), and the young modulus is negligible, the same concept reported by (Nguyen and Gupta, 2010); (Shamsuddin et al., 2013).

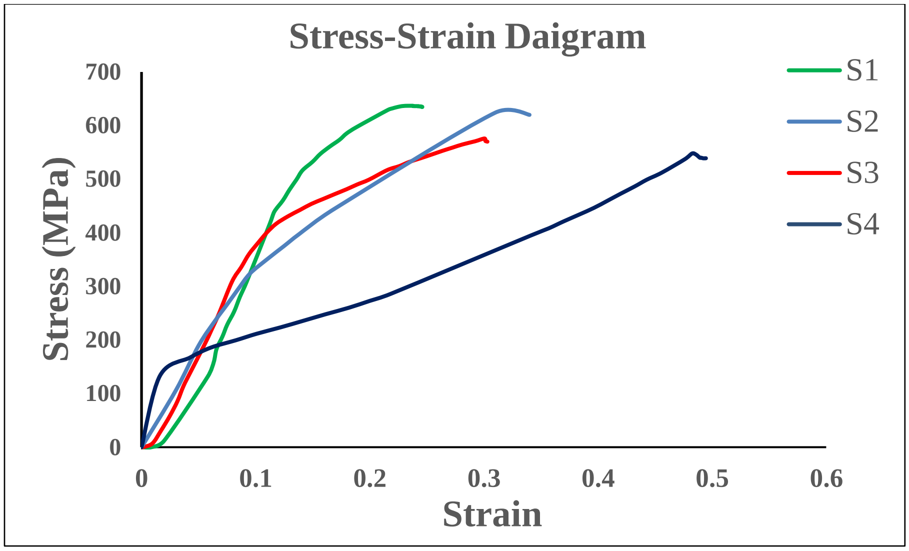

Figure 4.9 Stress- Strain Diagram of (S1, S2, S3, And S4)

Sample (S1) (Fe-5%NiTi-10Cr) scored first in the compression test and had the maximum compressive strength when compared to the other three samples due to its highest hardness and small pores. Therefore, the compressive strength is influenced by adding chromium rather than nitinol.

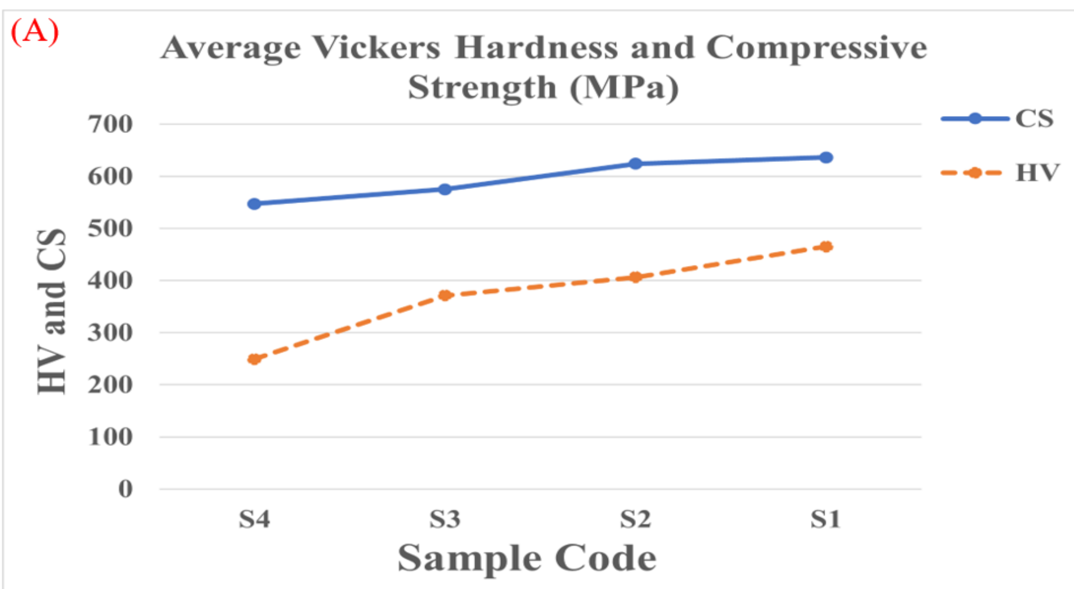

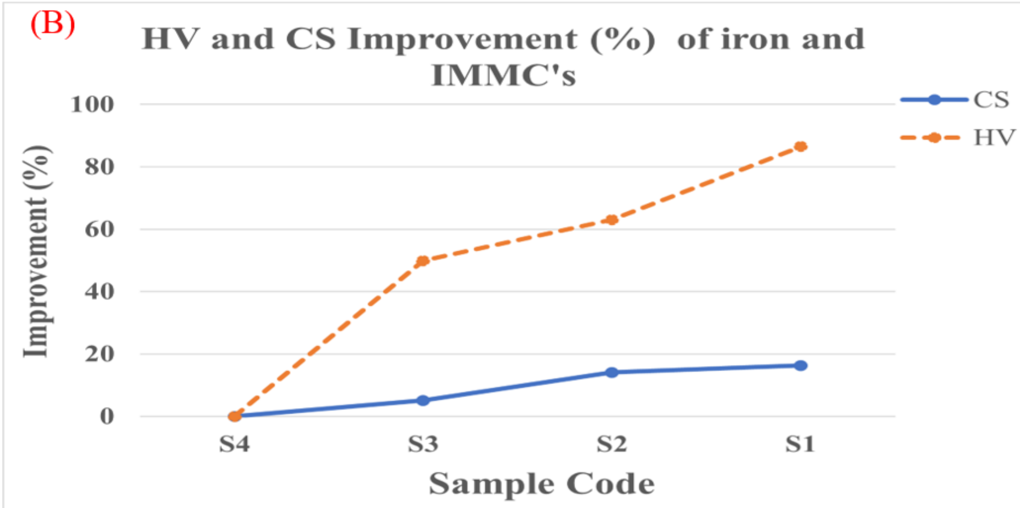

Figure 4.10 (A) Average Vickers Hardness and Compressive Strength, and (B) Improvement Recorded

4.6. Fracture Analysis Using SEM

At different magnifications, Figure 4.11 shows the fracture map of the surface morphology of the samples. The fracture processes of the composites were examined using SEM to explore the structure of the micrographs. The fractures and sections depicted in Figures 4.11 (a) and (b) indicate brittle cracking (fracture) in the IMMCs. Due to agglomeration during powder mixing, pores started to change in size during this period, from larger to smaller ones. This resulted in decreased mechanical characteristics and numerous indentations on the micrograph. Due to a force that was applied immediately perpendicular to the sample, there are several places where little cracks have started to spread. Due to its brittleness, there occurred cleavage cracking in some locations, which increased the fracture of composite samples.

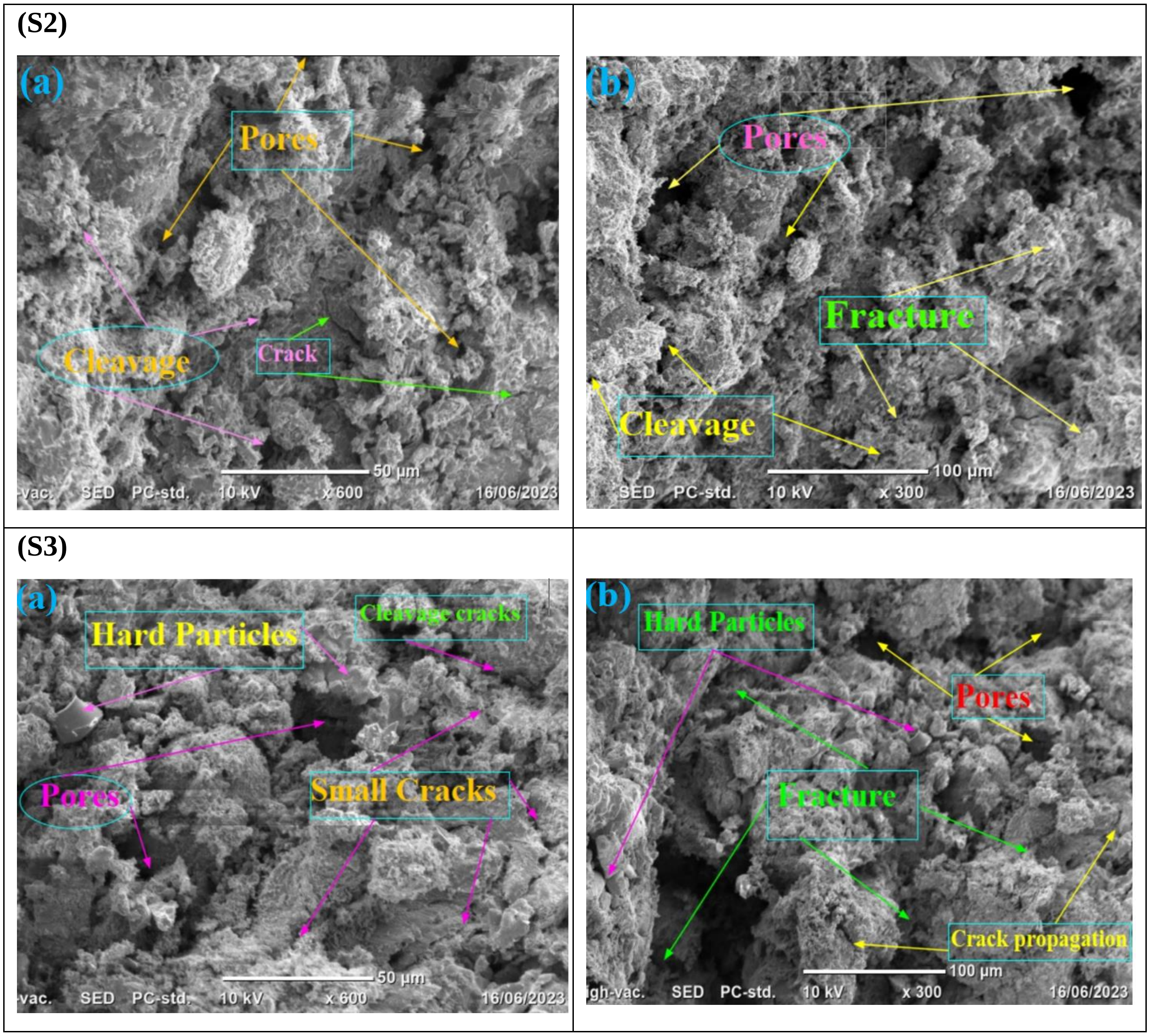

Figure 4.11 Fractography Analysis Using SEM for (S2) and (S3) at 50μm and 100 μm

4.7. Corrosion Study

In the ASTU material lab, corrosion experiments on various iron composite materials in 3.5 wt% NaCl solution were performed in a biological electrochemical cell with three electrodes connected to a biological instrument Potentiostat. A NaCl electrolyte was created by dissolving 3.5% (35g) of NaCl, and 150 mL of distilled water electrolyte was taken out for each experiment. Before beginning the testing, the electrodes were allowed to settle for about an hour in the electrolyte solution, and the open circuit potential (OCP) was recorded as shown in (appendix-4, (A)). At a scan rate of 1 mV/sec, potentiodynamic polarization curves in the 250–250 mV region was captured for OCP. The Tafel Plot or polarization curve (corrosion potential in Y-axis, versus corrosion current in X-axis) and electrochemical impedance spectroscopy (EIS) Nyquist plots (resistance in X-axis versus impedance in Y-axis) were processed and plotted in EC-LAB software after the sample was immersed in NaCl solution for an hour. The test was then terminated, and data from the numerous runs that were completed were extracted and plotted using the Origin Pro program.

4.7.1. Potentiodynamic Polarization Measurements

The Tafel estimation approach was utilized to detect potentiodynamic polarization in order to examine the corrosion behavior of the manufactured samples. Calculating the rate of action of corrosion reactions can be done using the shape of the polarization curve. Tafel plots offer a different electrochemical strategy that has the benefits of quickness and relative simplicity Olani et al. (2023). The Tafel plot for four samples from the potentiodynamic polarization test was displayed in the figure below using test data.

Corrosion current density (Icorr) and corrosion potential (Ecorr), as shown in (appendix 4, (B)), were obtained by projecting the cathodic and anodic linear segments of the Tafel plot to the intersection points using the Origin Graphs Analysis Method. The anodic and cathodic slopes of polarization were also assessed after Icorr and Ecorr were determined using the linear fitting dialog box, as shown in appendix (4).

The polarization resistance was then determined in relation to the anodic and cathodic polarization slopes as specified in the following Stern-Geary equation (4.2), (Andrade and Martínez, 2010).

$$\mathbf{Rp} = \frac{\boldsymbol{\beta a \beta c}}{\mathbf{2.303Icorr(\beta a + \beta c)}} \tag{4.2}$$

Where, $\boldsymbol{\beta a}$ and $\boldsymbol{\beta c}$ are anodic and cathodic slopes of polarization curves, and I is corrosion current density in (mA/cm^2).

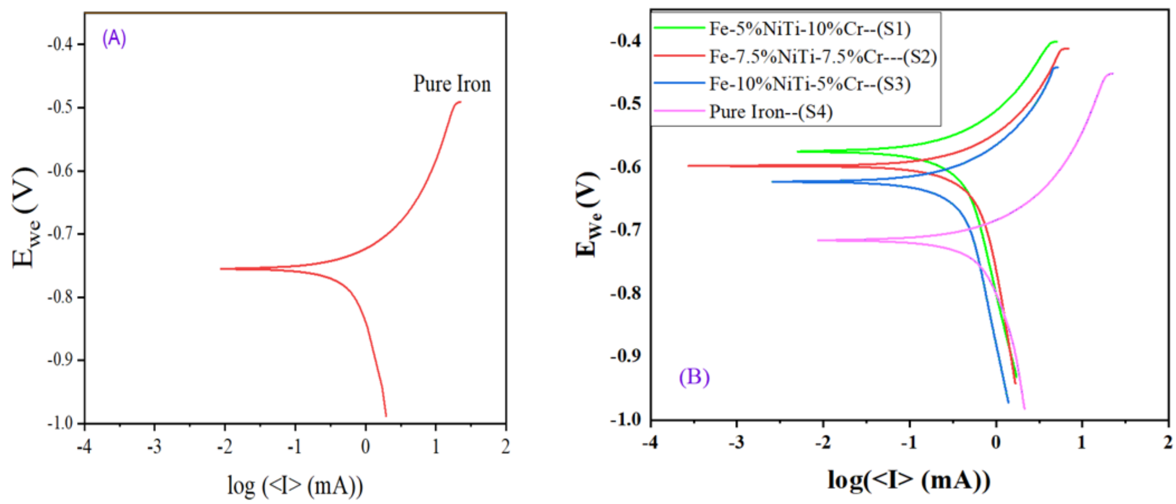

Figure 4.12 The Tafel Polarization Plot of Iron and IMMC's

Equations (3.12) and (3.13) from Chapter 3 were used to determine the corrosion rate and protection effectiveness of manufactured samples. The table below provides an overview of the Icorr, Ecorr, anodic and cathodic slopes, polarization resistance, corrosion rate, and protection efficiency.

Table 4.6 Tafel Polarization Experimental Parameters Values

Samples	Icorr (mA/cm^2)	Ecorr (mV)	βa (mV)	βc (mV)	R_P (Ω)	CR (mm/yr)	μ_p (%)
S1	19.27	-573.4	84.9	164.9	126.29	2.61	76.06
S2	27.44	-587.7	131.2	179.4	119.92	3.94	65.9
S3	28.22	-581.7	109.2	299.1	123.09	4.17	64.9
S4	55.25	-661.0	96.1	304.6	57.42	8.3	31.3
Pure iron	80.50	-896.67	55.25	350.2	25.64	10.3	-

According to Figure (4.12) and Table (4.6), the base metal (Fe) had the highest Icorr value of the four samples despite having the lowest Ecorr value. By dissolving into the solution, the Fe ions in the lattice thin the passive barrier on the metal surface, accelerating corrosion in the base material and the formation of rust on their surfaces (Kimura et al., 2005); (Konishi et al., 2005); (Szewczyk-Nykiel and Kazior, 2017). The effect of adding hybrid reinforcement particles to the base metal led the Ecorr to move in a favorable direction and the Icorr to decrease, as shown in Figure, which was proven by a potentiodynamic polarization test in a 3.5% NaCl solution. Since NiTi and Cr are resistant to severe corrosion attack, their addition may have an impact on the rate of corrosion and the polarization resistance.

Addition of chromium have significant improvement in corrosion (Santos et al., 2021) and Ni creates a stable inner oxide layer that serves as a barrier to stop corrosion (Konishi et al., 2005). According to reports in the literature, Ni is able to withstand the corrosive effects of Cl ions because it may form Fe-Ni alloy phases that are more resistant to damage caused by Cl ions (Singh et al., 2018). It has been discovered through examination of the rust layers that develop in situations with high salt concentrations that sodium ions (Na+) exist from the middle to outer rust layers, separate from the chloride ions, and permeate through an inner rust layer to the interface. When the chloride activity is greater than the hydroxyl activity, corrosion ensues ,(Usami et al., 2003); (Konishi et al., 2005).

According to the data in the table above, the base metal with the largest negative potential value or the lowest potential to resistance exhibits a high rate of corrosion and a low level of polarization resistance. The corrosion potential of composites increased from less negative to more negative from (S1-S4) to pure iron. The corrosion potentials were (-573.4, -587.7, -581.7, -661.0, and -896.67), respectively, for S1, S2, S3, S4, and pure iron. Maximum efficiency is shown by a high (low negative) Ecorr value, which also implies the lowest corrosion rate and highest corrosion resistance. The corrosion potential from (S1-S3) also marginally rose in parallel with a little increase in corrosion rate when Cr percentage decrease, (Bharat and Bose, 2021).

Therefore, a smart material with additional corrosive resistance at a 15 wt% (Cr and NiTi) has the capacity to reduce the corrosion rate and increase efficiency from 65% to 76%. addition, the protective efficiency of iron and IMMCs is in the sequence of (S1 >S2 > S3>S4) as shown in Table 4.7. Sample One (S1), which in this experiment shown high hardness, high compressive strength, uniform distribution of hybrid reinforcements and minimum porosity, had the highest protective efficiency and the lowest rate of corrosion. Furthermore, it is well known that materials with Tafel curves that show higher positive corrosion potential (Ecorr) and lower corrosion current density (Icorr) have superior corrosion resistance (low corrosion rate), many studies support the finding (Gupta et al., 2013); (Lei et al., 2012); (Singh et al., 2018); (Karabulut et al., 2022).

4.7.2. Electrochemical Impedance Spectroscopy (EIS) Analysis

After spending an hour submerged in 3.5% NaCl solutions, (Figure 4.12) displays the Nyquist plots made for the iron and IMMC sample electrodes at their open-circuit potential. A saturated calomel electrode (SCE) was used as the reference electrode, and a platinum electrode was used as the counter electrode. EIS spectra were obtained at open-circuit potential (OCP) of the specimens, with amplitude of 10 mV.

The diameter of the semicircle determines corrosion resistance, and the larger the diameter the higher the corrosion superior resistance (Balaraju et al., 2010); (Zhang et al., 2015); (Singh et al., 2018). The Nyquist plot showed that the diameter of semicircles increased from the base metal iron (S4) to (S3, S2, S1). From the Nyquist plot analysis larger diametric semicircles is exhibited, when the chromium reinforcement content increases from 5wt% to 10% (from S1 to S3) with respect to NiTi addition in the 3.5% NaCl solution. As compared the chromium and nitinol reinforcement, the increment of chromium particles have more effect on corrosion (Zhang et al., 2015), however the addition of nitinol up to 10 wt% also improve the corrosive resistance to some extent (Deepan Bharathi Kannan et al., 2016).

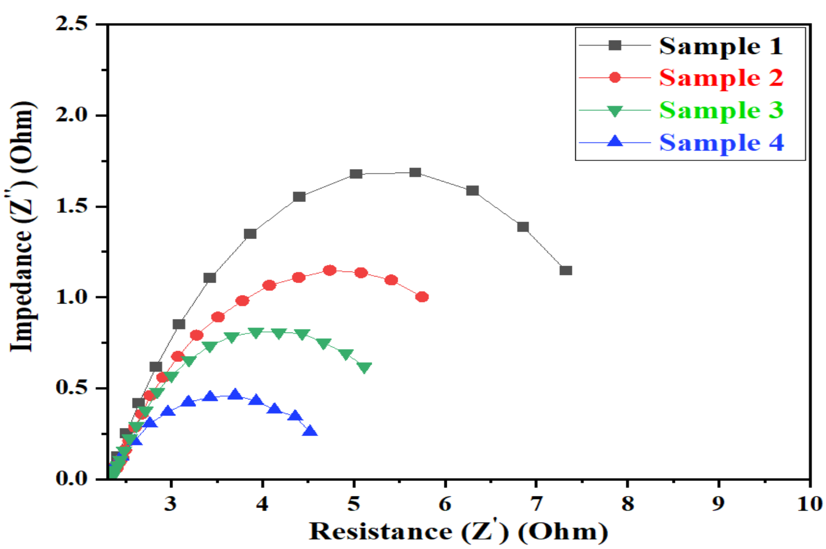

Figure 4.13 Electrochemical Impedance Nyquist Plots of Pure Iron and IMMC In 3.5 Wt% NaCl Solution.

Pure iron shows depressed diameter of semicircle which shows low corrosion resistance and (Fe-5NiTi-10%) (S1) shows higher diameter of semicircles, and it have good corrosion resistance from other three samples, the EIS data support this conclusion.

The results of the potentiodynamic polarization measurements and the EIS data are in good agreement. The increase in weight percentage of chromium reinforcements reduces the severity of the chloride ions against corrosion due to the oxide film and corrosion product thickening on the surface of the Fe and IMMCs, which is supported by all available data, and the base material (pure Fe) is easily attacked by corrosion compared to the reinforced IMMCs in 3.5% NaCl solutions.

4.7.3. Surface Investigation After Corrosion

After potentiodynamic polarization measurement, the corroded surface samples were characterized by using OM and SEM to see their morphology within the damaged surface.

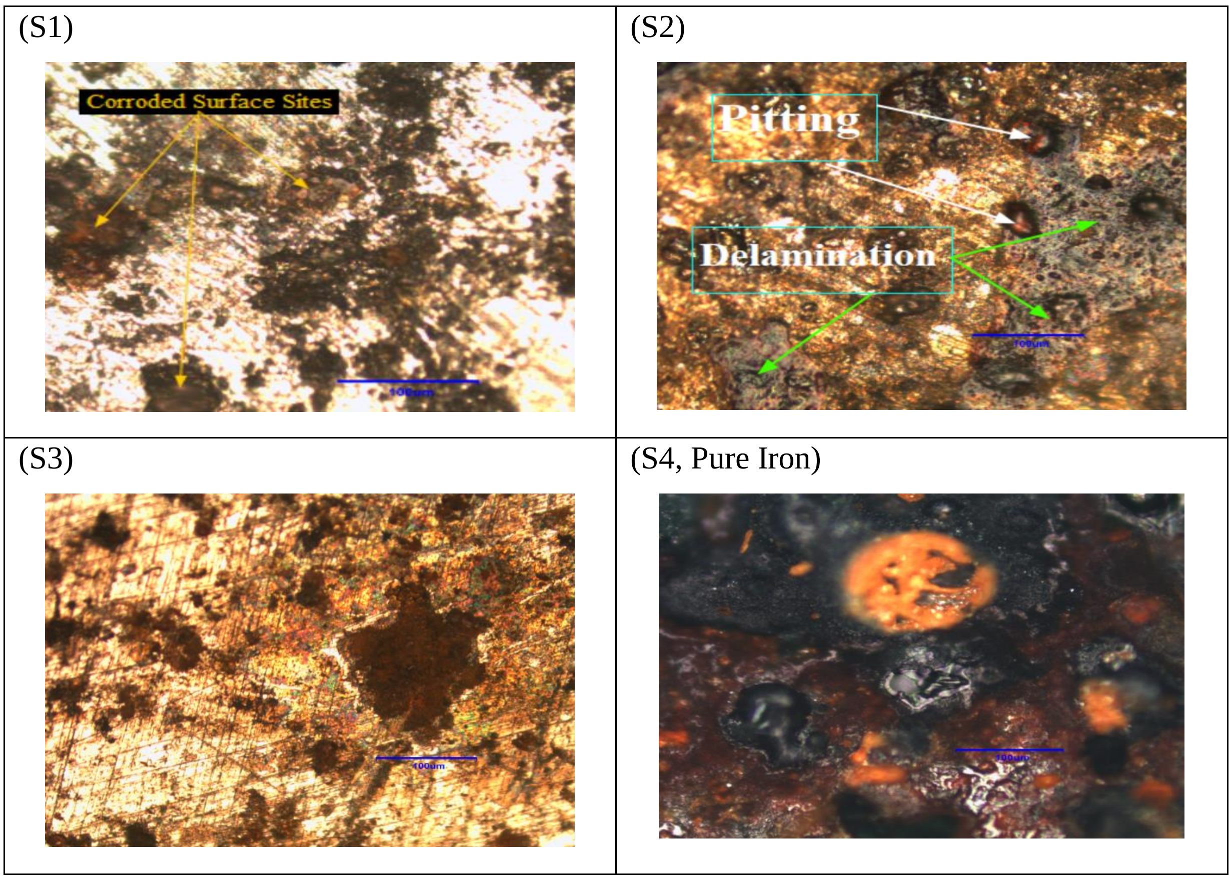

Figure 4. 14 OM Micrographs of Corroded for (S1, S2, S3, and S4) at 100μm

From the (SEM) micrographs it clearly observed that, there were cracking line, and surface microcracks existed around the grain boundary, may be due to pores and sintering temperatures (Bautista et al., 2008). Due to the separation between layer of particles and hard particles, the delamination showed in the micrographs. Fe-NiTi-Cr composite surface, the formation of (Fe-Ni) and (Fe-Cr) has contributed in resisting corrosion at the surface (Singh et al., 2018).

The pure iron (S4) sample's surface was found to be the most damaged of all the created samples. Figure (4.15) at (S2) illustrates the presence of white corrosion (pitting) due to small weight loss during fabrication and polishing, (El-saeed et al., 2009); (Zhang et al., 2014) products from the same layer under higher magnification. The most corrode area indicates that, the presence of maximum iron content iron covering the composite samples (Balaraju et al., 2010). The image makes clear that the interior of the corroded area has a significant number of tiny circular nodules.

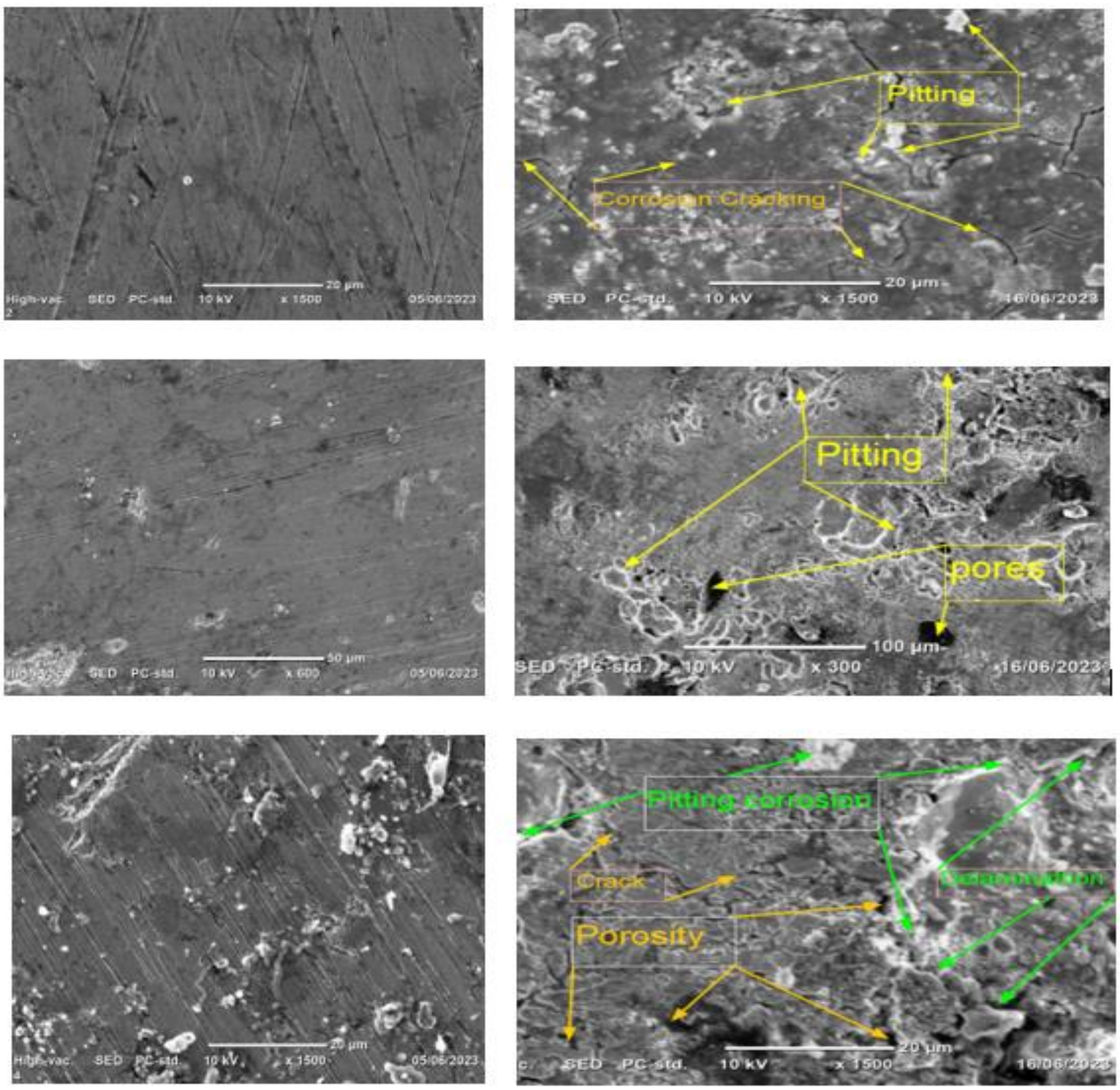

Figure 4. 15 SEM Micrographs Before and After Corrosion

CHAPTER 5

CONCLUSION AND RECOMMENDATION

In this study, the development of iron-based metal matrix composite reinforced with the ceramic particles like chromium and nitinol was carried out experimentally through powder metallurgy process. Different samples with various weight percentages of reinforcement were created and examined in order to determine the impact of reinforcement weight percentage on the microstructure, corrosion behavior, and mechanical properties of MMCs. The goal of the current research was to determine how smart particles such as chromium and nitinol can improve the metallurgical and mechanical properties of iron matrix-based composites.

5.1. Conclusions

Based on the result and discussion the following conclusion have been drawn:

1. Utilizing powder metallurgy, the novel Fe-NiTi-Cr (IMMC's) composites was created effectively. The results of the phase investigation showed that kamacite phases can be developed in (Fe-Ni) matrix and in separate (Fe-Cr) matrix. None of the composites showed any indication of the tiny phase development between the matrix and reinforcement phases.

2. The density of the sintered specimen after the addition of Nitinol and Chromium in the iron metal matrix indicates a slight reduction from base metal. Fe-5%NiTi-10%Cr-4%Mos2 had a low porosity (4.37%) and high relative density (95%) with minimal dislocation density and lattice strain as compared to other manufactured samples were recorded.

3. There was a uniform distribution of base metal and particulates which, were shown as seen on OM and SEM micrographs of fabricated samples. Fe-5%NiTi-10%Cr-4%Mos2 showed fine distribution of iron and particles, with little porosity and agglomeration on SEM image, which confirmed with good hardness. The existence of Fe-O bond stretching and bending, small Fe-O vibration spectrum in between (500-670) cm^{-1}, and the absence OH^- absorb zone spectrum which confirm the material ability to resist corrosion was analyzed using FT-IR test.

4. Due to reaction inside the matrix base metal, the addition of chromium and nitinol in Fe matrix has helped to improve the hardness and compressive strength of IMMCs. Hardness and

compressive strength increased with an increase in reinforcing fraction of up to 19%. Instead of nitinol, materials with chromium contents up to 10% exhibit a good improvement in hardness and compressive strength. As a result, Fe-5%NiTi-10Cr% exhibits 465HV hardness value and 636MPa compressive strength highest among all other fabricated samples.

5. The presence of Fe-Ni and Fe-Cr phases was responsible for the observed improvement in corrosion resistance. Corrosion resistance was improved as a result of adding NiTi and Cr particles to the matrix phase. Fe-5%NiTi-10%Cr composite was able to obtain the highest protection efficiency of 76% while using the least amount of corrosion current (19.27 mA cm^{-2}). Surface study (OM and SEM) was used to observe the impact of corrosion on various composite surfaces and showed outstanding agreement with the collected experimental results.

5.2. Recommendation

In order to prepare the components for IMMC with all the required factors, particularly during the compaction and sintering process, powder metallurgy techniques are being used more and more. Due to the remarkable improvement in hardness and corrosion resistance performances of these powder metallurgy iron-based metal matrix composite components, the outstanding result associated with near net shape production of these processes is of the greatest importance and could lead to a greater popularity of the alloy and particle reinforced iron metal matrix composites using powder metallurgy.

However, it is suggested to develop a method of improvement in reducing the porosity level gently and within concentration because the IMMCs have pores because they are interconnected in nature and easily agglomerated after milling to compaction. Every process parameter in powder metallurgy, including milling time, compaction pressure, sintering time, and sintering temperature, should be optimized in order to minimize their impact on the mechanical and physical properties of composites. It strongly encouraged that in the future, secondary operations such thermal stability and extrusion operations be carried out depending on their application requirements.

5.3. Future Work

- ✓ The study can be further extended to different fabrication techniques and study its parametric effect on mechanical and tribological behavior of developed IMMCs.
- ✓ The study can be extended for developed a composite on creep, fatigue, stiffness, etc.
- ✓ The study can be extended to study the effect of NiTi particle size and a small amount of MoS2 because the particle size and percentage volume fraction of the reinforcement play a significant role in mechanical and tribological behavior.
- ✓ The study can be extended to study the optimization of the content of reinforcements, process parameters milling time, compaction pressure and sintering temperature in powder metallurgy fabrication method.

REFERENCES

Ali Dad Chandio, A. D. C., Muhammad Basit Ansari, M. B. A., Shahid Hussain, S. H., & Muhammad Ali Siddiqui, M. A. S. (2019). Silicon Carbide Effect as Reinforcement on Aluminium Metal Matrix Composite. *Journal of the Chemical Society of Pakistan*, *41*(4), 650–650. https://doi.org/10.52568/000776/jcsp/41.04.2019

Altuntaş, G., Altuntaş, O., Öztürk, M. K., & Bostan, B. (2022). Metallurgical and Crystallographic Analysis of Different Amounts of Deformation Applied to Hadfield Steel. *International Journal of Metalcasting*, *17*(2), 1340–1349. https://doi.org/10.1007/s40962-022-00860-3

Anand, A., & Tiwari, S. K. (2022). Recent advancements in the production of hybrid metal matrix composites (HMMC): A Review. *IOP Conference Series: Materials Science and Engineering*, *1248*(1), 012087. https://doi.org/10.1088/1757-899x/1248/1/012087

Andrade, C., & Martínez, I. (2010). Techniques for measuring the corrosion rate (polarization resistance) and the corrosion potential of reinforced concrete structures. *Non-Destructive Evaluation of Reinforced Concrete Structures: Non-Destructive Testing Methods*, 284–316. https://doi.org/10.1533/9781845699604.2.284

Ankur, N., & Singh, N. (2021). Performance of cement mortars and concretes containing coal bottom ash: A comprehensive review. *Renewable and Sustainable Energy Reviews*, *149*(January), 111361. https://doi.org/10.1016/j.rser.2021.111361

Arif, S., Alam, M. T., Ansari, A. H., Siddiqui, M. A., & Mohsin, M. (2017). Study of mechanical and tribological behaviour of Al/SiC/ZrO2 hybrid composites fabricated through powder metallurgy technique. *Materials Research Express*, *4*(7). https://doi.org/10.1088/2053-1591/aa7b5f

Ashebir, D. A. (2022). *Synthesis , Characterization , and Testing of Self-Lubricating Tetra Hybrid Reinforced Al Matrix Composites via Powder Metallurgy Processing Synthesis , Characterization , and Testing of Self-Lubricating Tetra Hybrid Reinforced Al Matrix*

Composites via Po.

Augustin, M., & Balu, T. (2017). Estimation of Lattice Stress and Strain in Zinc and Manganese Ferrite Nanoparticles by Williamson-Hall and Size-Strain Plot Methods. *International Journal of Nanoscience*, *16*(3), 1–7. https://doi.org/10.1142/S0219581X16500356

Aydogmus, T. (2015). Processing of interpenetrating Mg-TiNi composites by spark plasma sintering. *Materials Science and Engineering A*, *624*, 261–270. https://doi.org/10.1016/j.msea.2014.11.092

Bahari, A., Sadeghi Nik, A., Roodbari, M., & Mirnia, N. (2012). Investigation the Al-Fe-Cr-Ti nano composites structures with using XRD and AFM techniques. *Sadhana - Academy Proceedings in Engineering Sciences*, *37*(6), 657–664. https://doi.org/10.1007/s12046-012-0103-3

Balaraju, J. N., Selvi, V. E., & Rajam, K. S. (2010). Electrochemical behavior of low phosphorus electroless Ni – P – Si 3 N 4 composite coatings. *Materials Chemistry and Physics*, *120*(2–3), 546–551. https://doi.org/10.1016/j.matchemphys.2009.11.047

Barrado, M., López, G. A., Nó, M. L., & San Juan, J. (2009). Composites with ultra high damping capacity based on powder metallurgy shape memory alloys. *Materials Science and Engineering A*, *521–522*, 363–367. https://doi.org/10.1016/j.msea.2008.10.075

Bautista, A., González-Centeno, A., Blanco, G., & Guzmán, S. (2008). Application of EIS to the study of corrosion behaviour of sintered ferritic stainless steels before and after high-temperature exposure. *Materials Characterization*, *59*(1), 32–39. https://doi.org/10.1016/j.matchar.2006.10.008

Bayu, D., Kumar, D., Venkatesh, C., Kumar, A., & Jha, P. (2021). Materials Today : Proceedings Mathematical modeling and mechanical characterization through process parameters optimization of AlMg-matrix SiC p reinforced composites produced by powder metallurgy route. *Materials Today: Proceedings*, *xxxx*. https://doi.org/10.1016/j.matpr.2021.03.078

Bharat, N., & Bose, P. S. C. (2021). An overview of production technologies and its application of metal matrix composites. *Advances in Materials and Processing Technologies*, *00*(00), 1–17. https://doi.org/10.1080/2374068X.2021.1878707

Bhowmik, R., & Naresh, N. (2011). Structure, ac conductivity and complex impedance study of Co_3O_4 and Fe_3O_4 mixed spinel ferrites. *International Journal of Engineering, Science and Technology*, *2*(8), 40–52. https://doi.org/10.4314/ijest.v2i8.63779

Bodunrin, M. O., Alaneme, K. K., & Chown, L. H. (2015). Aluminium matrix hybrid composites: A review of reinforcement philosophies; Mechanical, corrosion and tribological characteristics. *Journal of Materials Research and Technology*, *4*(4), 434–445. https://doi.org/10.1016/j.jmrt.2015.05.003

Borbély, A., & Groma, I. (2001). Variance method for the evaluation of particle size and dislocation density from x-ray Bragg peaks. *Applied Physics Letters*, *79*(12), 1772–1774. https://doi.org/10.1063/1.1404134

Bratu, V., Palacios, G., Nicoleta, I., & Ghit, C. (2013). *Applied Surface Science Tribological behaviour and statistical experimental design of sintered iron – copper based composites*. 72–85. https://doi.org/10.1016/j.apsusc.2013.08.007

Chami, A., Benabbou, R., Taleb, M., Rais, Z., & El, M. (2021). Materials Today : Proceedings Analysis of survey data on corrosion in the automotive industry. *Materials Today: Proceedings*, *xxxx*. https://doi.org/10.1016/j.matpr.2021.03.113

Chandel, R., Sharma, N., & Bansal, S. A. (2021). A review on recent developments of aluminum-based hybrid composites for automotive applications. *Emergent Materials*, *4*(5), 1243–1257. https://doi.org/10.1007/s42247-021-00186-6

Chandra Kandpal, B., Kumar, J., & Singh, H. (2018). Manufacturing and technological challenges in Stir casting of metal matrix composites- A Review. *Materials Today: Proceedings*, *5*(1), 5–10. https://doi.org/10.1016/j.matpr.2017.11.046

Chauhan, A., Vates, U. K., Kanu, N. J., Gupta, E., Singh, G. K., Sharma, B. P., & Gorrepati, S. R. (2020). Fabrication and characterization of novel nitinol particulate reinforced aluminium alloy metal matrix composites (NiTip/AA6061 MMCs). *Materials Today: Proceedings*, *38*(xxxx), 3027–3034. https://doi.org/10.1016/j.matpr.2020.09.326

Chauhan, S., Verma, V., Prakash, U., Tewari, P. C., & Khanduja, D. (2017). *Studies on induction hardening of powder-metallurgy-processed Fe – Cr / Mo alloys*. *24*(8), 918–925. https://doi.org/10.1007/s12613-017-1478-2

Chawla, N., & Deng, X. (2005). Microstructure and mechanical behavior of porous sintered steels. *Materials Science and Engineering A*, *390*(1–2), 98–112. https://doi.org/10.1016/j.msea.2004.08.046

Chu, C., Chen, W., Chen, Z., Jiang, Z., Wang, H., & Fu, Z. (2021). Microstructure and Mechanical Behavior of FeNiCoCr and FeNiCoCrMn High - Entropy Alloys Fabricated by Powder Metallurgy. *Acta Metallurgica Sinica (English Letters)*, *34*(4), 445–454. https://doi.org/10.1007/s40195-020-01150-9

Das, R., Mondal, M. K., & Pramanik, S. (2022). Strengthening Behaviour and Microstructural Properties during the Compaction of Reduced Blast Furnace Flue Dust—Fly Ash—Iron Metal Matrix Composite Fines using Powder Metallurgy Route. *Transactions of the Indian Institute of Metals*, *75*(9), 2255–2263. https://doi.org/10.1007/s12666-022-02592-8

Deepan Bharathi Kannan, T., Ramesh, T., & Sathiya, P. (2016). A Review of Similar and Dissimilar Micro-joining of Nitinol. *Jom*, *68*(4), 1227–1245. https://doi.org/10.1007/s11837-016-1836-y

Delavari, M., Salarvand, A., Rahi, A., & Shahri, F. (1970). The effect of powder metallurgy process parameters on mechanical properties of micro and nano-iron powder. *International Journal of Engineering, Science and Technology*, *3*(9), 86–94. https://doi.org/10.4314/ijest.v3i9.7

Duriagina, Z. A., Romanyshyn, M. R., Kulyk, V. V, Kovbasiuk, T. M., Trostianchyn, A. M., & Lemishka, I. A. (2020). *The character of the structure formation of model alloys of the Fe-Cr- (Zr , Zr-B) system synthesized by powder metallurgy*. *100*(2), 49–57. https://doi.org/10.5604/01.3001.0014.3344

El-saeed, O., Sroka, G., & Blake, G. (2009). *Gear Corrosion During the Manufacturing Process*. *October*, 60–65.

Fanani, E. W. A., Surojo, E., Prabowo, A. R., & Akbar, H. I. (2021). Recent progress in hybrid aluminum composite: Manufacturing and application. *Metals*, *11*(12). https://doi.org/10.3390/met11121919

Fisika, J., Fisika Indonesia, H., Khaerudini, D. S., Tetuko, A. P., & Ginting, M. (2008). Effect of Sintering Temperature and 5 WT.% Al(NO 3) 3 Additive to Metal Matrix by Powder Metallurgy Technique EFFECT OF SINTERING TEMPERATURE AND 5 WT.% Al(NO 3) 3 ADDITIVE TO METAL MATRIX COMPOSITES CHARACTERISTICS BY POWDER METALLURGY TECHNIQUE. *Jurnal Fisika Himpunan Fisika Indonesia*, *8*(1), 39–47.

Gagg, C. R., & Lewis, P. R. (2007). Wear as a product failure mechanism - Overview and case studies. *Engineering Failure Analysis*, *14*(8 SPEC. ISS.), 1618–1640. https://doi.org/10.1016/j.engfailanal.2006.11.064

Gupta, P., Kumar, D., Parkash, O., & Jha, A. K. (2013). Effect of sintering on wear characteristics of Fe-Al2O3 metal matrix composites. *Proceedings of the Institution of Mechanical Engineers, Part J: Journal of Engineering Tribology*, *228*(3), 362–368. https://doi.org/10.1177/1350650113508934

Han, T., Xiao, M., Zhang, Y., & Shen, Y. (2019). Laser cladding Ni-Ti-Cr alloy coatings with different process parameters. *Materials and Manufacturing Processes*, *34*(15), 1710–1718. https://doi.org/10.1080/10426914.2019.1686521

Hao, S., Cui, L., Jiang, D., Han, X., Ren, Y., Jiang, J., Liu, Y., Liu, Z., Mao, S., Wang, Y., Li, Y., Ren, X., Ding, X., Wang, S., Yu, C., Shi, X., Du, M., Yang, F., Zheng, Y., … Li, J. (2013). A transforming metal nanocomposite with large elastic strain, low modulus, and high strength. *Science*, *339*(6124), 1191–1194. https://doi.org/10.1126/science.1228602

Hao, S., Cui, L., Shao, Y., Jiang, J., Jiang, D., Wang, S., Du, M., Wang, Y., Brown, D. E., & Ren, Y. (2012). In situ X-ray diffraction study of deformation behavior in a Fe/NiTi composite. *Applied Physics Letters*, *101*(22), 2010–2014. https://doi.org/10.1063/1.4767993

Hill, H., Weber, S., Siebert, S., & Theisen, W. (2011). Investigation of corrosion and wear properties of fe based metal matrix composites consolidated by sintering and hot isostatic pressing. *Powder Metallurgy*, *54*(3), 455–462. https://doi.org/10.1179/003258910X12678035166656

Höhn, B. R., Stahl, K., Schudy, J., Tobie, T., & Zornek, B. (2012). FZG Rig-Based Testing of Flank Load-Carrying Capacity Internal Gears. *Gear Technology*, *June/July*(July), 60–69.

Honnaiah, C., Srinath, M. S., & Shashank Lingappa, M. (2023). Metallographical characterization of Al-SiCP metal matrix composites processed through microwave sintering technique. *Materials Today: Proceedings*. https://doi.org/https://doi.org/10.1016/j.matpr.2023.03.077

Imataka, H., Tanaka, K., Maeda, S., Yuya, M., & Kobayashi, A. (2017). Development of High-strength Nitriding Steel for Gear. *Nippon Steel & Sumitomo Emtal Technical Report*, *116*, 9–13.

Issa, S. A. M., Almutairi, A. M., Albalawi, K., Dakhilallah, O. K., Zakaly, H. M. H., Ene, A., Abulyazied, D. E., Ahmed, S. M., Youness, R. A., & Taha, M. A. (2023). Production of Hybrid Nanocomposites Based on Iron Waste Reinforced with Niobium Carbide/Granite Nanoparticles with Outstanding Strength and Wear Resistance for Use in Industrial Applications. *Nanomaterials*, *13*(3). https://doi.org/10.3390/nano13030537

Ivannikov, A. Y., Grebennikov, I. K., Klychevskikh, Y. A., Mikhailova, A. V., Sergienko, K. V., & Kaplan, M. A. (2022). *Elemental Powders*.

Jabur, A. S. (2013). Effect of powder metallurgy conditions on the properties of porous bronze. *Powder Technology*, *237*, 477–483. https://doi.org/10.1016/j.powtec.2012.12.027

Jacob, J., & Khadar, M. A. (2010). Investigation of mixed spinel structure of nanostructured nickel ferrite. *Journal of Applied Physics*, *107*(11). https://doi.org/10.1063/1.3429202

Jha, P., Kumar, D., & Mishra, V. K. (2022). Development of mathematical models to predict the density and hardness of Fe-ZrO2 composites. *Advances in Materials and Processing Technologies*, *8*(3), 3042–3056. https://doi.org/10.1080/2374068X.2021.1945298

Jiang, T. (2012). *Design of High Performance NiTi-based Shape Memory Alloys for Automotive Actuator Applications*. *August*, 1–161.

Jojith, R., & Radhika, N. (2019). Mechanical and tribological properties of LM13/TiO2/MoS2 hybrid metal matrix composite synthesized by stir casting. *Particulate Science and Technology*, *37*(5), 566–578. https://doi.org/10.1080/02726351.2017.1407381

Karabulut, H., Erden, M. A., Karacif, K., & Gündüz, S. (2022). Investigation of the effects of SiC reinforcement ratio in iron-based composite materials on corrosion properties. *Journal of the Southern African Institute of Mining and Metallurgy*, *122*(6), 317–322. https://doi.org/10.17159/2411-9717/1059/2022

Kesarwani, P., Jahan, S. J., & Kesarwani, K. (2015). Composite : Classification and its manufacturing process. *International Journal of Applied Research*, *1*(9), 352–358. www.allresearchjournal.com

Khazaal, S. M., Nimer, N. S. M., Szabolcs, S., Al Ansari, luay S., & Abdulsamad, H. J. (2022). Study of manufacturing and material properties of the hybrid composites with metal matrix as tool materials. *Results in Engineering*, *16*(August). https://doi.org/10.1016/j.rineng.2022.100647

Khitouni, M., Mhadhbi, M., Escoda, L., Suñol, J. J., & Dammak, M. (2010). Characterization of mechanically alloyed nanocrystalline Fe(Al): Crystallite size and dislocation density. *Journal of Nanomaterials*, *2010*. https://doi.org/10.1155/2010/712407

Khuntia, S. K., & Samal, B. P. (2019). *Fabrication of Ferrous based Composites via Different Processes and their Characterization*. *14*(12), 2817–2820.

Kimura, M., Kihira, H., Ohta, N., Hashimoto, M., & Senuma, T. (2005). Control of Fe(O,OH)6 nano-network structures of rust for high atmospheric-corrosion resistance. *Corrosion Science*, *47*(10), 2499–2509. https://doi.org/10.1016/j.corsci.2005.04.005

Konishi, H., Yamashita, M., Uchida, H., & Mizuki, J. (2005). Characterization of rust layer formed on Fe, Fe-Ni and Fe-Cr alloys exposed to Cl-rich environment by Cl and Fe K-Edge XANES measurements. *Materials Transactions*, *46*(2), 329–336. https://doi.org/10.2320/matertrans.46.329

Kulkarni, S. G., Lal, A., & Menghani, J. V. (2016). Effect of reinforcement type and porosity on strength of metal matrix composite. *International Journal of Computational Materials Science and Engineering*, *5*(1). https://doi.org/10.1142/S2047684116500068

Kumar, L., Kumar, P., Narayan, A., & Kar, M. (2013). Rietveld analysis of XRD patterns of different sizes of nanocrystalline cobalt ferrite. *International Nano Letters*, *3*(1), 1–12. https://doi.org/10.1186/2228-5326-3-8

Kumar, N., Bharti, A., & Dixit, M. (2021). Powder Compaction Dies and Compressibility of Various Materials. *Powder Metallurgy and Metal Ceramics*, *60*(7–8), 403–409. https://doi.org/10.1007/s11106-021-00253-x

Kumar, N., Bharti, A., & Saxena, K. K. (2021). A re-investigation: Effect of powder metallurgy parameters on the physical and mechanical properties of aluminium matrix composites. *Materials Today: Proceedings*, *44*, 2188–2193. https://doi.org/10.1016/j.matpr.2020.12.351

Kumar, S., Singh, R., & Hashmi, M. S. J. (2020). Metal matrix composite: a methodological review. *Advances in Materials and Processing Technologies*, *6*(1), 13–24. https://doi.org/10.1080/2374068X.2019.1682296

Lee, M. Y., Choi, Y. J., Woo, H. J., Kim, S. W., & Lee, B. W. (2022). Microwave absorption properties of Ni0.6Zn0.4Fe2O4 composites with nonmagnetic nanoferrite percentages. *Ceramics International*, *48*(14), 20187–20193. https://doi.org/10.1016/j.ceramint.2022.03.297

Lei, T., Tang, W., Cai, S. H., Feng, F. F., & Li, N. F. (2012). On the corrosion behaviour of newly developed biodegradable Mg-based metal matrix composites produced by in situ reaction. *Corrosion Science*, *54*(1), 270–277. https://doi.org/10.1016/j.corsci.2011.09.027

Li, J., Zhu, Z., Peng, Y., & Shen, G. (2020). Microstructure and wear characteristics of novel fe-ni matrix wear-resistant composites on the middle chute of the scraper conveyor. *Journal of Materials Research and Technology*, *9*(1), 935–947. https://doi.org/10.1016/j.jmrt.2019.11.033

Li, Y., Li, C., Tang, S., Zheng, Q., Wang, J., Zhang, Z., & Wang, Z. (2019). *Interfacial Bonding and Abrasive Wear Behavior of Iron Matrix Composite Reinforced by Ceramic Particles*. *3*.

López, G. A., Barrado, M., San Juan, J., & Nó, M. L. (2009). Mechanical spectroscopy measurements on SMA high-damping composites. *Materials Science and Engineering A*, *521–522*, 359–362. https://doi.org/10.1016/j.msea.2008.09.121

Manohar, G., Pandey, K. M., & Ranjan Maity, S. (2020). Effect of compaction pressure on mechanical properties of AA7075/B4C/graphite hybrid composite fabricated by powder metallurgy techniques. *Materials Today: Proceedings*, *38*(xxxx), 2157–2161. https://doi.org/10.1016/j.matpr.2020.05.194

Mavhungu, S. T., Akinlabi, E. T., Onitiri, M. A., & Varachia, F. M. (2017). Aluminum Matrix Composites for Industrial Use: Advances and Trends. *Procedia Manufacturing*, *7*, 178–182. https://doi.org/10.1016/j.promfg.2016.12.045

McCall, J. L. (1986). Systematic analysis of gear failures. *Metallography*, *19*(2), 249. https://doi.org/10.1016/0026-0800(86)90042-x

Meher, B. S., Saha, R., & Chaira, D. (2021). Fabrication of MWCNTs reinforced iron metal matrix composite by powder metallurgy: Effects of wet and dry milling. *Journal of Alloys and Compounds*, *872*, 159688. https://doi.org/10.1016/j.jallcom.2021.159688

Meignanamoorthy, M., & Ravichandran, M. (2018). Synthesis of metal matrix composites via powder metallurgy route: A review. *Mechanics and Mechanical Engineering*, *22*(1), 65–75. https://doi.org/10.2478/mme-2018-0007

Milani, A. S., Shanian, A., Madoliat, R., & Nemes, J. A. (2005). The effect of normalization norms in multiple attribute decision making models: A case study in gear material selection. *Structural and Multidisciplinary Optimization*, *29*(4), 312–318. https://doi.org/10.1007/s00158-004-0473-1

Nguyen, B., & Gupta, M. (2010). Enhancing compressive response of AZ31B using nano-Al 2O 3 and copper additions. *Journal of Alloys and Compounds - J ALLOYS COMPOUNDS*, *490*, 382–387. https://doi.org/10.1016/j.jallcom.2009.09.188

Obadele, B. A., Ramabulana, K., Alaneme, K. K., & Durowoju, M. O. (2015). *composite coatings on AISI 316 stainless steel*. *June*.

Öksüz, K. E., Çevik, M., Bozdağ, A. E., Özer, A., & Şimşir, M. (2014). *Production of (V-B) Reinforced Fe Matrix Composites*. *8*(8), 800–804.

Olani, M., Kumar, D., & Asrat, G. (2023). Mechanical and corrosion properties of Fe–SiC–ZrO2 hybrid composite fabricated through powder metallurgy process. *Results in Engineering*, *17*(November 2022), 100866. https://doi.org/10.1016/j.rineng.2022.100866

Panda, D. (2016). *Development of Al-Fe 3 Al Composites by Powder Metallurgy Route National Institute of Technology Rourkela Supervisors ' Certificate*.

Parande, G., Manakari, V., Wakeel, S., Kujur, M. S., & Gupta, M. (2018). Enhancing mechanical response of monolithic magnesium using nano-NiTi (Nitinol) particles. *Metals*, *8*(12), 1–13. https://doi.org/10.3390/met8121014

Parveen, A., Chauhan, N. R., & Suhaib, M. (2021). Influence of Process Parameters and Reinforcements on Aluminum Hybrid Composites Developed by Powder Metallurgy Process. *Physics of Metals and Metallography*, *122*(10), 1007–1013. https://doi.org/10.1134/S0031918X21100094

Paswan, S. K., Kumari, S., Kar, M., Singh, A., Pathak, H., Borah, J. P., & Kumar, L. (2021). Optimization of structure-property relationships in nickel ferrite nanoparticles annealed at different temperature. *Journal of Physics and Chemistry of Solids*, *151*(January), 109928. https://doi.org/10.1016/j.jpcs.2020.109928

Patange, S. M., Shirsath, S. E., Jadhav, S. P., Hogade, V. S., Kamble, S. R., & Jadhav, K. M. (2013). Elastic properties of nanocrystalline aluminum substituted nickel ferrites prepared by co-precipitation method. *Journal of Molecular Structure*, *1038*, 40–44. https://doi.org/10.1016/j.molstruc.2012.12.053

Praveena, B. A., Santhosh, N., Buradi, A., Srikanth, H. V., Shankar, G., Ramesha, K., Manjunath, N., Karthik, S. N., Rudra Naik, M., & Praveen Kumar, S. (2022). Experimental Investigation on Density and Volume Fraction of Void, and Mechanical Characteristics of Areca Nut Leaf Sheath Fiber-Reinforced Polymer Composites. *International Journal of Polymer Science*, *2022*. https://doi.org/10.1155/2022/6445022

Rai, A., Rai, P., Kumar, A., Chaturvedi, R. K., & Singh, V. K. (2023). Study of Mechanical Characteristics of Silicon Carbide Reinforced Zn-Mg Based Metal-Ceramic Composite. *Silicon*, *0123456789*. https://doi.org/10.1007/s12633-023-02474-8

Rajak, D. K., Pagar, D. D., Kumar, R., & Pruncu, C. I. (2019). Recent progress of reinforcement materials: A comprehensive overview of composite materials. *Journal of Materials Research and Technology*, *8*(6), 6354–6374. https://doi.org/10.1016/j.jmrt.2019.09.068

Rajesh Kumar, L., Saravanakumar, A., Bhuvaneswari, V., Gokul, G., Dinesh Kumar, D., & Jithin Karunan, M. P. (2019). Optimization of wear behaviour for AA2219-MoS2 metal matrix composites in dry and lubricated condition. *Materials Today: Proceedings*, *27*(xxxx), 2645–2649. https://doi.org/10.1016/j.matpr.2019.11.087

Raturi, A. (2019). *Analysis Of Mechanical And Micro Structural Behaviour Of Al Based Metal Matrix Composite Reinforced With Ball Milled Nano Particles : A Review*. *1*(1), 11–29.

Sajan, S., & Philip Selvaraj, D. (2021). A review on polymer matrix composite materials and their applications. *Materials Today: Proceedings*, *47*(xxxx), 5493–5498. https://doi.org/10.1016/j.matpr.2021.08.034

Sankar, S., & Nataraj, M. (2011). Profile modification-a design approach for increasing the tooth strength in spur gear. *International Journal of Advanced Manufacturing Technology*, *55*(1–4), 1–10. https://doi.org/10.1007/s00170-010-3034-3

Santos, R. F., Rocha, A. M. F., Bastos, A. C., Cardoso, J. P., Rodrigues, F., Fernandes, C. M., Sacramento, J., Ferreira, M. G. S., Senos, A. M. R., Fonseca, C., Vieira, M. F., & Malheiros, L. F. (2021). The effect of Cr content on the corrosion resistance of WC-Ni-Cr-Mo composites. *International Journal of Refractory Metals and Hard Materials*, *95*(October 2020), 105434. https://doi.org/10.1016/j.ijrmhm.2020.105434

Shamsuddin, S., Jamaludin, S. B., Hussain, Z., & Arifin, Z. (2014). Enhancing properties of Fe-Cr-alumina composites prepared by powder metallurgy. *Jurnal Intelek*, *8*(2), 20–26.

Shamsuddin, S., Jamaludin, S., Hussain, Z. H., & Ahmad, Z. (2008). Characterization of Fe-Cr-Al2O3 Composites Fabricated by Powder Metallurgy Method with Varying Weight

Percentage of Alumina. *Journal of Physical Science*, *44*(8), 085201. http://arxiv.org/abs/1011.1669%0Ahttp://dx.doi.org/10.1088/1751-8113/44/8/085201%0Ahttps://iopscience.iop.org/article/10.1088/1751-8113/44/8/085201

Shamsuddin, S., Shamsul, B. J., Hussain, Z., & Zainal, A. A. (2013). Compressive and wear resistance of alumina reinforced Fe-Cr matrix composites. *Advanced Materials Research*, *620*(January), 362–367. https://doi.org/10.4028/www.scientific.net/AMR.620.362

Sharma, A. K., Bhandari, R., & Aherwar, A. (2020). *Materials Today : Proceedings Matrix materials used in composites : A comprehensive study*. *21*, 1559–1562. https://doi.org/10.1016/j.matpr.2019.11.086

Sharma, D. K., Mahant, D., & Upadhyay, G. (2019). Manufacturing of metal matrix composites: A state of review. *Materials Today: Proceedings*, *26*(xxxx), 506–519. https://doi.org/10.1016/j.matpr.2019.12.128

Sharma, N., Jangra, K., & Raj, T. (2015). Applications of Nickel-Titanium Alloy. *Journal of Engineering and Technology*, *5*(1), 1. https://doi.org/10.4103/0976-8580.149472

Singh, A., Singh, J., Sinha, M. K., & Kumar, R. (2022). *Ferrous Metal Matrix Composites Status Scope and Challenges*. http://arxiv.org/abs/2204.09999

Singh, N., Banerjee, S., Parkash, O., & Kumar, D. (2018). Tribological and corrosion behavior of (100-x)(Fe70Ni30)-(x)ZrO2 composites synthesized by powder metallurgy. *Materials Chemistry and Physics*, *205*, 261–268. https://doi.org/10.1016/j.matchemphys.2017.11.031

Singh, P., Abhash, A., Yadav, B. N., Shafeeq, M., Singh, I. B., & Mondal, D. P. (2019). Effect of milling time on powder characteristics and mechanical performance of Ti4wt%Al alloy. *Powder Technology*, *342*, 275–287. https://doi.org/10.1016/j.powtec.2018.09.075

Skotnicova, K., Kirillova, V. M., Ermishkin, V. A., Cegan, T., Jurica, J., Kraus, M., & Burkhanov, G. S. (2015). Influence of alloying and testing conditions on mechanical properties and deformation behavior of <100> tungsten-based single crystals. *Materials Science and Engineering A*, *636*, 536–542. https://doi.org/10.1016/j.msea.2015.03.126

Song, G. Q., & Sun, Q. P. (2000). Effect of microstructure on the mechanical behavior of NiTi shape memory alloy reinforced aluminum matrix composite. *Smart Materials and Structures*, *9*(5), 693–700. https://doi.org/10.1088/0964-1726/9/5/314

Szewczyk-Nykiel, A., & Kazior, J. (2017). Effect of Aging Temperature on Corrosion Behavior of Sintered 17-4 PH Stainless Steel in Dilute Sulfuric Acid Solution. *Journal of Materials Engineering and Performance*, *26*(7), 3450–3456. https://doi.org/10.1007/s11665-017-2778-4

T.Somasekhar, & P Niteesh kumar. (2018). *Review Paper on Processing of Metal Matrix Composites & Its Properties*. 284–287. www.ijcrt.org

Tai, Q., Yuen, R. K. K., Yang, W., Qiao, Z., Song, L., & Hu, Y. (2012). Iron-montmorillonite and zinc borate as synergistic agents in flame-retardant glass fiber reinforced polyamide 6 composites in combination with melamine polyphosphate. *Composites Part A: Applied Science and Manufacturing*, *43*(3), 415–422. https://doi.org/10.1016/J.COMPOSITESA.2011.10.012

Usami, A., Kihira, H., & Kusunoki, T. (2003). 3%-Ni weathering steel plate for uncoated bridges at high airborne salt environment. *Nippon Steel Technical Report*, *87*, 21–23.

Varadaraj, K. R., Kumar, S., Vitala, H. R., Ravishankar, M. K., & Dileep, B. P. (2023). *Effect of Chromium on Mechanical and Corrosion Behaviour of Ferrous Metal Matrix Composites by Using Powder Metallurgy Route BT - Recent Developments in Mechanics and Design* (S. Hegde, A. Mishra, & D. K. Singh (eds.); pp. 225–234). Springer Nature Singapore.

Veličković, S., Miladinović, S., Stojanović, B., Nikolić, R. R., Hadzima, B., & Arsić, D. (2018). Influence of load and reinforcement content on selected tribological properties of Al/SiC/Gr hybrid composites. *Production Engineering Archives*, *18*(18), 18–23. https://doi.org/10.30657/pea.2018.18.03

Venkateswarlu, K., Sandhyarani, M., Nellaippan, T. A., & Rameshbabu, N. (2014). Estimation of Crystallite Size, Lattice Strain and Dislocation Density of Nanocrystalline Carbonate Substituted Hydroxyapatite by X-ray Peak Variance Analysis. *Procedia Materials Science*, *5*(August 2015), 212–221. https://doi.org/10.1016/j.mspro.2014.07.260

Wang, M., Wang, Z., Yang, Z., Jin, J., Ling, G., & Zong, Y. (2021). Sintering and Mechanical Properties of (SiC + TiCx)p/Fe Composites Synthesized from Ti3AlC2, SiC, and Fe Powders. *Materials*, *14*, 2453. https://doi.org/10.3390/ma14092453

Wu, M. W., & Hwang, K. S. (2010). Formation mechanism of weak ferrite areas in Ni-containing powder metal steels and methods of strengthening them. *Materials Science and Engineering: A*, *527*(21), 5421–5429. https://doi.org/https://doi.org/10.1016/j.msea.2010.05.089

Xie, C. L., Hailat, M., Wu, X., Newaz, G., Taya, M., & Raju, B. (2007). Development of short fiber-reinforced NiTi/Al6061 composite. *Journal of Engineering Materials and Technology*, *129*(1), 69–76. https://doi.org/10.1115/1.2400271

Xie, L., Xu, Z., Qi, Y., Liang, J., He, P., Shen, Q., & Wang, C. (2023). Effect of ball milling time on the microstructure and compressive properties of the Fe-Mn-Al porous steel. *International Journal of Minerals, Metallurgy and Materials*, *30*(5), 917–929. https://doi.org/10.1007/s12613-022-2568-3

Zhang, H., Zou, Y., Zou, Z., & Shi, C. (2014). Effects of chromium addition on microstructure and properties of TiC-VC reinforced Fe-based laser cladding coatings. *Journal of Alloys and Compounds*, *614*, 107–112. https://doi.org/10.1016/j.jallcom.2014.06.073

Zhang, H., Zou, Y., Zou, Z., & Wu, D. (2015). Microstructure and properties of Fe-based composite coating by laser cladding Fe-Ti-V-Cr-C-CeO2 powder. *Optics and Laser Technology*, *65*, 119–125. https://doi.org/10.1016/j.optlastec.2014.06.016

Zhou, Z., Liu, B., Guo, W., Fu, A., Duan, H., & Li, W. (2021). Corrosion behavior and mechanism of FeCrNi medium entropy alloy prepared by powder metallurgy. *Journal of Alloys and Compounds*, *867*, 1–9. https://doi.org/10.1016/j.jallcom.2021.159094

Zhu, P., Yan, H., Zhou, J., Zhou, Y., Zhang, Y., & Chen, Z. (2023). Microstructure of Gear Steels Treated by Shot Peening by X-Ray Line Profile Analysis Method. *Metals and Materials International*, *0123456789*. https://doi.org/10.1007/s12540-023-01436-4

APPENDIX

Appendix -1

(A) Crystalline size (CS), Dislocation density (DD), and Lattice Strain (LS) measurment in origin software using Gausses curve fit analysis from XRD data.

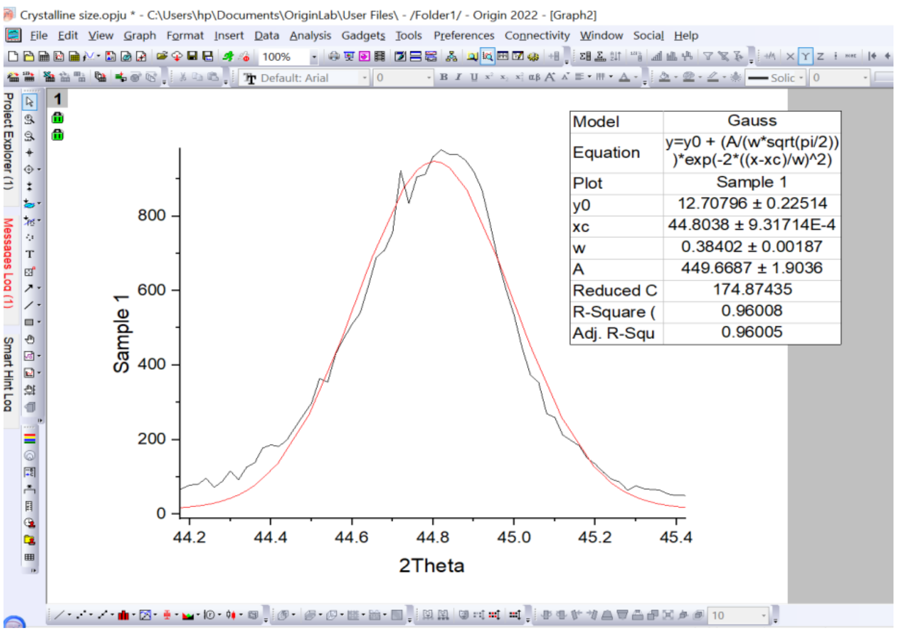

Appendix-2

Vickers Hardness Measurements for (S4, S3, S2, and S1) at trial 1, 2, 3

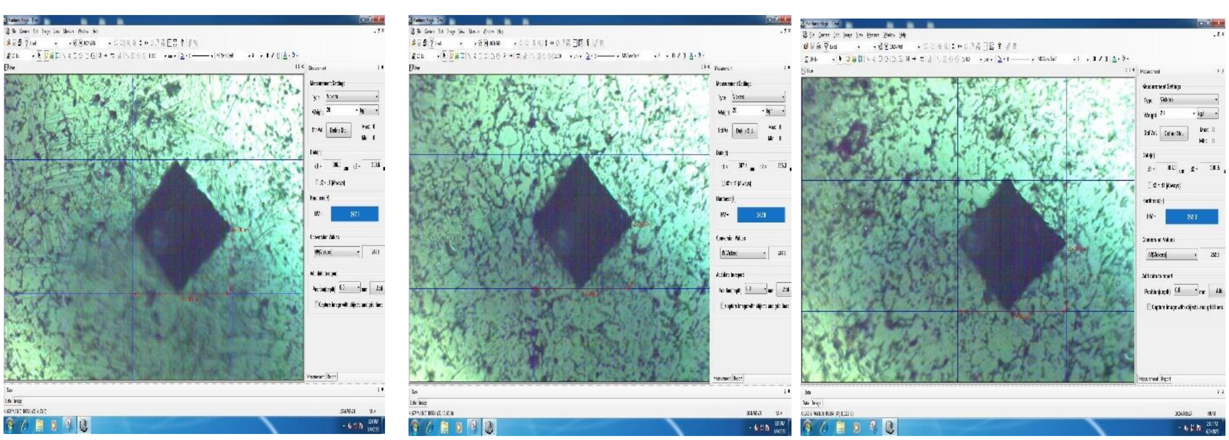

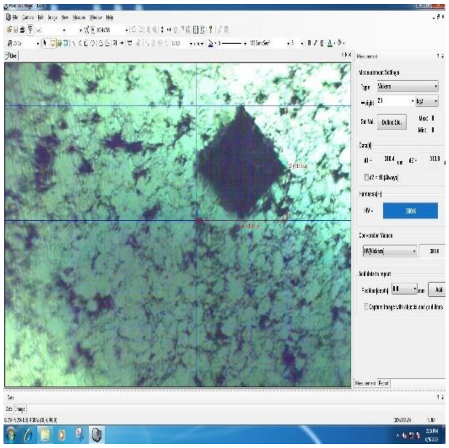
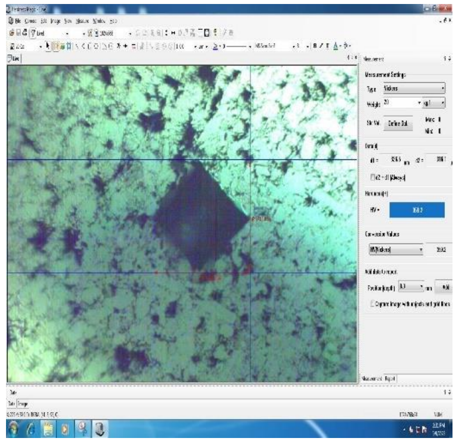
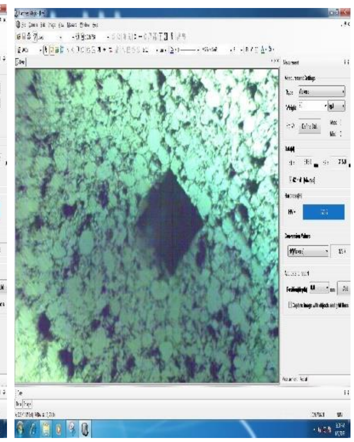
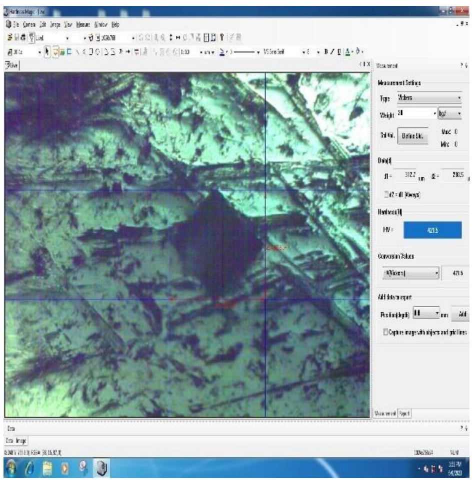
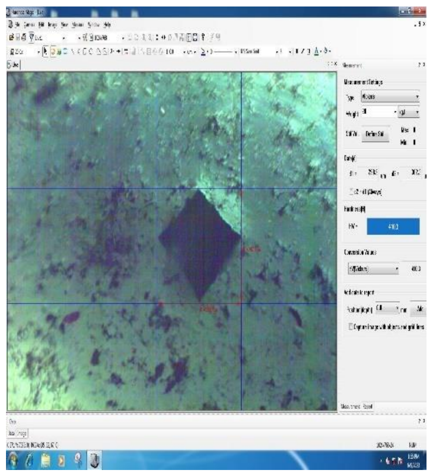
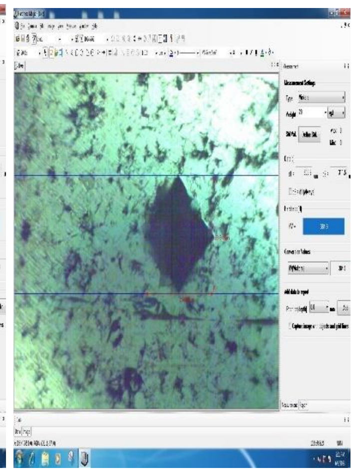
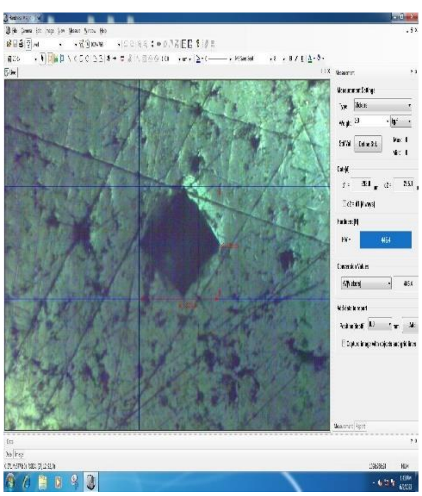
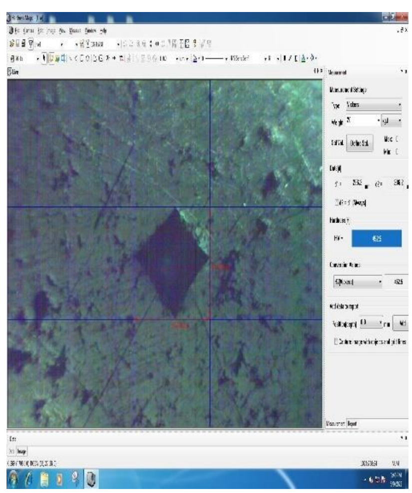
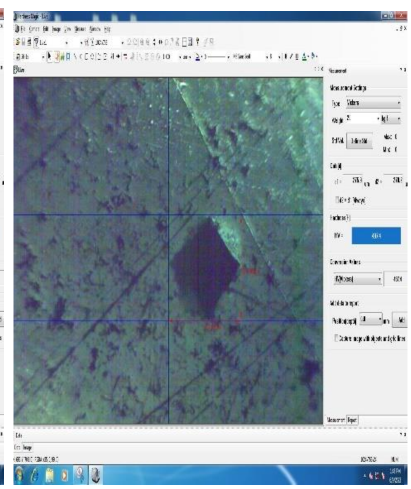

Appendix- 3

Compression Test (Stress-Elongation Curve for (S4) And Test Report For (S4)

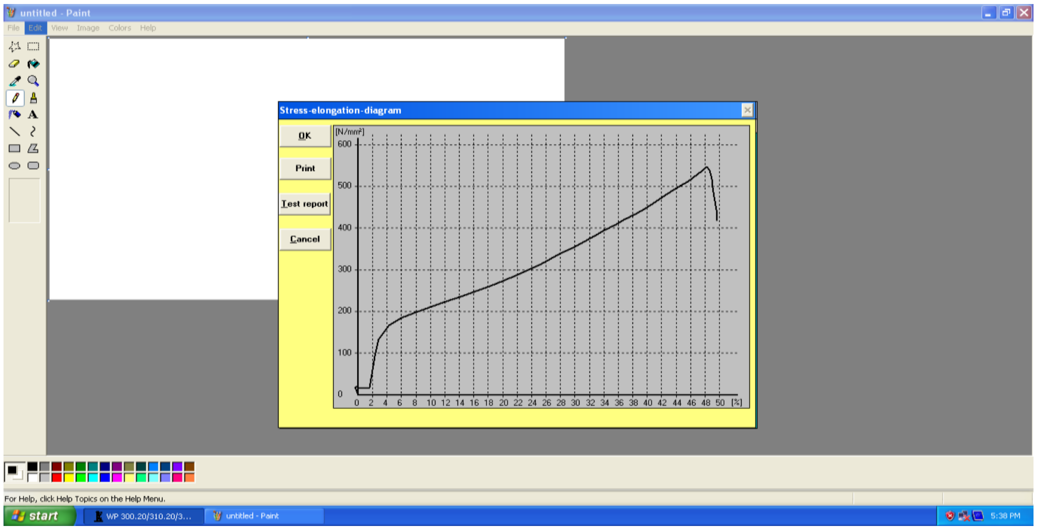

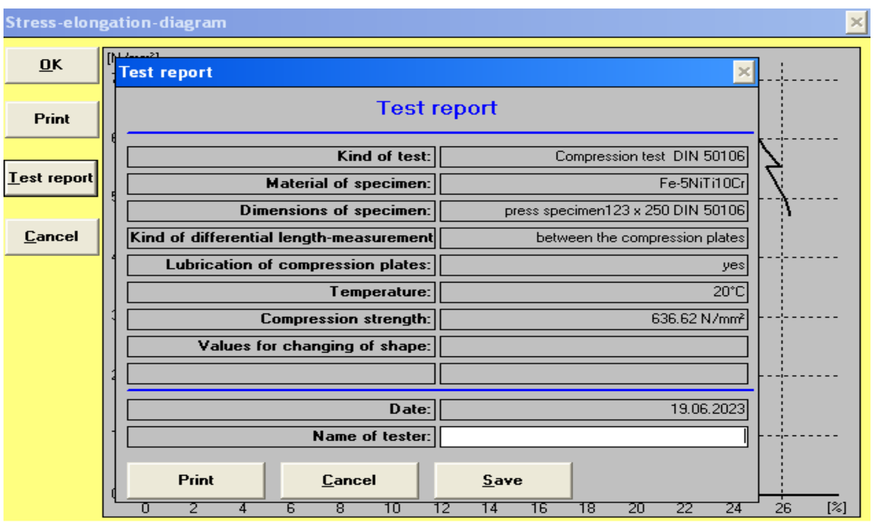

Stress-elongation-diagram

Test report

Kind of test:	Compression test DIN 50106
Material of specimen:	Fe-5NiTi10Cr
Dimensions of specimen:	press specimen123 x 250 DIN 50106
Kind of differential length-measurement	between the compression plates
Lubrication of compression plates:	yes
Temperature:	20°C
Compression strength:	636.62 N/mm²
Values for changing of shape:	
Date:	19.06.2023
Name of tester:	

Print Cancel Save

Appendix-4

(A) Open circuit potential (OCP) (Potential with Time)

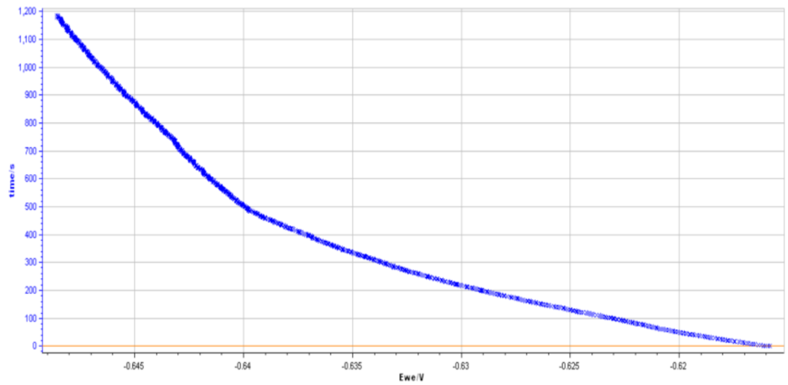

(B) Polarization Resistance and Corrosion Rate Calculation from Tafel Plot

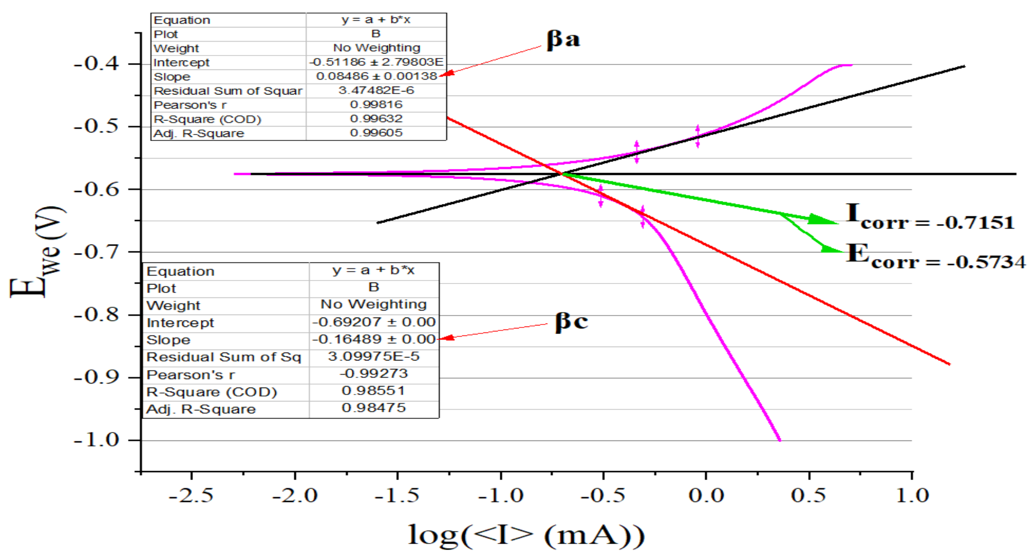

Samples Code	Icorr Log(mA/cm^2)	Ecorr (mV)	βc (V)	βc (V)
S1	-0.7151	-0.5734	0.0849	-0.1649
S2	-0.5616	-0.5877	0.1312	-0.1794
S3	-0.5494	-0.5817	0.1092	-0.2991
S4	-0.2577	-0.661	0.0961	-0.3046